Asymptotic Theory and Linear Stability in the Presence of Sinusoidal Bottom Topography

Imperial College London

Jack Davies

CID: 01534407

Supervisor: Pavel Berloff

September 12, 2019

ABSTRACT

We investigate the linear stability theory (LST) for a two-layer quasi-geostrophic (QG) model with sinusoidal bottom irregularities. By considering Fourier solutions for the perturbation streamfunctions, we formulate the associated eigenvalue problem. With the aid of MATLAB, we find solutions for the eigenfrequencies and eigenfunctions numerically and compare with the LST for the flat bottom correspondence. To complement this, we include an asymptotic analysis due to Benilov, which assumes the horizontal length scale of topography is small relative to the horizontal length scale of the flow disturbance and the vertical length scale of topography is small relative to the bottom layer depth. Finally, we compare the asymptotic theory with numerical results in an attempt to identify similarities and differences between the results obtained in both cases.

DECLARATION

I acknowledge that the work presented in this thesis, along with the MATLAB codes used to produce the plots, are my own, unless stated otherwise.

Signature:

ACKNOWLEDGEMENTS

I would like to express my immense gratitude to Dr Hemant Khatri and my supervisor Dr Pavel Berloff for their invaluable wealth of knowledge and continuous support throughout the process of writing this thesis. Words cannot begin to describe how lucky I am to have had my parents, Natalie and Paul, brother Ryan and girlfriend Jade with me every step of the way throughout this endeavour. I am forever thankful.

CONTENTS

CHAPTER 1

INTRODUCTION

Fluid dynamics is an extremely vast discipline which deals with many complicated ideas, such as: wave motion [1], vortex dynamics [2], boundary layers [3], hydrodynamic stability [4], and the list goes on. To even make sense of the subject, one must have at the very least a solid background in: differential equations [5], vector calculus [6], linear algebra [7], numerical analysis [8], and some probability and statistics [9] would only be beneficial. So it is safe to say we need a broad understanding of mathematics to even scratch the surface.

What we present in this dissertation is a problem which stems from the study of geophysical fluid dynamics (GFD). There have been a plethora of papers published on research in this field, some of which (but not limited to) include: linear and nonlinear analysis of mesoscale eddies [10, 11], investigations of multiple jets [12, 13] and the study of oceanic gyres [14, 15, 16]. The focus of this study will be on the problem of flow instability in a two-layer quasi-geostrophic (QG) model with sinusoidal bottom topography. The linear stability theory (LST) in the presence of a flat bottom is already well understood, and despite there already being a variety of publications considering variable bottom irregularities (some of which being [17, 18, 19, 20]), the linear and nonlinear analysis in the presence of sinusoidal topography does not appear to be heavily researched. Hence, we aim to expand our understanding of how the dynamics of oceanic flows is influenced by sinusoidal bottom irregularities. For simplicity, we shall restrict our attention to the cases of zonal and meridional topography only, as well as neglect terms due to viscosity and bottom friction.

To begin with, in chapter 2, we present some elementary theory from GFD and derive the one and two-layer QG model equations with general bottom topography. Before we focus our attention on the two-layer problem, we use chapter 3 to demonstrate the mathematical

techniques we shall employ by considering the simpler one-layer problem. Since this section is intended to ease us into the mathematical analysis moving forward, we shall not solve the sinusoidal problem numerically, but only construct it. Moving on, in chapter 4, we formulate and solve numerically the two-layer linearised problem in the presence of sinusoidal bottom topography by considering Fourier solutions for the perturbation streamfunctions. With the help of MATLAB, we plot various graphs such as dispersion relations and unstable mode distributions to illustrate our numerical findings. With these in mind, we solve the flat bottom case to identify how the stability of the flow changes in the presence of topography. Following this, we take an in depth look at an asymptotic analysis due to Benilov [21] in chapter 5. To conclude this section, we look at how the results obtained by solving the LST problem asymptotically differ from our numerical solutions in chapter 4. Finally, we summarise the main results of this thesis and suggest ways in which we can improve and expand on what we have done in 6.

Remark. *Throughout this thesis, when referring to some physical quantity, we shall use notation to distinguish whether we are working with dimensions or not. For example, if we are considering the energy in a system, then we shall write* $\hat{E}$ *to mean dimensional energy, and* E *to mean dimensionless energy. Moreover, regarding the presentation of referencing, we will use the labelling* $[S, pg.\, P]$*, where* S *refers to the source we are referring to and* P *refers to the page numbers of particular interest. As seen in this introduction, we will not always pay mention to page numbers when referring to different source materials.*

CHAPTER 2

REVIEW OF ESSENTIAL GEOPHYSICAL FLUID DYNAMICS

Before we can make any significant progress with the problem we wish to solve in this dissertation, we must first take some time to review the elementary theory. This chapter is intended to introduce some fundamental ideas in the study of geophysical fluid dynamics (GFD). By no means should this be considered as a complete overview of the field as the subject is too vast to cover here. However, the results we establish shall be used throughout the thesis, and so a firm understanding of this chapter is a prerequisite moving forward. Despite what we choose to present here being needed to understand our discussion later on, the more knowledge, the better, and so for a more in depth look at GFD, we suggest the textbooks [22], [23] and [24].

2.1 ELEMENTARY CONCEPTS

NAVIER-STOKE'S IN A ROTATING COORDINATE SYSTEM

We shall start our exploration of the exciting field of GFD by introducing the fundamental equations governing the dynamics of fluid motion. Since these equations are already well established in the literature, we will not dwell on the derivation here, but refer to [25, pg. 200-208] for the mathematical details involved.

In a *fixed Cartesian* $(\hat{x}, \hat{y}, \hat{z})$-frame of reference, the *Navier-Stoke's* equations can be compactly written as the vector equation (2.1a), along with the *Continuity equation* (2.1b):

$$\frac{\mathrm{D}\hat{\boldsymbol{u}}}{\mathrm{D}\hat{t}} = -\frac{1}{\hat{\rho}}\hat{\nabla}\hat{p} + \hat{\nu}\hat{\nabla}^2\hat{\boldsymbol{u}} + \hat{\boldsymbol{F}}_b, \tag{2.1a}$$

$$\frac{\mathrm{D}\hat{\rho}}{\mathrm{D}\hat{t}} + \hat{\rho}\hat{\nabla}\cdot\hat{\boldsymbol{u}} = 0, \tag{2.1b}$$

where $\hat{\boldsymbol{u}} = (\hat{u}, \hat{v}, \hat{w})$ is the *velocity profile*, $\hat{\rho}$ is the *density* of the fluid, $\hat{p}$ is the *pressure field*,

$\hat{\nu}$ is the *kinematic viscosity coefficient*[1], $\hat{\boldsymbol{F}}_b$ is representative of *body forces* such as those due to gravity, and the *material derivative*, *gradient* and *Laplacian* operators are defined as:

$$\frac{\mathrm{D}}{\mathrm{D}\hat{t}} := \frac{\partial}{\partial \hat{t}} + (\hat{\boldsymbol{u}} \cdot \hat{\nabla}), \quad \hat{\nabla} := \left(\frac{\partial}{\partial \hat{x}}, \frac{\partial}{\partial \hat{y}}, \frac{\partial}{\partial \hat{z}} \right) \text{ and } \hat{\nabla}^2 := \frac{\partial^2}{\partial \hat{x}^2} + \frac{\partial^2}{\partial \hat{y}^2} + \frac{\partial^2}{\partial \hat{z}^2},$$

respectively. When working on problems in geophysical fluid dynamics, it is useful to express (2.1) w.r.t. the *Earth's rotation*, $\hat{\boldsymbol{\Omega}}$. To do this, we must move to a coordinate system which rotates with *angular velocity* $\hat{\boldsymbol{\Omega}}$. This is achieved by noting that the rate of change of some arbitrary vector, $\hat{\boldsymbol{b}}$, in an *inertial* reference frame, $\mathscr{I}$, transforms to a rotating frame, $\mathscr{R}$, by the following rule:

$$\left[\frac{\mathrm{d}\hat{\boldsymbol{b}}}{\mathrm{d}\hat{t}} \right]_{\mathscr{I}} = \left[\frac{\mathrm{d}\hat{\boldsymbol{b}}}{\mathrm{d}\hat{t}} \right]_{\mathscr{R}} + \hat{\boldsymbol{\Omega}} \wedge \hat{\boldsymbol{b}}, \tag{2.2}$$

where we have assumed $\mathscr{R}$ rotates with angular velocity $\hat{\boldsymbol{\Omega}}$. If, in place of $\hat{\boldsymbol{b}}$, we consider the *position vector* $\hat{\boldsymbol{x}}$, then we find that:

$$\begin{aligned} \left[\frac{\mathrm{d}\hat{\boldsymbol{x}}}{\mathrm{d}\hat{t}} \right]_{\mathscr{I}} &= \left[\frac{\mathrm{d}\hat{\boldsymbol{x}}}{\mathrm{d}\hat{t}} \right]_{\mathscr{R}} + \hat{\boldsymbol{\Omega}} \wedge \hat{\boldsymbol{x}} \\ \implies \quad \hat{\boldsymbol{u}}_{\mathscr{I}} &= \hat{\boldsymbol{u}}_{\mathscr{R}} + \hat{\boldsymbol{\Omega}} \wedge \hat{\boldsymbol{x}}. \end{aligned}$$

From this, it follows that the *acceleration* of $\hat{\boldsymbol{u}}_{\mathscr{I}}$, that is the material derivative in (2.1a), transforms as:

$$\begin{aligned} \left[\frac{\mathrm{d}\hat{\boldsymbol{u}}_{\mathscr{I}}}{\mathrm{d}\hat{t}} \right]_{\mathscr{I}} &= \left[\frac{\mathrm{d}\hat{\boldsymbol{u}}_{\mathscr{I}}}{\mathrm{d}\hat{t}} \right]_{\mathscr{I}} + \left[\frac{\mathrm{d}}{\mathrm{d}\hat{t}} (\hat{\boldsymbol{\Omega}} \wedge \hat{\boldsymbol{x}}) \right]_{\mathscr{I}} \\ &= \left\{ \left[\frac{\mathrm{d}\hat{\boldsymbol{u}}_{\mathscr{R}}}{\mathrm{d}\hat{t}} \right]_{\mathscr{R}} + \hat{\boldsymbol{\Omega}} \wedge \hat{\boldsymbol{u}}_{\mathscr{R}} \right\} + \left\{ \hat{\boldsymbol{\Omega}} \wedge \hat{\boldsymbol{u}}_{\mathscr{R}} + \left[\frac{\mathrm{d}\hat{\boldsymbol{\Omega}}}{\mathrm{d}\hat{t}} \right]_{\mathscr{R}} \wedge \hat{\boldsymbol{x}} + \hat{\boldsymbol{\Omega}} \wedge (\hat{\boldsymbol{\Omega}} \wedge \hat{\boldsymbol{x}}) \right\} \\ &= \left[\frac{\mathrm{d}\hat{\boldsymbol{u}}_{\mathscr{R}}}{\mathrm{d}\hat{t}} \right]_{\mathscr{R}} + \underbrace{2\hat{\boldsymbol{\Omega}} \wedge \hat{\boldsymbol{u}}_{\mathscr{R}}}_{\text{Coriolis force}} + \underbrace{\hat{\boldsymbol{\Omega}} \wedge (\hat{\boldsymbol{\Omega}} \wedge \hat{\boldsymbol{x}})}_{\text{centrifugal force}}, \end{aligned}$$

where the final equality is obtained by assuming the rotation of the Earth to be constant. Since the *centrifugal* term is a body force, it can conveniently be absorbed into $\hat{\boldsymbol{F}}_b$. Hence, in a frame rotating with angular velocity $\hat{\boldsymbol{\Omega}}$, the Navier-Stoke's equations read in vector form as:

$$\frac{\mathrm{D}\hat{\boldsymbol{u}}}{\mathrm{D}\hat{t}} + 2\hat{\boldsymbol{\Omega}} \wedge \hat{\boldsymbol{u}} = -\frac{1}{\hat{\rho}} \hat{\nabla} \hat{p} + \hat{\nu} \hat{\nabla}^2 \hat{\boldsymbol{u}} + \hat{\boldsymbol{F}}_b, \tag{2.3}$$

with Continuity equation as defined in (2.1b).

[1]The kinematic viscosity coefficient is defined as $\hat{\nu} = \hat{\mu}/\hat{\rho}$, where $\hat{\mu}$ is the so called *dynamic viscosity coefficient*, which is a measure of the viscosity of the fluid in question.

Spherical Equations

So far, we have been working in a Cartesian coordinate system, despite the fact the Earth is approximately spherical. As such, it makes sense to rewrite (2.3) in terms of *spherical coordinates*, $(\lambda, \theta, \hat{r})$, where λ is the *longitude* coordinate, θ is the *latitude* coordinate and $\hat{r}$ is the *altitude* coordinate[2]. If, for simplicity, we assume viscous effects to be negligible, then in the presence of gravity, $\hat{\boldsymbol{g}} = (0, 0, -\hat{g})$, with the Earth's rotation given by $\hat{\boldsymbol{\Omega}} = (0, \hat{\Omega}\cos\hat{\theta}, \hat{\Omega}\sin\hat{\theta})$, we can rewrite (2.3) in spherical coordinates as:

$$\frac{\mathrm{D}\hat{u}}{\mathrm{D}\hat{t}} - \left(2\hat{\Omega} + \frac{\hat{u}}{\hat{r}\cos\theta}\right)(\hat{v}\sin\theta - \hat{w}\cos\theta) = -\frac{1}{\hat{\rho}\hat{r}\cos\theta}\frac{\partial\hat{p}}{\partial\hat{\lambda}}, \tag{2.4a}$$

$$\frac{\mathrm{D}\hat{v}}{\mathrm{D}\hat{t}} + \frac{\hat{v}\hat{w}}{\hat{r}} + \left(2\hat{\Omega} + \frac{\hat{u}}{\hat{r}\cos\theta}\right)\hat{u}\sin\theta = -\frac{1}{\hat{\rho}\hat{r}}\frac{\partial\hat{p}}{\partial\theta}, \tag{2.4b}$$

$$\frac{\mathrm{D}\hat{w}}{\mathrm{D}\hat{t}} - \frac{\hat{u}^2 + \hat{v}^2}{\hat{r}} - 2\hat{\Omega}\hat{u}\cos\theta = -\frac{1}{\hat{\rho}}\frac{\partial\hat{p}}{\partial\hat{r}} - \hat{g}, \tag{2.4c}$$

$$\frac{\partial\hat{\rho}}{\partial\hat{t}} + \frac{1}{\hat{r}\cos\theta}\frac{\partial}{\partial\lambda}(\hat{u}\hat{\rho}) + \frac{1}{\hat{r}\cos\theta}\frac{\partial}{\partial\theta}(\hat{v}\hat{\rho}\cos\theta) + \frac{1}{\hat{r}^2}\frac{\partial}{\partial\hat{r}}(\hat{r}^2\hat{w}\hat{\rho}) = 0, \tag{2.4d}$$

where (2.4a), (2.4b) and (2.4c) are the spherical representation of Navier-Stoke's, and (2.4d) corresponds to the Continuity equation. Since we will not be working with this particular equation set later on, but rather an approximation of (2.4), we shall not concern ourself with the details of the derivation here and instead refer to [22, pg. 61-65] for a complete mathematical breakdown explaining the specific details and how the system of equations is obtained.

Local Cartesian Approximation

For large scale motions, the equation set (2.4) is a useful tool to work with. However, when concerning ourselves with small-scale motions, it becomes inconvenient to work with spherical coordinates since the equations in question are very complicated and the rotation of the Earth no longer plays a pivotal role in the dynamics of the problem under consideration. Instead, it turns out to be more beneficial to introduce a *tangent plane* to the surface of the Earth. If we position the tangent plane at some point $(\lambda_0, \hat{r}_0, \theta_0)$ on the sphere, then an approximation to (2.4) in the tangent plane (preserving the velocity profile) can be achieved by introducing the change of variables:

$$\hat{x} = \underbrace{\lambda\hat{r}_0\cos(\theta_0)}_{\text{longitude}}, \quad \hat{y} = \underbrace{(\theta - \theta_0)\hat{r}_0}_{\text{latitude}}, \quad \hat{z} = \underbrace{\hat{r} - \hat{r}_0}_{\text{altitude}}. \tag{2.5}$$

[2]The longitude and latitude parameters are dimensionless quantities, which is the reason for denoting them by λ and θ rather than $\hat{\lambda}$ and $\hat{\theta}$.

It follows under the assumption that nonlinear terms in (2.4) are negligible and the *Eotvos effect* is small, when introducing the *Coriolis parameter*, $\hat{f}(\theta) = 2\hat{\Omega}\sin\theta$, the change of coordinates (2.5) yields the *local Cartesian approximation*:

$$\frac{\mathrm{D}\hat{u}}{\mathrm{D}\hat{t}} - \hat{f}\hat{v} = -\frac{1}{\hat{\rho}}\frac{\partial \hat{p}}{\partial \hat{x}}, \tag{2.6a}$$

$$\frac{\mathrm{D}\hat{v}}{\mathrm{D}\hat{t}} + \hat{f}\hat{u} = -\frac{1}{\hat{\rho}}\frac{\partial \hat{p}}{\partial \hat{y}}, \tag{2.6b}$$

$$\frac{\mathrm{D}\hat{w}}{\mathrm{D}\hat{t}} = -\frac{1}{\hat{\rho}}\frac{\partial \hat{p}}{\partial \hat{z}} - \hat{g}, \tag{2.6c}$$

with Continuity equation the same as (2.1b). In the neighbourhood of the point where the plane is tangent to the sphere, the Coriolis parameter can of course be Taylor expanded:

$$\begin{aligned} \hat{f}(\theta) &= \hat{f}(\theta_0) + (\theta - \theta_0)\frac{\mathrm{d}\hat{f}}{\mathrm{d}\theta}(\theta_0) + \mathcal{O}\big[(\theta-\theta_0)^2\big] \\ \implies \hat{f}(\hat{y}) &= 2\hat{\Omega}\sin\theta_0 + \hat{y}\frac{2\hat{\Omega}\cos\theta_0}{\hat{r}_0} + \mathcal{O}(\hat{y}^2) \\ &\approx \hat{f}_0 + \hat{\beta}\hat{y}, \end{aligned}$$

for $\hat{f}_0 = 2\hat{\Omega}\sin\theta_0$ and the *meridional gradient* of the Coriolis parameter, $\hat{\beta} = 2\hat{\Omega}\cos\theta_0/\hat{r}_0$. Though we can expand the Coriolis parameter further, for theoretical purposes it proves useful to work with the $\hat{f}$-plane and $\hat{\beta}$-plane approximations, $\hat{f} = \hat{f}_0$ and $\hat{f} = \hat{f}_0 + \hat{\beta}\hat{y}$ respectively. The later of which accounts for changes in latitude, and so incorporates some important elements of the sphericity of the Earth.

2.2 SHALLOW WATER THEORY

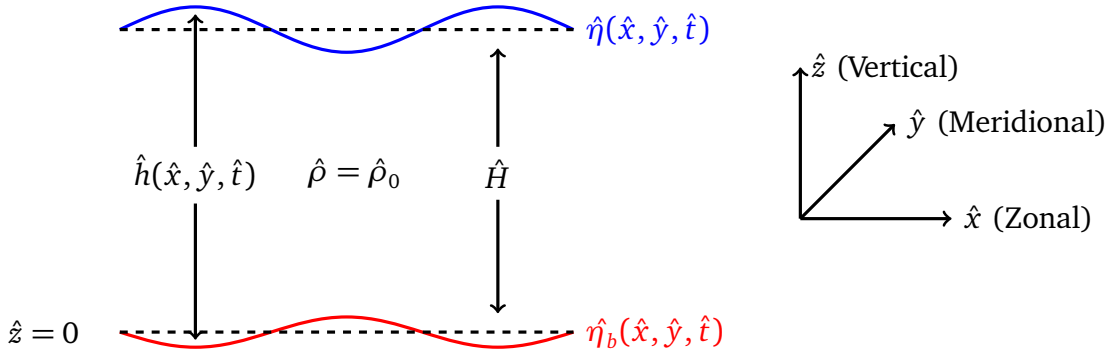

Figure 2.1: A one-layer shallow-water model in a Cartesian $(\hat{x},\hat{y},\hat{z})$-plane with constant fluid density $\hat{\rho}_0$, variable layer depth $\hat{h}(\hat{x},\hat{y},\hat{t})$, average layer depth $\hat{H}$, and variable bottom topography defined by $\hat{\eta}_b(\hat{x},\hat{y},\hat{t})$.

Now that we have obtained the local Cartesian approximation for our governing equations, we would like to construct from them the *shallow water model*. The assumptions under which this particular model is formulated are the following:

- The fluid density is constant, i.e. $\hat{\rho} = \hat{\rho}_0$,
- The *hydrostatic approximation* applies, i.e. vertical acceleration is small relative to gravity.

With these in mind, the vertical momentum equation (2.6c) becomes:

$$\frac{\partial \hat{p}}{\partial \hat{z}} = -\hat{\rho}_0 \hat{g},$$

which when integrated w.r.t. $\hat{z}$, results in the pressure field:

$$\hat{p}(\hat{x}, \hat{y}, \hat{z}, \hat{t}) = \hat{\rho}_0 \hat{g}\big[\hat{h}(\hat{x}, \hat{y}, \hat{t}) - \hat{z}\big], \tag{2.7}$$

where we have assumed pressure continuity at the free-surface and taken atmospheric pressure to be zero, i.e. $\hat{p}|_{\hat{z}=\hat{h}(\hat{x},\hat{y},\hat{t})} = 0$. From (2.7), we see that the horizontal pressure gradients are independent of $\hat{z}$, that is, we have:

$$\frac{\partial}{\partial \hat{z}}\left(\frac{\partial \hat{p}}{\partial \hat{x}}\right) = \frac{\partial}{\partial \hat{z}}\left(\frac{\partial \hat{p}}{\partial \hat{y}}\right) = 0,$$

and so, as a consequence of (2.6a) and (2.6b), the horizontal velocities $\hat{u}$ and $\hat{v}$ are independent of $\hat{z}$[3]. Furthermore, (2.7) reduces (2.6a) and (2.6b) to the form:

$$\frac{\mathrm{D}\hat{u}}{\mathrm{D}\hat{t}} - \hat{f}\hat{v} = -\hat{g}\frac{\partial \hat{h}}{\partial \hat{x}}, \tag{2.8a}$$

$$\frac{\mathrm{D}\hat{v}}{\mathrm{D}\hat{t}} + \hat{f}\hat{u} = -\hat{g}\frac{\partial \hat{h}}{\partial \hat{y}}, \tag{2.8b}$$

which is the system of momentum equations governing shallow-water dynamics.

Continuity Derivation for Shallow Water

We have yet to find the complete equation set describing the dynamics in a shallow-water model since we still have to identify the associated Continuity equation. To do this, we work from first principles by noting that the *mass flux* across the boundary of a fluid column with cross-sectional area $\hat{A}$ and variable height $\hat{h}$ must balance with the *mass change* in the fluid column. If we denote an outward unit normal vector to the column by $\hat{\boldsymbol{n}}$, and represent a

[3] Physically, this corresponds to fluid flowing in columns of variable height $\hat{h}$.

surface element of the vertical section of the fluid column by $\hat{h}\,\mathrm{d}\hat{s}$ (for some line element $\mathrm{d}\hat{s}$), then the mass flux across the boundary can be written as:

$$\text{Flux} = -\oint \hat{\rho}_0 \hat{\boldsymbol{u}} \cdot \hat{\boldsymbol{n}} \hat{h}\,\mathrm{d}\hat{s} = -\int_{\hat{A}} \hat{\nabla} \cdot (\hat{\rho}_0 \hat{h} \hat{\boldsymbol{u}})\,\mathrm{d}\hat{A},$$

where the second equality is a consequence of the *divergence theorem* (details of which can be found in [6, pg. 81-83]). Hence, since the mass of fluid is given by the integral:

$$\hat{m} = \int_{\hat{A}} \hat{\rho}_0 \hat{h}\,\mathrm{d}\hat{A},$$

by the balance we stated earlier, we find that:

$$\begin{aligned} -\int_{\hat{A}} \hat{\nabla} \cdot (\hat{\rho}_0 \hat{h} \hat{\boldsymbol{u}})\,\mathrm{d}\hat{A} &= \int_{\hat{A}} \hat{\rho}_0 \frac{\partial \hat{h}}{\partial \hat{t}}\,\mathrm{d}\hat{A} \\ \implies \int_{\hat{A}} \frac{\partial \hat{h}}{\partial \hat{t}} + \hat{\nabla} \cdot (\hat{\rho}_0 \hat{h} \hat{\boldsymbol{u}})\,\mathrm{d}\hat{A} &= 0. \end{aligned}$$

Since this has to hold for arbitrary $\hat{A}$, we must have the integrand equal to zero, giving us the shallow-water Continuity equation:

$$\frac{\mathrm{D}\hat{h}}{\mathrm{D}\hat{t}} + \hat{h}\left(\frac{\partial \hat{u}}{\partial \hat{x}} + \frac{\partial \hat{v}}{\partial \hat{y}}\right) = 0. \tag{2.9}$$

Conservation of Potential Vorticity

With the equation set for a one-layer shallow water model identified, we can now derive an important *conservation law*. If we take the *curl* of (2.8) and define *relative vorticity* by:

$$\hat{\zeta} = \frac{\partial \hat{v}}{\partial \hat{x}} - \frac{\partial \hat{u}}{\partial \hat{y}}, \tag{2.10}$$

then we obtain the aptly named *vorticity equation*:

$$\begin{aligned} &\frac{\partial}{\partial \hat{y}}\left[\frac{\mathrm{D}\hat{u}}{\mathrm{D}\hat{t}} - \hat{f}\hat{v}\right] - \frac{\partial}{\partial \hat{x}}\left[\frac{\mathrm{D}\hat{v}}{\mathrm{D}\hat{t}} + \hat{f}\hat{u}\right] = -\hat{g}\left[\frac{\partial^2 \hat{h}}{\partial \hat{y}\partial \hat{x}} - \frac{\partial^2 \hat{h}}{\partial \hat{x}\partial \hat{y}}\right] = 0 \\ \implies &\frac{\partial}{\partial \hat{t}}\left(\frac{\partial \hat{u}}{\partial \hat{y}}\right) + \frac{\partial \hat{u}}{\partial \hat{y}}\frac{\partial \hat{u}}{\partial \hat{x}} + \hat{u}\frac{\partial \hat{u}^2}{\partial \hat{x}\partial \hat{y}} + \frac{\partial \hat{v}}{\partial \hat{y}}\frac{\partial \hat{u}}{\partial \hat{y}} + \hat{v}\frac{\partial^2 \hat{u}}{\partial \hat{y}^2} - \hat{v}\frac{\mathrm{d}\hat{f}}{\mathrm{d}\hat{y}} - \hat{f}\frac{\partial \hat{v}}{\partial \hat{y}} \\ &- \left[\frac{\partial}{\partial \hat{t}}\left(\frac{\partial \hat{v}}{\partial \hat{x}}\right) + \frac{\partial \hat{u}}{\partial \hat{x}}\frac{\partial \hat{v}}{\partial \hat{x}} + \hat{u}\frac{\partial^2 \hat{v}}{\partial \hat{x}^2} + \frac{\partial \hat{v}}{\partial \hat{x}}\frac{\partial \hat{v}}{\partial \hat{y}} + \hat{v}\frac{\partial^2 \hat{v}}{\partial \hat{x}\partial \hat{y}} + \hat{f}\frac{\partial \hat{u}}{\partial \hat{x}}\right] = 0 \\ \implies &\frac{\mathrm{D}\hat{\zeta}}{\mathrm{D}\hat{t}} + (\hat{f} + \hat{\zeta})\left[\frac{\partial \hat{u}}{\partial \hat{x}} + \frac{\partial \hat{v}}{\partial \hat{y}}\right] + \hat{v}\frac{\mathrm{d}\hat{f}}{\mathrm{d}\hat{y}} = 0. \end{aligned}$$

With the aid of (2.9), we can reduce this further, arriving at the statement of *potential vorticity* conservation:

$$\frac{\mathrm{D}\hat{q}}{\mathrm{D}\hat{t}} = 0, \quad \hat{q} = \frac{\hat{f} + \hat{\zeta}}{\hat{h}}, \tag{2.11}$$

for potential vorticity $\hat{q}$. In other words, this tells us that the quantity $\hat{q}$ is constant and dictated by changes in $\hat{f}$, $\hat{\zeta}$ and $\hat{h}$ only. This is an extremely powerful result as it turns the problem of solving for the dynamic description of fluid motion to one where we must solve for the evolution of a scalar quantity which is materially conserved.

This conservation law in fact holds for variable Coriolis parameter $\hat{f}$ as well as large-scale topography (when considering sinusoidal topography, the mention of large-scale bottom irregularities refers to the amplitude of topography being allowed to scale with the average depth of the fluid layer). However, we can further simplify this by means of *linearisation* if we make several assumptions:

- The Rossby number is very small, i.e. $\varepsilon = \hat{U}/\hat{f}_0\hat{L} \ll 1$,
- The bottom topography under consideration is small-scale, i.e. $|\hat{\eta}_b|/\hat{H} = \mathcal{O}(\varepsilon)$,
- The perturbation of the free-surface is small when compared with the characteristic layer depth, i.e. $|\hat{\eta}|/\hat{H} = \mathcal{O}(\varepsilon)$,
- The contribution to the Coriolis parameter due to beta is small, i.e. $|\hat{\beta}\hat{y}|/\hat{f}_0 = \mathcal{O}(\varepsilon)$.

Under these assumptions, we can approximate potential vorticity:

$$\begin{aligned}
\hat{q} &= \frac{\hat{f}_0 + \hat{\beta}\hat{y} + \hat{\zeta}}{\hat{H} + \hat{\eta} - \hat{\eta}_b} \\
&= \frac{\hat{f}_0}{\hat{H}}\left[\frac{1 + \hat{\beta}\hat{y}/\hat{f}_0 + \hat{\zeta}/\hat{f}_0}{1 + \hat{\eta}/\hat{H} - \hat{\eta}_b/\hat{H}}\right] \\
&= \frac{\hat{f}_0}{\hat{H}}\left(1 + \frac{\hat{\beta}\hat{y}}{\hat{f}_0} + \frac{\hat{\zeta}}{\hat{f}_0}\right)\left[1 + \frac{(\hat{\eta} - \hat{\eta}_b)}{\hat{H}}\right]^{-1} \\
&= \frac{\hat{f}_0}{\hat{H}}\left(1 + \frac{\hat{\beta}\hat{y}}{\hat{f}_0} + \frac{\hat{\zeta}}{\hat{f}_0}\right)\left[1 - \frac{(\hat{\eta} - \hat{\eta}_b)}{\hat{H}} + \mathcal{O}(\varepsilon^2)\right] \\
&= \frac{\hat{f}_0}{\hat{H}} + \frac{\hat{\beta}\hat{y}}{\hat{H}} + \frac{\hat{\zeta}}{\hat{H}} - \frac{\hat{f}_0(\hat{\eta} - \hat{\eta}_b)}{\hat{H}^2} + \mathcal{O}(\varepsilon^2),
\end{aligned}$$

where we were able to Taylor expand due to the presence of small-scale ratios[4]. We notice that the first term in this expansion is constant and will be forgotten when taking the material derivative, whereas, the following three terms are of order ε, and are thus larger than the remaining terms of order ε^2 (as a consequence of assuming the Rossby number to be small).

[4]The expansion,

$$(1 + x)^{-1} = \sum_{j=0}^{\infty}(-1)^j x^j,$$

is convergent provided $|x| < 1$ and divergent otherwise.

Therefore, substitution of these findings into our conservation law, and neglecting terms of order ε^2, it follows that:

$$\frac{\mathrm{D}}{\mathrm{D}\hat{t}}\left[\hat{\beta}\,\hat{y}+\hat{\zeta}-\frac{\hat{f}_0(\hat{\eta}-\hat{\eta}_b)}{\hat{H}}\right]=0, \tag{2.12}$$

where we have multiplied through by $\hat{H}$ for completeness. This is the so-called *quasi-geostrophic* (QG) representation of the PV conservation law in the absence of external forces. In fact, we can rewrite this further by making use of the *geostrophic relations*:

$$\hat{f}_0\hat{v}=\hat{g}\frac{\partial\hat{\eta}}{\partial\hat{x}},\quad \hat{f}_0\hat{u}=-\hat{g}\frac{\partial\hat{\eta}}{\partial\hat{y}}. \tag{2.13}$$

From these, we have equalities for $\hat{u}$ and $\hat{v}$, and so by recalling (2.10), we are able to express the relative vorticity term as:

$$\hat{\zeta}=\frac{\hat{g}}{\hat{f}_0}\hat{\nabla}^2\hat{\eta}.$$

We can tidy this up somewhat by defining the flow *streamfunction*:

$$\hat{\psi}=\frac{\hat{g}}{\hat{f}_0}\hat{\eta}. \tag{2.14}$$

Making use of (2.14), one finds that the relative vorticity relation can be rewritten in the form:

$$\hat{\zeta}=\hat{\nabla}^2\hat{\psi}. \tag{2.15}$$

With these relations established, we are now in a position to rewrite the QG conservation law for PV. It follows by means of substituting these parameters in terms of streamfunctions into the QG equation, (2.12), that:

$$\frac{\mathrm{D}}{\mathrm{D}\hat{t}}\left[\nabla^2\hat{\psi}-\frac{\hat{f}_0^2\hat{\psi}}{\hat{g}\hat{H}}+\hat{\beta}\,\hat{y}+\frac{\hat{f}_0}{\hat{H}}\hat{\eta}_b\right]=0, \tag{2.16}$$

where the material derivative operator in terms of flow streamfunctions reads as:

$$\frac{\mathrm{D}}{\mathrm{D}\hat{t}}=\frac{\partial}{\partial\hat{t}}-\frac{\partial\hat{\psi}}{\partial\hat{y}}\frac{\partial}{\partial\hat{x}}+\frac{\partial\hat{\psi}}{\partial\hat{x}}\frac{\partial}{\partial\hat{y}}.$$

2.3 DERIVATION OF THE TWO-LAYER QUASI-GEOSTROPHIC MODEL

A natural means of extending the one-layer shallow water model is the addition of multiple fluid layers. For the purpose of our study later on, we shall focus our attention on the two-layer extension, though in principle, an arbitrary number of layers can be considered. The way in

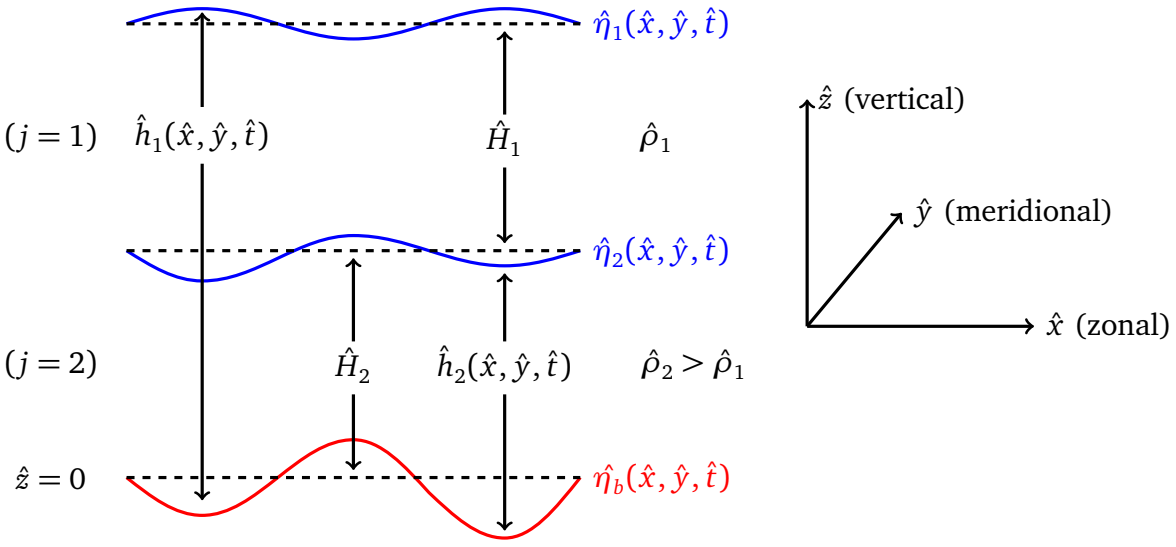

Figure 2.2: A two-layer shallow-water model (j indicating the layer of reference) with variable bottom irregularities defined by $\hat{\eta}_b(\hat{x},\hat{y},\hat{t})$, layer density defined by $\hat{\rho}_j$, variable layer depth defined by $\hat{h}_j(\hat{x},\hat{y},\hat{t})$, and characteristic (or average) layer depth defined by $\hat{H}_j$.

which we proceed with deriving the model equations is by obtaining a governance for each layer separately. Clearly, from figure 2.2, we see that the variable layer depths can be expressed in the form:

$$\hat{h}_1(\hat{x},\hat{y},\hat{t}) = \hat{H}_1 + \hat{H}_2 + \hat{\eta}_1(\hat{x},\hat{y},\hat{t}) - \hat{\eta}_b(\hat{x},\hat{y},\hat{t}), \tag{2.17a}$$

$$\hat{h}_2(\hat{x},\hat{y},\hat{t}) = \hat{H}_2 + \hat{\eta}_2(\hat{x},\hat{y},\hat{t}) - \hat{\eta}_b(\hat{x},\hat{y},\hat{t}). \tag{2.17b}$$

Now, making use of the shallow-water assumptions established earlier, it follows that the fluid pressure for each layer can be expressed as:

$$\hat{p}_j(\hat{x},\hat{y},\hat{z},\hat{t}) = -\hat{\rho}_j\hat{g}\hat{z} + \hat{P}_j(\hat{x},\hat{y},\hat{t}),$$

If we consider the top layer, referenced by $j=1$, we can assume pressure continuity at the free surface to identify the arbitrary function $\hat{P}_1$. Assuming for simplicity that atmospheric pressure is zero, we must have that $\hat{p}_1|_{\hat{z}=\hat{h}_1} = 0$, which results in:

$$\hat{p}_1 = \underbrace{\hat{\rho}_1\hat{g}(\hat{H}_1+\hat{H}_2-\hat{z})}_{\text{static contribution}} + \underbrace{\hat{\rho}_1\hat{g}(\hat{\eta}_1-\hat{\eta}_b)}_{\text{dynamic contribution}},$$

where the later term is time dependent and so represents the dynamic pressure contribution. Regarding the bottom layer, referenced by $j=2$, we must have pressure continuity at the layer interface. Mathematically, this can be expressed as the statement $\hat{p}_2|_{\hat{z}=\hat{h}_2} = \hat{p}_1|_{\hat{z}=\hat{h}_2}$, giving us:

$$\hat{p}_2 = \underbrace{\hat{g}\Big[\hat{\rho}_1\hat{H}_1 + \hat{\rho}_2\hat{g}(\hat{H}_2-\hat{z})\Big]}_{\text{static contribution}} + \underbrace{\hat{g}\Big[\hat{\rho}_1(\hat{\eta}_1-\hat{\eta}_b) + (\hat{\rho}_2-\hat{\rho}_1)\hat{\eta}_2 - \hat{\rho}_2\hat{\eta}_b\Big]}_{\text{dynamic contribution}}.$$

We can now substitute these pressure representations into our local Cartesian approximation, (2.6), to obtain the set of governing equations:

$$(j=1)\quad \begin{cases} \dfrac{\mathrm{D}\hat{u}_1}{\mathrm{D}\hat{t}} - \hat{f}\hat{v}_1 = -\hat{g}\dfrac{\partial}{\partial \hat{x}}(\hat{\eta}_1 - \hat{\eta}_b), \\ \dfrac{\mathrm{D}\hat{v}_1}{\mathrm{D}\hat{t}} + \hat{f}\hat{u}_1 = -\hat{g}\dfrac{\partial}{\partial \hat{y}}(\hat{\eta}_1 - \hat{\eta}_b), \end{cases} \tag{2.18a}$$

$$(j=2)\quad \begin{cases} \dfrac{\mathrm{D}\hat{u}_2}{\mathrm{D}\hat{t}} - \hat{f}\hat{v}_2 = -\dfrac{\hat{g}}{\hat{\rho}_2}\left[\dfrac{\partial \hat{\eta}_1}{\partial \hat{x}} + (\hat{\rho}_2 - \hat{\rho}_1)\dfrac{\partial \hat{\eta}_2}{\partial \hat{x}} - (\hat{\rho}_1 + \hat{\rho}_2)\dfrac{\partial \hat{\eta}_b}{\partial \hat{x}}\right], \\ \dfrac{\mathrm{D}\hat{v}_2}{\mathrm{D}\hat{t}} + \hat{f}\hat{u}_2 = -\dfrac{\hat{g}}{\hat{\rho}_2}\left[\dfrac{\partial \hat{\eta}_1}{\partial \hat{y}} + (\hat{\rho}_2 - \hat{\rho}_1)\dfrac{\partial \hat{\eta}_2}{\partial \hat{y}} - (\hat{\rho}_1 + \hat{\rho}_2)\dfrac{\partial \hat{\eta}_b}{\partial \hat{y}}\right], \end{cases} \tag{2.18b}$$

along with the layer Continuity equations:

$$(j=1)\quad \left\{\frac{\mathrm{D}}{\mathrm{D}\hat{t}}(\hat{h}_1 - \hat{h}_2) + (\hat{h}_1 - \hat{h}_2)\left[\frac{\partial \hat{u}_1}{\partial \hat{x}} + \frac{\partial \hat{v}_1}{\partial \hat{y}}\right] = 0, \right. \tag{2.19a}$$

$$(j=2)\quad \left\{\frac{\mathrm{D}\hat{h}_2}{\mathrm{D}\hat{t}} + \hat{h}_2\left[\frac{\partial \hat{u}_2}{\partial \hat{x}} + \frac{\partial \hat{v}_2}{\partial \hat{y}}\right] = 0, \right. \tag{2.19b}$$

which are motivated by the one-layer Continuity equation, (2.9). As we saw previously, we can take the curl of the momentum equations and make use of the Continuity relations to derive the corresponding layer PV conservation laws. These derivations are similar to the one-layer case, and yield:

$$(j=1)\quad \left\{\frac{\mathrm{D}\hat{q}_1}{\mathrm{D}\hat{t}} = 0, \;\; \hat{q}_1 = \frac{\hat{\zeta}_1 + \hat{f}}{\hat{h}_1 - \hat{h}_2}, \right. \tag{2.20a}$$

$$(j=2)\quad \left\{\frac{\mathrm{D}\hat{q}_2}{\mathrm{D}\hat{t}} = 0, \;\; \hat{q}_2 = \frac{\hat{\zeta}_2 + \hat{f}}{\hat{h}_2}, \right. \tag{2.20b}$$

with relative vorticity in each layer defined by:

$$\hat{\zeta}_j = \frac{\partial \hat{u}_j}{\partial \hat{y}} - \frac{\partial \hat{v}_j}{\partial \hat{x}}.$$

As we did with the PV conservation for the one-layer model, we proceed by linearising (2.20) to formulate the corresponding QG governance. We shall make use of the previously established QG assumptions for the one-layer case, with the alteration that now $(\hat{\eta}_1 - \hat{\eta}_2) \ll \hat{H}_1$ and $(\hat{\eta}_2 + \hat{\eta}_b) \ll \hat{H}_2$. linearisation leads to $\hat{q}_1$ becoming:

$$\begin{aligned} \hat{q}_1 &= \frac{\hat{\zeta}_1 + \hat{f}_0 + \hat{\beta}\hat{y}}{(\hat{H}_1 + \hat{H}_2 + \hat{\eta}_1 - \hat{\eta}_b) - (\hat{H}_2 + \hat{\eta}_2 - \hat{\eta}_b)} \\ &= \frac{\hat{\zeta}_1 + \hat{f}_0 + \hat{\beta}\hat{y}}{\hat{H}_1 + \hat{\eta}_1 - \hat{\eta}_2} \\ &= \frac{\hat{f}_0}{\hat{H}_1}\left[\frac{1 + \hat{\zeta}_1/\hat{f}_0 + \hat{\beta}\hat{y}/\hat{f}_0}{1 + (\hat{\eta}_1 - \hat{\eta}_2)/\hat{H}_1}\right] \\ &= \frac{\hat{f}_0}{\hat{H}_1}\left(1 + \frac{\hat{\zeta}_1}{\hat{f}_0} + \frac{\hat{\beta}\hat{y}}{\hat{f}_0}\right)\left[1 + \frac{(\hat{\eta}_1 - \hat{\eta}_2)}{\hat{H}_1}\right]^{-1} \\ &= \frac{\hat{f}_0}{\hat{H}_1} + \frac{\hat{\beta}\hat{y}}{\hat{H}_1} + \frac{\hat{\zeta}_1}{\hat{H}_1} - \frac{\hat{f}_0(\hat{\eta}_1 - \hat{\eta}_2)}{\hat{H}_1^2} + \mathcal{O}(\varepsilon^2). \end{aligned}$$

A similar computation reveals that $\hat{q}_2$ can be expressed as:

$$\begin{aligned}\hat{q}_2 &= \frac{\hat{\zeta}_2 + \hat{f}_0 + \hat{\beta}\hat{y}}{\hat{H}_2 + \hat{\eta}_2 - \hat{\eta}_b} \\ &= \frac{\hat{f}_0}{\hat{H}_2} + \frac{\hat{\beta}\hat{y}}{\hat{H}_2} + \frac{\hat{\zeta}_2}{\hat{H}_2} - \frac{\hat{f}_0(\hat{\eta}_2 - \hat{\eta}_b)}{\hat{H}_2^2} + \mathcal{O}(\varepsilon^2),\end{aligned}$$

and so the linearised representation for (2.20) reads as:

$$(j=1)\quad \left\{\frac{\mathrm{D}}{\mathrm{D}\hat{t}}\left[\hat{\zeta}_1 + \hat{\beta}\hat{y} - \frac{\hat{f}_0(\hat{\eta}_1 - \hat{\eta}_2)}{\hat{H}_1}\right] = 0, \tag{2.21a}$$

$$(j=2)\quad \left\{\frac{\mathrm{D}}{\mathrm{D}\hat{t}}\left[\hat{\zeta}_2 + \hat{\beta}\hat{y} - \frac{\hat{f}_0(\hat{\eta}_2 - \hat{\eta}_b)}{\hat{H}_2}\right] = 0, \tag{2.21b}$$

in terms of relative vorticity. In order to express (2.21) in terms of streamfunctions, we note that:

$$\hat{\eta}_1 = \frac{\hat{f}_0}{\hat{g}}\hat{\psi}_1, \quad \hat{\eta}_2 = \frac{\hat{f}_0}{\hat{g}'}(\hat{\psi}_2 - \hat{\psi}_1),$$

where $\hat{g}' = (\hat{\rho}_2 - \hat{\rho}_1)\hat{g}/\hat{\rho}_2$ is the *reduced gravity* coefficient. Hence, substitution of these in (2.21) leads to the system:

$$(j=1)\quad \left\{\frac{\mathrm{D}}{\mathrm{D}\hat{t}}\left[\hat{\nabla}^2\hat{\psi}_1 + \hat{\beta}\hat{y} + \frac{\hat{f}_0^2(\hat{\psi}_2 - \hat{\psi}_1)}{\hat{g}'\hat{H}_1} - \frac{\hat{f}_0^2\hat{\psi}_1}{\hat{g}\hat{H}_1}\right] = 0, \tag{2.22a}$$

$$(j=2)\quad \left\{\frac{\mathrm{D}}{\mathrm{D}\hat{t}}\left[\hat{\nabla}^2\hat{\psi}_2 + \hat{\beta}\hat{y} + \frac{\hat{f}_0^2(\hat{\psi}_1 - \hat{\psi}_2)}{\hat{g}'\hat{H}_2} + \frac{\hat{f}_0\hat{\eta}_b}{\hat{H}_2}\right] = 0, \tag{2.22b}$$

with the material derivative operator in each layer now defined as:

$$\frac{\mathrm{D}}{\mathrm{D}\hat{t}} = \frac{\partial}{\partial\hat{t}} - \frac{\partial\hat{\psi}_j}{\partial\hat{y}}\frac{\partial}{\partial\hat{x}} + \frac{\partial\hat{\psi}_j}{\partial\hat{x}}\frac{\partial}{\partial\hat{y}}.$$

Finally, under the *Boussinesq approximation*, that is $\hat{\rho}_1 \approx \hat{\rho}_2$, we can safely neglect the last term in (2.22a), which leaves us with the QG two-layer model with bottom topography:[5]

$$\frac{\mathrm{D}\hat{Q}_1}{\mathrm{D}\hat{t}} = 0, \quad \hat{Q}_1 = \hat{\nabla}^2\hat{\psi}_1 + \frac{\hat{f}_0^2(\hat{\psi}_2 - \hat{\psi}_1)}{\hat{g}'\hat{H}_1} + \hat{\beta}\hat{y}, \tag{2.23a}$$

$$\frac{\mathrm{D}\hat{Q}_2}{\mathrm{D}\hat{t}} = 0, \quad \hat{Q}_2 = \hat{\nabla}^2\hat{\psi}_2 + \frac{\hat{f}_0^2(\hat{\psi}_1 - \hat{\psi}_2)}{\hat{g}'\hat{H}_1} + \hat{\beta}\hat{y} + \frac{\hat{f}_0\hat{\eta}_b}{\hat{H}_2}. \tag{2.23b}$$

Clearly, (2.23) is invariant under addition of constants, and so we in fact have a more powerful conservation law, namely *absolute potential vorticity conservation*, where we define absolute PV to be the quantity:

$$\hat{\Pi}_j = \hat{Q}_j + \hat{f}_0. \tag{2.24}$$

[5] In the absence of bottom topography, that is we are working with a flat bottomed ocean model, we simply set $\hat{\eta}_b = 0$ in (2.23b).

CHAPTER 3

ONE-LAYER LINEAR STABILITY ANALYSIS

3.1 FORMULATING THE ONE-LAYER PROBLEM

Before we dive into the main focus of this thesis, that being the analysis of the two-layer QG model with sinusoidal bottom irregularities, we shall consider the one-layer problem first to ease the reader into the mathematical analysis that is involved. Since the purpose of this section is to ease us into the problem this thesis deals with, we shall not solve this particular problem numerically. However, later on when dealing with the two-layer case, we shall discuss numerical results.

SINUSOIDAL BOTTOM TOPOGRAPHY

Recall that in chapter 2 we derived the one-layer QG model with bottom topography on the beta plane:

$$\frac{\mathrm{D}\hat{Q}}{\mathrm{D}\hat{t}} = 0, \;\; \hat{Q} = \hat{\nabla}^2\hat{\psi} - \hat{S}\hat{\psi} + \hat{\beta}\hat{y} + \frac{\hat{f}_0}{\hat{H}}\hat{\eta}_b, \tag{3.1}$$

where $(\hat{x}, \hat{y})$ denotes horizontal spatial Cartesian coordinates, $\hat{t}$ is the temporal coordinate, $\hat{f}_0$ is the Coriolis parameter, $\hat{\beta}$ is the corresponding meridional gradient, $\hat{\psi}(\hat{x}, \hat{y}, \hat{t})$ represents the flow streamfunction, $\hat{H}$ denotes the mean-layer depth, $\hat{\eta}_b(\hat{x}, \hat{y})$ defines the behaviour of the bottom topography, $\hat{S} = \hat{f}_0^2/\hat{g}\hat{H}$ is the stratification parameter (with acceleration due to gravity, $\hat{g}$), $\hat{Q}$ refers to the quasi-geostrophic layer PV, and we have made use of the material derivative and Laplacian operators:

$$\frac{\mathrm{D}}{\mathrm{D}\hat{t}} := \frac{\partial}{\partial\hat{t}} - \frac{\partial\hat{\psi}}{\partial\hat{y}}\frac{\partial}{\partial\hat{x}} + \frac{\partial\hat{\psi}}{\partial\hat{x}}\frac{\partial}{\partial\hat{y}} \;\text{ and }\; \hat{\nabla}^2 := \frac{\partial^2}{\partial\hat{x}^2} + \frac{\partial^2}{\partial\hat{y}^2},$$

respectively. There are a variety of means in which we can analyse this model, however, for our purposes, we shall attempt to analyse the *linear stability* of (3.1). In order to achieve this, we must first identify the nonlinearities present in the system that we wish to neglect. To do such, we have to linearise (3.1) about a state of rest, i.e. we write $\hat{\psi} = 0 + \delta\hat{\Psi}$, where $0 < \delta \ll 1$, making $\delta\hat{\Psi}$ a small perturbation (if we assumed some background velocity in the flow, then we would linearise about this moving state rather than linearising about a rest state). Hence, perturbing (3.1) about a state of rest, we find that:

$$\frac{\mathrm{D}}{\mathrm{D}\hat{t}}\left[\hat{\beta}\,\hat{y} + \frac{\hat{f}_0}{\hat{H}}\hat{\eta}_b + \delta\left(\hat{\nabla}^2\hat{\Psi} - \hat{S}\hat{\Psi}\right)\right] = 0. \tag{3.2}$$

We would now like to collect terms in order of magnitude, which when expanding (3.2), can be seen to be:

$$\underbrace{\delta\left[\frac{\partial}{\partial\hat{t}}\left(\hat{\nabla}^2\hat{\Psi} - \hat{S}\hat{\Psi}\right) + \frac{\hat{f}_0}{\hat{H}}\hat{J}\left(\hat{\Psi},\hat{\eta}_b\right) + \hat{\beta}\frac{\partial\hat{\Psi}}{\partial\hat{x}}\right]}_{\text{linear system}} + \delta^2\underbrace{\hat{J}\left(\hat{\Psi},\hat{\nabla}^2\hat{\Psi} - \hat{S}\hat{\Psi}\right)}_{\text{nonlinear contribution}} = 0,$$

where we have introduced the *Jacobian operator*:

$$\hat{J}(a,b) = \frac{\partial a}{\partial\hat{x}}\frac{\partial b}{\partial\hat{y}} - \frac{\partial a}{\partial\hat{y}}\frac{\partial b}{\partial\hat{x}},$$

for arbitrary functions a and b. Clearly, by how we have chosen to define δ, $\delta^2 \ll \delta$, and so we can assume the nonlinear terms to be negligible. Thus, keeping terms of order δ, we find the linearised system about a state of rest to be:

$$\frac{\partial}{\partial\hat{t}}\left(\hat{\nabla}^2\hat{\Psi} - \hat{S}\hat{\Psi}\right) + \left[\hat{\beta} + \frac{\hat{f}_0}{\hat{H}}\frac{\partial\hat{\eta}_b}{\partial\hat{y}}\right]\frac{\partial\hat{\Psi}}{\partial\hat{x}} - \frac{\hat{f}_0}{\hat{H}}\frac{\partial\hat{\eta}_b}{\partial\hat{x}}\frac{\partial\hat{\Psi}}{\partial\hat{y}} = 0, \tag{3.3}$$

where for clarity, we have expanded the Jacobian term. So far, we have assumed the bottom topography to be a general function of the spatial coordinates. Moving forward, we shall restrict our attention to the simple case of *sinusoidal* topography. In particular, we shall consider two types: namely sinusoidal *zonal* topography:

$$\hat{\eta}_b = \hat{\mathscr{A}}\sin(\hat{\alpha}\hat{y}), \tag{3.4}$$

and sinusoidal *meridional* topography:

$$\hat{\eta}_b = \hat{\mathscr{A}}\sin(\hat{\alpha}\hat{x}), \tag{3.5}$$

with parameters $\hat{\mathscr{A}}$ and $\hat{\alpha}$ refering to the amplitude and wavenumber of bottom topography respectively. With these considerations in mind, (3.3) reduces to the system of equations:

$$\frac{\partial}{\partial \hat{t}}\left(\hat{\nabla}^2\hat{\Psi}-\hat{S}\hat{\Psi}\right)+\left[\hat{\beta}+\frac{\hat{\mathscr{A}}\hat{\alpha}\hat{f}_0}{\hat{H}}\cos(\hat{\alpha}\hat{y})\right]\frac{\partial\hat{\Psi}}{\partial\hat{x}}=0, \quad \text{for } \hat{\eta}_b \text{ as in (3.4)}, \tag{3.6a}$$

$$\frac{\partial}{\partial \hat{t}}\left(\hat{\nabla}^2\hat{\Psi}-\hat{S}\hat{\Psi}\right)+\hat{\beta}\frac{\partial\hat{\Psi}}{\partial\hat{x}}-\frac{\hat{\mathscr{A}}\hat{\alpha}\hat{f}_0}{\hat{H}}\cos(\hat{\alpha}\hat{x})\frac{\partial\hat{\Psi}}{\partial\hat{y}}=0, \quad \text{for } \hat{\eta}_b \text{ as in (3.5)}. \tag{3.6b}$$

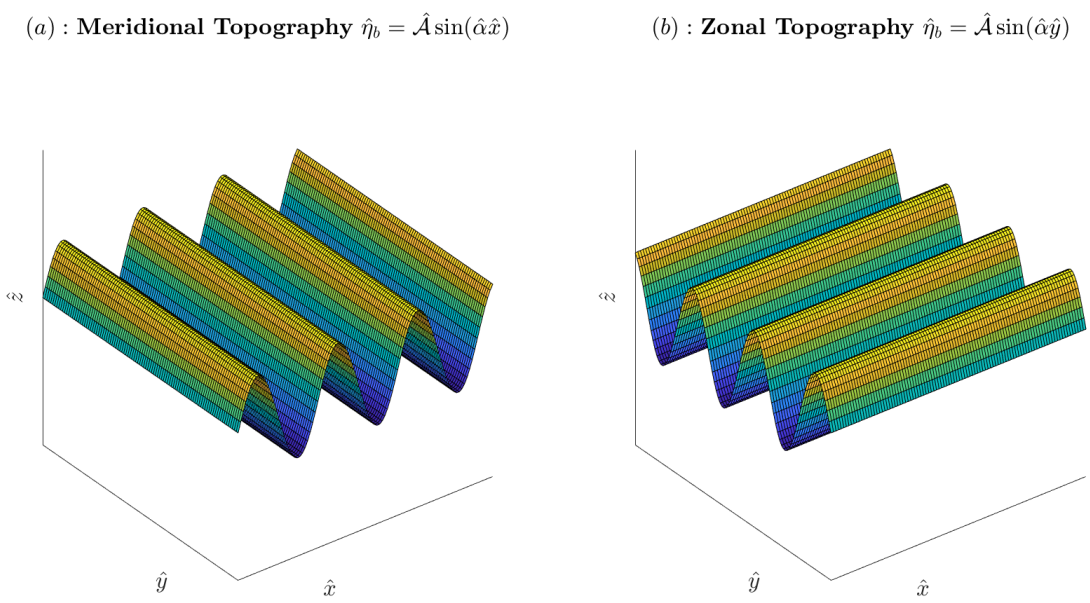

Figure 3.1: Plots to illustrate the various bottom irregularities under consideration in this study, that is (a): meridional (zonally varying) topography, and (b): zonal (meridonally varying) topography.

3.2 CONSTRUCTING THE EIGENVALUE PROBLEM

Now that we have our linearised system, we would ideally like to solve for the perturbation streamfunction, $\hat{\Psi}$. In hydrodynamic stability theory, it is standard to consider *Fourier/normal mode* solutions when working with linearised equations. Due to the presence of topography in our problem, (3.6) has variable coefficients in the spatial coordinates, which suggests we seek solutions of the form:

$$\hat{\Psi}(\hat{x},\hat{y},\hat{t}) = \begin{cases} \sum_{k,\ell}\hat{\phi}(\hat{k},\hat{y},\hat{\omega})e^{i(\hat{k}\hat{x}-\hat{\omega}\hat{t})}, & \text{in (3.6}a\text{)}, \\ \sum_{k,\ell}\hat{\phi}(\hat{x},\hat{\ell},\hat{\omega})e^{i(\hat{\ell}\hat{y}-\hat{\omega}\hat{t})}, & \text{in (3.6}b\text{)}, \end{cases}$$

where $\hat{\phi}$ is the amplitude of the perturbation streamfunction, $\hat{k}, \hat{\ell}$ are the horizontal wavenumbers and $\hat{\omega}$ is the wave frequency (it is understood that we are only concerned with the real contribution of these solutions). Despite these being reasonable solutions to consider, since we are working with sinusoidal topography, we can actually solve the problem exactly by seeking solutions of the form:

$$\hat{\Psi}(\hat{x},\hat{y},\hat{t}) = \sum_{k,\ell} \hat{\phi}(\hat{k},\hat{\ell},\hat{\omega}) e^{i((\hat{k}\hat{x}+\hat{\ell}\hat{y}-\hat{\omega}\hat{t})}. \tag{3.7}$$

In fact, since our equations are linear, we can consider the single mode solutions:

$$\hat{\Psi}(\hat{x},\hat{y},\hat{t}) = \hat{\phi}(\hat{k},\hat{\ell},\hat{\omega}) e^{i((\hat{k}\hat{x}+\hat{\ell}\hat{y}-\hat{\omega}\hat{t})},$$

and the complete solution will simply be a linear combination of these. We seek these solutions in particular since for arbitrary θ, the cosine function can be expressed in the exponential form:

$$\cos(\theta) = \frac{e^{i\theta} + e^{-i\theta}}{2},$$

which makes it possible to *Fourier transform* (3.6) w.r.t. $\hat{x}, \hat{y}$ and $\hat{t}$ to obtain an *eigenvalue problem* for the *spectrum* of $\hat{\Psi}$ (a review of the Fourier transform can be found in [5, pg. 133-149]. To illustrate the construction of the eigenvalue problem, consider (3.6a). It follows by Fourier transforming w.r.t. $\hat{x}, \hat{y}$ and $\hat{t}$ that:

$$\begin{aligned}
&\mathscr{F}\left\{\frac{\partial}{\partial \hat{t}}\left(\hat{\nabla}^2\hat{\Psi} - \hat{S}\hat{\Psi}\right) + \left[\hat{\beta} + \frac{\hat{\mathscr{A}}\hat{\alpha}\hat{f}_0}{\hat{H}}\cos(\hat{\alpha}\hat{y})\right]\frac{\partial \hat{\Psi}}{\partial \hat{x}}\right\} = 0 \\
\implies &\mathscr{F}\left[\hat{\nabla}^2\frac{\partial \hat{\Psi}}{\partial \hat{t}}\right] - \hat{S}\mathscr{F}\left[\frac{\partial \hat{\Psi}}{\partial \hat{t}}\right] + \hat{\beta}\mathscr{F}\left[\frac{\partial \hat{\Psi}}{\partial \hat{x}}\right] + \frac{\hat{\mathscr{A}}\hat{\alpha}\hat{f}_0}{2\hat{H}}\left\{\mathscr{F}\left[e^{i\hat{\alpha}\hat{y}}\frac{\partial \hat{\Psi}}{\partial \hat{x}}\right] + \mathscr{F}\left[e^{-i\hat{\alpha}\hat{y}}\frac{\partial \hat{\Psi}}{\partial \hat{x}}\right]\right\} = 0 \\
\implies &i\hat{\omega}(\hat{k}^2 + \hat{\ell}^2 + \hat{S})\hat{\phi}(\hat{k},\hat{\ell},\hat{\omega}) + i\hat{k}\left\{\hat{\beta}\hat{\phi}(\hat{k},\hat{\ell},\hat{\omega}) + \frac{\hat{\mathscr{A}}\hat{\alpha}\hat{f}_0}{2\hat{H}}\left[\hat{\phi}(\hat{k},\hat{\ell}+\hat{\alpha},\hat{\omega}) + \hat{\phi}(\hat{k},\hat{\ell}-\hat{\alpha},\hat{\omega})\right]\right\} = 0,
\end{aligned}$$

where we have made use of the fact that the Fourier transform is a linear operator. Thus, after some rearrangement and dividing through by a common factor of i, the eigenvalue problem in (k,ℓ)-space is found to be:

$$-\hat{k}\left\{\frac{\hat{\mathscr{A}}\hat{\alpha}\hat{f}_0}{2\hat{H}}\left[\hat{\phi}(\hat{k},\hat{\ell}+\hat{\alpha},\hat{\omega}) + \hat{\phi}(\hat{k},\hat{\ell}-\hat{\alpha},\hat{\omega})\right] + \hat{\beta}\hat{\phi}(\hat{k},\hat{\ell},\hat{\omega})\right\} = \hat{\omega}(\hat{k}^2 + \hat{\ell}^2 + \hat{S})\hat{\phi}(\hat{k},\hat{\ell},\hat{\omega}), \tag{3.8}$$

for *eigenfunctions* $\hat{\phi}$ and *eigenfrequencies* $\hat{\omega}$. By a similar argument of Fourier transform, or simply substitution of (3.7), the eigenvalue problem for (3.6b) in $(\hat{k},\hat{\ell})$-space is given by:

$$\frac{\hat{\mathscr{A}}\hat{\alpha}\hat{f}_0\hat{\ell}}{2\hat{H}}\Big[\hat{\phi}(\hat{k}+\hat{\alpha},\hat{\ell},\hat{\omega})+\hat{\phi}(\hat{k}-\hat{\alpha},\hat{\ell},\hat{\omega})\Big]-\hat{k}\hat{\beta}\hat{\phi}(\hat{k},\hat{\ell},\hat{\omega})=\hat{\omega}(\hat{k}^2+\hat{\ell}^2+\hat{S})\hat{\phi}(\hat{k},\hat{\ell},\hat{\omega}). \tag{3.9}$$

Nondimensionalisation

Now that we have formulated the desired eigenvalue problems, we would like to rewrite them in terms of nondimensional parameters. To do this, we must *nondimensionalise* (3.8) and (3.9). This involves rewriting the terms in our problem as products of characteristic scales (consistent with the dimension of the terms) and parameters of order unity. The choice of scaling is very much arbitrary, however, for physical insight, it is convenient to choose characteristic scales which appear in the problem of interest. For our purposes, we shall introduce *length* and *time* scales, $\hat{L}_h=\hat{R}_d/2\pi$, $\hat{L}_v=2\hat{H}$ and $\hat{T}=1/\hat{f}_0$, respectively, i.e. we will change variables according to the transformation:

$$\begin{aligned}(\hat{x},\hat{y})&=\hat{L}_h(x,y),\quad \hat{t}=\hat{T}t,\quad \hat{S}=\frac{S}{\hat{L}_h^2},\quad \hat{\phi}=\frac{\hat{L}_h^2\phi}{\hat{T}},\\ (\hat{k},\hat{\ell})&=\frac{1}{\hat{L}_h}(k,\ell),\quad \hat{\omega}=\frac{\omega}{\hat{T}},\quad \hat{\mathscr{A}}=\hat{L}_v\mathscr{A},\quad \hat{\alpha}=\frac{\alpha}{\hat{L}_h},\end{aligned} \tag{3.10}$$

where $\hat{R}_d=\sqrt{\hat{g}\hat{H}}/\hat{f}_0$ is the *barotropic Rossby deformation radius* and $x,y,t,S,\phi,k,\ell,\omega,\mathscr{A}$ and α are all constants of order unity. The inclusion of 2π in the scaling for some of these parameters is simply a matter of preference, but is motivated by the fact that k,ℓ and α are all multiples of 2π. In addition to this, the factor of 2 when scaling the amplitude for bottom topography is intended to eliminate the factor of $1/2$ in both (3.8) and (3.9).

With the change of variables, (3.10), established, we can rewrite (3.8) and (3.9) such that they are dimensionless. Starting with (3.8):

$$\begin{aligned}&-\frac{k}{\hat{L}_h}\left\{\frac{\hat{L}_v\mathscr{A}}{2\hat{H}}\frac{\alpha}{\hat{L}_h}\hat{f}_0\Big[\phi(k,\ell+\alpha,\omega)+\phi(k,\ell-\alpha,\omega)\Big]+\hat{\beta}\phi\right\}\frac{\hat{L}_h^2}{\hat{T}}=\frac{\omega}{\hat{T}}\frac{1}{\hat{L}_h^2}(k^2+\ell^2+S)\frac{\hat{L}_h^2\phi}{\hat{T}}\\ \implies\ &-\hat{L}_h\hat{T}k\left\{\frac{\hat{L}_v\mathscr{A}}{2\hat{H}}\frac{\alpha}{\hat{L}_h}\hat{f}_0\Big[\phi(k,\ell+\alpha,\omega)+\phi(k,\ell-\alpha,\omega)\Big]+\hat{\beta}\phi\right\}=\omega(k^2+\ell^2+S)\phi\\ \implies\ &-k\left\{\frac{\hat{L}_v\mathscr{A}}{2\hat{H}}\hat{T}\hat{f}_0\alpha\Big[\phi(k,\ell+\alpha,\omega)+\phi(k,\ell-\alpha,\omega)\Big]+\hat{L}_h\hat{T}\hat{\beta}\phi\right\}=\omega(k^2+\ell^2+S)\phi,\end{aligned}$$

which after some simplification can be expressed in the form:

$$-k\left\{\mathscr{A}\alpha\Big[\phi(k,\ell+\alpha,\omega)+\phi(k,\ell-\alpha,\omega)\Big]+\beta\phi\right\}=\omega(k^2+\ell^2+S)\phi, \tag{3.11}$$

with $\beta=\hat{\beta}\hat{R}_d/2\pi\hat{f}_0$ denoting the nondimensional meridional gradient of the Coriolis parameter and $\hat{\phi}=\hat{\phi}(\hat{k},\hat{\ell},\hat{\omega})$. Following the same procedure, we find the nondimensional equivalent of (3.9) to be:

$$\mathscr{A}\ell\alpha\Big[\phi(k+\alpha,\ell,\omega)+\phi(k-\alpha,\ell,\omega)\Big]-\beta k\phi=\omega(k^2+\ell^2+S)\phi. \tag{3.12}$$

Nondimensional solutions to these eigenvalue problems in real space take the form (by assumption):

$$\begin{aligned}\Psi(x,y,t)&=\sum_{k,\ell}\phi(k,\ell,\omega)e^{i(kx+\ell y-\omega t)}\\&=\sum_{k,\ell}\phi(k,\ell,\omega)e^{i(kx+\ell y)}e^{-i\omega t}\\&=\sum_{k,\ell}\phi(k,\ell,\omega)e^{i(kx+\ell y)}e^{-i\omega_r t}e^{\omega_i t},\end{aligned}$$

where we have set $\omega=\omega_r+i\omega_i$. From this, we see that as $t\to\infty$, we either have:

- $\Psi\to 0$ provided $\omega_i<0$, i.e. the flow is *stable*,
- $\Psi\to\infty$ provided $\omega_i>0$, i.e. the flow is *unstable*.

These criteria for stability will prove useful later on in chapter 4 when we solve the two-layer problem numerically.

The Matrix Formulation

Now that we have derived the nondimensional eigenvalue problems in (k,ℓ)-space, we proceed by solving the eigenvalue problems for various values of k and ℓ. If we consider the values $k,\ell=-N/2,-N/2+1,\cdots,N/2-1$, for even N, then for fixed α, the number of equations we have to solve for each eigenvalue problem is N^2 equations. The greater the number of values we use, the more accurate our numerical solution will be. To better picture this, take (3.11) as an example. If we fix the value of k and set $\alpha=1$, then for various values of ℓ we obtain the following system of equations in matrix form:

$$\mathscr{M}\phi=\omega\mathscr{N}\phi,$$

with

$$\phi = \begin{bmatrix} \phi(k,-N/2,\omega) \\ \phi(k,-N/2+1,\omega) \\ \vdots \\ \phi(k,N/2-2,\omega) \\ \phi(k,N/2-1,\omega) \end{bmatrix}, \quad \mathscr{M} = -k \begin{bmatrix} \beta & \mathscr{A} & 0 & 0 & 0 \\ \mathscr{A} & \beta & \mathscr{A} & 0 & 0 \\ \ddots & \ddots & \ddots & \ddots & \ddots \\ 0 & 0 & \mathscr{A} & \beta & \mathscr{A} \\ 0 & 0 & 0 & \mathscr{A} & \beta \end{bmatrix},$$

and

$$\mathscr{N} = \begin{bmatrix} k^2+\frac{N^2}{4}+S & 0 & \ddots & 0 & 0 \\ 0 & k^2+\left(-\frac{N}{2}+1\right)^2+S & \ddots & 0 & 0 \\ \ddots & \ddots & \ddots & \ddots & \ddots \\ 0 & 0 & \ddots & k^2+\left(\frac{N}{2}-2\right)^2+S & 0 \\ 0 & 0 & \ddots & 0 & k^2+\left(\frac{N}{2}-1\right)^2+S \end{bmatrix}.$$

This corresponds to having to solve N equations when k is fixed. Hence, if we allow k to vary, the problem becomes one in which we have to solve N^2 equations. Note that this matrix form is specifically for when $\alpha = 1$. In general, the matrix $\mathscr{M}$ will vary with α as a consequence of the presence of $\ell \pm \alpha$ in the eigenvalue problem. For example, when $\alpha = 2$, the matrix $\mathscr{M}$ becomes

$$\mathscr{M} = -k \begin{bmatrix} \beta & 0 & 2\mathscr{A} & 0 & 0 & \ddots & 0 & 0 \\ 0 & \beta & 0 & 2\mathscr{A} & 0 & \ddots & 0 & 0 \\ 2\mathscr{A} & 0 & \beta & 0 & 2\mathscr{A} & \ddots & 0 & 0 \\ \ddots & \ddots & \ddots & \ddots & \ddots & \ddots & \ddots & \ddots \end{bmatrix}.$$

We can also formulate the corresponding matrix problem for (3.12). Again, to illustrate this, we shall take $\alpha = 1$. Then, for various k, we have

$$\phi = \begin{bmatrix} \phi(-N/2,\ell,\omega) \\ \phi(-N/2+1,\ell,\omega) \\ \vdots \\ \phi(N/2-2,\ell,\omega) \\ \phi(N/2-1,\ell,\omega) \end{bmatrix},$$

$$\mathscr{M} = \begin{bmatrix} \frac{\beta N}{2} & \mathscr{A}\alpha\ell & 0 & \ddots & 0 & 0 & 0 \\ \mathscr{A}\alpha\ell & -\beta\left(-\frac{N}{2}+1\right) & \mathscr{A}\alpha\ell & \ddots & 0 & 0 & 0 \\ \ddots & \ddots & \ddots & \ddots & \ddots & \ddots & \ddots \\ \ddots & \ddots & \ddots & \ddots & \ddots & \ddots & \ddots \\ \ddots & \ddots & \ddots & \ddots & \ddots & \ddots & \ddots \\ \ddots & \ddots & \ddots & \ddots & \mathscr{A}\alpha\ell & -\beta\left(\frac{N}{2}-2\right) & \mathscr{A}\alpha\ell \\ \ddots & \ddots & \ddots & \ddots & \ddots & \mathscr{A}\alpha\ell & -\beta\left(\frac{N}{2}-1\right) \end{bmatrix},$$

and

$$\mathscr{N} = \begin{bmatrix} \frac{N^2}{4}+\ell^2+S & 0 & \ddots & 0 & 0 \\ 0 & \left(-\frac{N}{2}+1\right)^2+\ell^2+S & \ddots & 0 & 0 \\ \ddots & \ddots & \ddots & \ddots & \ddots \\ 0 & 0 & \ddots & \left(\frac{N}{2}-2\right)^2+\ell^2+S & 0 \\ 0 & 0 & \ddots & 0 & \left(\frac{N}{2}-1\right)^2+\ell^2+S \end{bmatrix}.$$

To proceed, we can solve these numerically with the aid of MATLAB. Though we will not concern ourselves with this here as the purpose of this section was to demonstrate how to formulate the problem we want to solve. When we do this for the two-layer model in chapter 4, we shall complement the analysis with numerical results.

As an aside, we can also formulate the flat bottom correspondence. To do this, we must first rewrite the layer governance in the absence of variable bottom irregularities. This is easily done by neglecting terms due to topography, leaving us with the dimensionless system:

$$\Big[\omega(k^2+\ell^2+S)+k\beta\Big]\phi = 0.$$

From this, we can obtain the eigenfrequencies for the flat bottom case directly by dividing through by ϕ. The result of this is:

$$\omega = -\frac{k\beta}{k^2+\ell^2+S}.$$

CHAPTER 4

TWO-LAYER LINEAR STABILITY ANALYSIS

4.1 FORMULATING THE TWO-LAYER PROBLEM

We now turn our attention to the main focus of this thesis, which involves extending the linear stability theory used in chapter 3 to a QG model with two fluid layers and sinusoidal bottom irregularities. As seen in chapter 2, the inviscid form for a QG model on the beta plane with topography, $\hat{\eta}_b = \hat{\eta}_b(\hat{x}, \hat{y})$, is given by the coupled conservation laws:

$$\frac{\mathrm{D}_1 \hat{Q}_1}{\mathrm{D}\hat{t}} = 0, \;\; \hat{Q} = \hat{\nabla}^2 \hat{\psi}_1 + \hat{S}_1(\hat{\psi}_2 - \hat{\psi}_1) + \hat{\beta}\hat{y}, \tag{4.1a}$$

$$\frac{\mathrm{D}_2 \hat{Q}_2}{\mathrm{D}\hat{t}} = 0, \;\; \hat{Q}_2 = \hat{\nabla}^2 \hat{\psi}_2 + \hat{S}_2(\hat{\psi}_1 - \hat{\psi}_2) + \hat{\beta}\hat{y} + \frac{\hat{f}_0}{\hat{H}_2}\hat{\eta}_b, \tag{4.1b}$$

with spatial Cartesian coordinates $(\hat{x}, \hat{y})$, temporal coordinate $\hat{t}$, Coriolis parameter defined as $\hat{f} = \hat{f}_0 + \hat{\beta}\hat{y}$, j^{th}-layer streamfunctions denoted by $\hat{\psi}_j(\hat{x}, \hat{y}, \hat{t})$, layer depths $\hat{H}_j$, stratification parameters $\hat{S}_j = \hat{f}_0^2/\hat{g}'\hat{H}_j$ (with reduced gravity, $\hat{g}' = \hat{g}(\hat{\rho}_2 - \hat{\rho}_1)/\hat{\rho}$, and fluid layer densities, ρ_j), and potential vorticity in each layer represented by $\hat{Q}_j$. These equations can be rewritten by expanding the material derivative operator:

$$\frac{\mathrm{D}_j}{\mathrm{D}\hat{t}} = \frac{\partial}{\partial \hat{t}} - \frac{\partial \hat{\psi}_j}{\partial \hat{y}}\frac{\partial}{\partial \hat{x}} + \frac{\partial \hat{\psi}_j}{\partial \hat{x}}\frac{\partial}{\partial \hat{y}},$$

such that the linear and nonlinear contributions present in both layers can be easily separated.

LINEARISATION

We now would like to linearise our system of equations. To do this, we shall assume in the top layer ($j = 1$) we have a meridionaly sheared, but zonally uniform background flow, whilst in the bottom layer ($j = 2$), the flow is at rest. This amounts to linearising about the background

flow in the top layer and linearising about the state of rest in the bottom layer, that is we set $\hat{\psi}_1 = -\hat{U}\hat{y} + \delta\hat{\Psi}_1$ and $\hat{\psi}_2 = 0 + \delta\hat{\Psi}_2$, where $0 < \delta \ll 1$ and $\hat{\Psi}_j$ are perturbation streamfunctions for the j^{th}-layer. With this in mind, substitution yields the top layer governance:

$$\begin{aligned}
&\frac{\mathrm{D}_1}{\mathrm{D}\hat{t}}\left\{(\hat{S}_1\hat{U}+\hat{\beta})\hat{y} + \delta\left[\hat{\nabla}^2\Psi_1 + \hat{S}_1(\hat{\Psi}_2 - \hat{\Psi}_1)\right]\right\} = 0 \\
\implies &\frac{\mathrm{D}_1}{\mathrm{D}\hat{t}}\left[(\hat{S}_1\hat{U}+\hat{\beta})\hat{y}\right] + \delta\frac{\mathrm{D}_1}{\mathrm{D}\hat{t}}\left[\hat{\nabla}^2\Psi_1 + \hat{S}_1(\hat{\Psi}_2 - \hat{\Psi}_1)\right] = 0 \\
\implies &\delta\left\{(\hat{S}_1\hat{U}+\hat{\beta})\frac{\partial\hat{\Psi}_1}{\partial\hat{x}} + \left(\frac{\partial}{\partial\hat{t}} + \hat{U}\frac{\partial}{\partial\hat{x}}\right)\left[\hat{\nabla}^2\hat{\Psi}_1 + \hat{S}_1(\hat{\Psi}_2 - \hat{\Psi}_1)\right]\right\} \\
&+ \delta^2\hat{J}\left[\hat{\Psi}_1, \hat{\nabla}^2\hat{\Psi}_1 + \hat{S}_1(\hat{\Psi}_2 - \hat{\Psi}_1)\right] = 0.
\end{aligned}$$

As for the bottom layer governance, it follows that:

$$\begin{aligned}
&\frac{\mathrm{D}_2}{\mathrm{D}\hat{t}}\left\{(\hat{\beta}-\hat{S}_2\hat{U})\hat{y} + \frac{\hat{f}_0}{\hat{H}_2}\hat{\eta}_b + \delta\left[\hat{\nabla}^2\Psi_2 + \hat{S}_2(\hat{\Psi}_1 - \hat{\Psi}_2)\right]\right\} = 0 \\
\implies &\frac{\mathrm{D}_2}{\mathrm{D}\hat{t}}\left[(\hat{\beta}-\hat{S}_2\hat{U})\hat{y} + \frac{\hat{f}_0}{\hat{H}_2}\hat{\eta}_b\right] + \delta\frac{\mathrm{D}_2}{\mathrm{D}\hat{t}}\left[\hat{\nabla}^2\Psi_2 + \hat{S}_2(\hat{\Psi}_1 - \hat{\Psi}_2)\right] = 0 \\
\implies &\delta\left\{(\hat{\beta}-\hat{S}_2\hat{U})\frac{\partial\hat{\Psi}_2}{\partial\hat{x}} + \frac{\hat{f}_0}{\hat{H}_2}\hat{J}(\hat{\Psi}_2, \hat{\eta}_b) + \frac{\partial}{\partial\hat{t}}\left[\hat{\nabla}^2\Psi_2 + \hat{S}_2(\hat{\Psi}_1 - \hat{\Psi}_2)\right]\right\} \\
&+ \delta^2\hat{J}\left[\hat{\Psi}_2, \hat{\nabla}^2\Psi_2 + \hat{S}_2(\hat{\Psi}_1 - \hat{\Psi}_2)\right] = 0.
\end{aligned}$$

From this analysis, we can see that the nonlinear contributions are small relative to linear components since $\delta^2 \ll \delta$, and so we can neglect these nonlinear terms and arrive at the linearised system of equations:

$$\left(\frac{\partial}{\partial\hat{t}} + \hat{U}\frac{\partial}{\partial\hat{x}}\right)\left[\hat{\nabla}^2\hat{\Psi}_1 + \hat{S}_1(\hat{\Psi}_2 - \hat{\Psi}_1)\right] + (\hat{S}_1\hat{U}+\hat{\beta})\frac{\partial\hat{\Psi}_1}{\partial\hat{x}} = 0, \tag{4.2a}$$

$$\frac{\partial}{\partial\hat{t}}\left[\hat{\nabla}^2\Psi_2 + \hat{S}_2(\hat{\Psi}_1 - \hat{\Psi}_2)\right] + \left(\hat{\beta} - \hat{S}_2\hat{U} + \frac{\hat{f}_0}{\hat{H}_2}\frac{\partial\hat{\eta}_b}{\partial\hat{y}}\right)\frac{\partial\hat{\Psi}_2}{\partial\hat{x}} - \frac{\hat{f}_0}{\hat{H}_2}\frac{\partial\hat{\eta}_b}{\partial\hat{x}}\frac{\partial\hat{\Psi}_2}{\partial\hat{y}} = 0, \tag{4.2b}$$

where we have expanded out the Jacobian term in the bottom layer governance for the sake of clarity.

So far, we have only considered general bottom topography, but we are particularly interested in the case where the topography is sinusoidal. Since (4.2a) does not include terms due to topography, the only equation which will change w.r.t. changes in topography is (4.2b). Therefore, substituting the topographies defined in (3.4) and (3.5) into (4.2b), the two-layer model reduces to the system (4.2a), with either:

$$\frac{\partial}{\partial\hat{t}}\left[\hat{\nabla}^2\hat{\Psi}_2 + \hat{S}_2(\hat{\Psi}_1 - \hat{\Psi}_2)\right] + \left[\hat{\beta} - \hat{S}_2\hat{U} + \frac{\hat{\mathscr{A}}\hat{\alpha}\hat{f}_0}{\hat{H}_2}\cos(\hat{\alpha}\hat{y})\right]\frac{\partial\hat{\Psi}_2}{\partial\hat{x}} = 0, \text{ if } \hat{\eta}_b \text{ is (3.4)}, \tag{4.3a}$$

$$\frac{\partial}{\partial\hat{t}}\left[\hat{\nabla}^2\hat{\Psi}_2 + \hat{S}_2(\hat{\Psi}_1 - \hat{\Psi}_2)\right] + (\hat{\beta} - \hat{S}_2\hat{U})\frac{\partial\hat{\Psi}_2}{\partial\hat{x}} - \frac{\hat{\mathscr{A}}\hat{f}_0\hat{\alpha}}{\hat{H}_2}\cos(\hat{\alpha}\hat{x})\frac{\partial\hat{\Psi}_2}{\partial\hat{y}} = 0, \text{ if } \hat{\eta}_b \text{ is (3.5)}. \tag{4.3b}$$

As we did with the one-layer model in chapter 3, we shall Fourier transform (4.3) to obtain the corresponding eigenvalue problem in $(\hat{k},\hat{\ell})$-space. Starting with the top layer governance, (4.3a) becomes:

$$\mathscr{F}\left\{\left(\frac{\partial}{\partial \hat{t}}+\hat{U}\frac{\partial}{\partial \hat{x}}\right)\left[\hat{\nabla}^2\hat{\Psi}_1+\hat{S}_1(\hat{\Psi}_2-\hat{\Psi}_1)\right]+(\hat{S}_1\hat{U}+\hat{\beta})\frac{\partial \hat{\Psi}_1}{\partial \hat{x}}\right\}=0$$
$$\implies (\hat{\omega}-\hat{k}\hat{U})\left[(\hat{k}^2+\hat{\ell}^2+\hat{S}_1)\hat{\phi}_1(\hat{k},\hat{\ell},\hat{\omega})-\hat{S}_1\hat{\phi}_2(\hat{k},\hat{\ell},\hat{\omega})\right]+\hat{k}(\hat{S}_1\hat{U}+\hat{\beta})\hat{\phi}_1(\hat{k},\hat{\ell},\hat{\omega})=0,$$

where we have made use of linearity of the Fourier transform and have divided through by common factors of i. Rewriting in the form of an eigenvalue problem, we find that for the top layer, we have:

$$\hat{k}\left\{\left[\hat{\beta}-(\hat{k}^2+\hat{\ell}^2)\hat{U}\right]\hat{\phi}_1+\hat{S}_1\hat{U}\hat{\phi}_2\right\}=\hat{\omega}\left[\hat{S}_1\hat{\phi}_2-(\hat{k}^2+\hat{\ell}^2+\hat{S}_1)\hat{\phi}_1\right], \tag{4.4}$$

where $\hat{\phi}_j=\hat{\phi}_j(\hat{k},\hat{\ell},\hat{\omega})$. As for the bottom layer, similar to the one-layer case, we rewrite the cosine functions in (4.3) in terms of exponentials and Fourier transform to obtain the eigenvalue problems:

$$\begin{aligned}\hat{k}\left\{(\hat{\beta}-\hat{S}_2\hat{U})\hat{\phi}_2+\frac{\hat{\mathscr{A}}\hat{\alpha}\hat{f}_0}{2\hat{H}_2}\left[\hat{\phi}_2(\hat{k},\hat{\ell}+\hat{\alpha},\hat{\omega})+\hat{\phi}_2(\hat{k},\hat{\ell}-\hat{\alpha},\hat{\omega})\right]\right\}\\ =\hat{\omega}\left[\hat{S}_2\hat{\phi}_1-(\hat{k}^2+\hat{\ell}^2+\hat{S}_2)\hat{\phi}_2\right],\end{aligned} \tag{4.5}$$

which corresponds to (4.3a), and:

$$\begin{aligned}\hat{k}(\hat{\beta}-\hat{S}_2\hat{U})\hat{\phi}_2-\frac{\hat{\mathscr{A}}\hat{\alpha}\hat{f}_0\hat{\ell}}{2\hat{H}_2}\left[\hat{\phi}_2(\hat{k}+\hat{\alpha},\hat{\ell},\hat{\omega})+\hat{\phi}_2(\hat{k}-\hat{\alpha},\hat{\ell},\hat{\omega})\right]\\ =\hat{\omega}\left[\hat{S}_2\hat{\phi}_1-(\hat{k}^2+\hat{\ell}^2+\hat{S}_2)\hat{\phi}_2\right],\end{aligned} \tag{4.6}$$

which corresponds to (4.3b).

NONDIMENSIONALISATION

Reminiscent of our analysis in chapter 3, we shall introduce a change of variables which gives us a dimensionless form for the eigenvalue problems we previously derived. For simplicity, we

shall assume the layer depths to be the same, i.e. $\hat{H}_1 = \hat{H}_2 = \hat{H}$ (so that the total depth of the model is $2\hat{H}$). With this in mind, the stratification parameters can be assumed equal, i.e. $\hat{S}_1 = \hat{S}_2 = \hat{S}$. Thus, if we introduce the horizontal length scale $\hat{L}_h = \hat{R}_d/2\pi$, vertical length scale $\hat{L}_v = 2\hat{H}$, time scale $\hat{T} = 1/\hat{f}_0$ and velocity scale $\hat{V} = \hat{f}_0\hat{R}_d/2\pi$, we obtain the nondimensional transform:

$$\begin{aligned}(\hat{x},\hat{y}) &= \hat{L}_h(x,y),\ \ \hat{t} = \hat{T}t,\ \ \hat{U} = \hat{V}U,\ \ \hat{\phi} = \hat{L}_h\hat{V}\phi_j,\\ (\hat{k},\hat{\ell}) &= \frac{1}{\hat{L}_h}(k,\ell),\ \ \hat{\omega} = \frac{\omega}{\hat{T}},\ \ \hat{\mathscr{A}} = \hat{L}_v\mathscr{A},\ \ \hat{\alpha} = \frac{\alpha}{\hat{L}_h},\ \ \hat{S}_j = \frac{S_j}{\hat{L}_h^2},\end{aligned} \tag{4.7}$$

where we have included factors of 2 and 2π in our dimensional scales to eliminate terms in our model without physical significance.

Applying (4.7) to (4.4), we see that:

$$\begin{aligned}&\frac{k}{\hat{L}_h}\left\{\left[\hat{\beta} - \frac{\hat{V}(k^2+\ell^2)U}{\hat{L}_h^2}\right]\phi_1 + \frac{\hat{V}SU\phi_2}{\hat{L}_h^2}\right\}\hat{L}_h\hat{V} = \frac{\omega}{\hat{L}_h^2\hat{T}}\left[S\phi_2 - (k^2+\ell^2+S)\phi_1\right]\hat{L}_h\hat{V}\\ \implies &\hat{L}_h\hat{T}k\left\{\left[\hat{\beta} - \frac{\hat{V}(k^2+\ell^2)U}{\hat{L}_h^2}\right]\phi_1 + \frac{\hat{V}SU\phi_2}{\hat{L}_h^2}\right\} = \omega\left[S\phi_2 - (k^2+\ell^2+S)\phi_1\right]\\ \implies &k\left\{\left[\hat{L}_h\hat{T}\hat{\beta} - \frac{\hat{T}\hat{V}(k^2+\ell^2)U}{\hat{L}_h}\right]\phi_1 + \frac{\hat{T}\hat{V}SU\phi_2}{\hat{L}_h}\right\} = \omega\left[S\phi_2 - (k^2+\ell^2+S)\phi_1\right]\end{aligned}$$

which when expressed in simplest form, reads as the following:

$$k\left\{\left[\beta - (k^2+\ell^2)U\right]\phi_1 + SU\phi_2\right\} = \omega\left[S\phi_2 - (k^2+\ell^2+S)\phi_1\right], \tag{4.8}$$

where $\beta = \hat{\beta}\hat{R}_d/2\pi\hat{f}_0$. For the layer with topography, the calculation is not very different. To illustrate this, we see that for (4.5) we find the eigenvalue problem to be:

$$\begin{aligned}&\frac{\hat{L}_h\hat{V}k}{\hat{L}_h}\left\{\left[\hat{\beta} - \frac{\hat{V}SU}{\hat{L}_h^2}\right]\phi_2 + \frac{\hat{L}_v\mathscr{A}}{2\hat{H}}\frac{\alpha}{\hat{L}_h}\hat{f}_0\left[\phi_2(k,\ell+\alpha,\omega) + \phi_2(k,\ell-\alpha,\omega)\right]\right\}\\ &= \frac{\hat{L}_h\hat{V}\omega}{\hat{L}_h^2\hat{T}}\left[S\phi_1 - (k^2+\ell^2+S)\phi_2\right]\\ \implies &\hat{L}_h\hat{T}k\left\{\left[\hat{\beta} - \frac{\hat{V}SU}{\hat{L}_h^2}\right]\phi_2 + \frac{\hat{L}_v\mathscr{A}}{2\hat{H}}\frac{\alpha}{\hat{L}_h}\hat{f}_0\left[\phi_2(k,\ell+\alpha,\omega) + \phi_2(k,\ell-\alpha,\omega)\right]\right\}\\ &= \omega\left[S\phi_1 - (k^2+\ell^2+S)\phi_2\right]\\ \implies &k\left\{\left[\beta - \frac{\hat{T}\hat{V}SU}{\hat{L}_h}\right]\phi_2 + \frac{\hat{L}_v\mathscr{A}}{2\hat{H}}\hat{T}\hat{f}_0\alpha\left[\phi_2(k,\ell+\alpha,\omega) + \phi_2(k,\ell-\alpha,\omega)\right]\right\}\\ &= \omega\left[S\phi_1 - (k^2+\ell^2+S)\phi_2\right],\end{aligned}$$

which when simplified becomes:

$$k\Big\{(\beta - SU)\phi_2 + \mathscr{A}\alpha\Big[\phi_2(k,\ell+\alpha,\omega) + \phi_2(k,\ell-\alpha,\omega)\Big]\Big\} = \omega\Big[S\phi_1 - (k^2+\ell^2+S)\phi_2\Big]. \tag{4.9}$$

Following the same procedure for (4.6), we obtain the eigenvalue problem:

$$k(\beta - SU)\phi_2 - \mathscr{A}\ell\alpha\Big[\phi_2(k+\alpha,\ell,\omega) + \phi_2(k-\alpha,\ell,\omega)\Big] = \omega\Big[S\phi_1 - (k^2+\ell^2+S)\phi_2\Big]. \tag{4.10}$$

Naturally, we can also formulate the bottom layer governance where topography exhibits both zonal and meridional variation. If we do this, we see that:

$$\begin{aligned} k(\beta - SU)\phi_2 + \mathscr{A}\alpha\Big\{k\Big[\phi_2(k,\ell+\alpha,\omega) + \phi_2(k,\ell-\alpha,\omega)\Big] \\ -\ell\Big[\phi_2(k+\alpha,\ell,\omega) + \phi_2(k-\alpha,\ell,\omega)\Big]\Big\} = \omega\Big[S\phi_1 - (k^2+\ell^2+S)\phi_2\Big]. \end{aligned} \tag{4.11}$$

Unfortunately, solving for this is a very computationally taxing task, and so we shall neglect this case moving forward and restrict our attention to (4.9) and (4.10).

Matrix Formulation

As seen in chapter 3, we would like to proceed by constructing the corresponding matrix formulation for our system of eigenvalue problems. Due to the addition of a second fluid layer, this turns out to be slightly different to the one-layer case. To illustrate this, consider the system of equations consisting of (4.8) and (4.9). Since we are working with two fluid layers as opposed to one, our matrices will have the composition $2N \times 2N$, rather than $N \times N$ as in chapter 3, since our eigenvector now consists on $2N$ eigenfunctions. As we did in the one-layer instance, if we attempt to rewrite our system in the matrix form:

$$\mathscr{M}\phi = \omega\mathscr{N}\phi,$$

with eigenvector:

$$\phi = \begin{bmatrix} \phi_1(k,-N/2,\omega) \\ \phi_1(k,-N/2+1,\omega) \\ \vdots \\ \phi_1(k,N/2-1,\omega) \\ \phi_2(k,-N/2,\omega) \\ \vdots \\ \phi_2(k,N/2-1,\omega) \end{bmatrix},$$

then if we limit our attention to bottom topography with a single ridge, that is when $\alpha = 1$, for simplicity, then the matrix $\mathscr{M}$ can be expressed in terms of block matrices as:

$$\mathscr{M} = k \begin{bmatrix} \mathscr{M}_1 \\ \mathscr{M}_2 \end{bmatrix},$$

where $\mathscr{M}_1$ is the $N \times 2N$ matrix:

$$\begin{bmatrix} \beta - \left(k^2 + \frac{N^2}{4}\right)U & 0 & \ddots & 0 & SU & 0 & \ddots & 0 \\ 0 & \beta - \left\{k + \left(-\frac{N}{2}+1\right)^2\right\}U & \ddots & 0 & 0 & SU & \ddots & 0 \\ \ddots & \ddots & \ddots & \ddots & \ddots & \ddots & \ddots & \ddots \\ 0 & 0 & \ddots & \beta - \left\{k + \left(\frac{N}{2}-1\right)^2\right\}U & 0 & 0 & \ddots & SU \end{bmatrix},$$

and $\mathscr{M}_2$ is the $N \times 2N$ matrix:

$$\begin{bmatrix} 0 & 0 & \ddots & 0 & \beta - SU & \mathscr{A} & 0 & \ddots & 0 \\ 0 & 0 & \ddots & 0 & \mathscr{A} & \beta - SU & \mathscr{A} & \ddots & 0 \\ \ddots & \ddots & \ddots & \ddots & \ddots & \ddots & \ddots & \ddots & \ddots \end{bmatrix}.$$

In addition to this, we have the matrix $\mathscr{N}$ defined by:

$$\mathscr{N} = \begin{bmatrix} \mathscr{N}_1 \\ \mathscr{N}_2 \end{bmatrix},$$

with $\mathscr{N}_1$ being the $N \times 2N$ matrix:

$$\begin{bmatrix} -\left(k^2 + \frac{N^2}{4} + S\right) & 0 & \ddots & 0 & S & 0 & \ddots & 0 \\ 0 & -\left\{k^2 + \left(-\frac{N}{2}+1\right)^2 + S\right\} & \ddots & 0 & 0 & S & \ddots & 0 \\ \ddots & \ddots & \ddots & \ddots & \ddots & \ddots & \ddots & \ddots \\ 0 & 0 & \ddots & -\left\{k^2 + \left(\frac{N}{2}-1\right)^2 + S\right\} & 0 & 0 & \ddots & S \end{bmatrix},$$

and with $\mathscr{N}_2$ being the $N \times 2N$ matrix:

$$\begin{bmatrix} S & 0 & \ddots & 0 & -\left(k^2+\frac{N^2}{4}+S\right) & 0 & \ddots & 0 \\ 0 & S & \ddots & 0 & 0 & -\left\{k^2+\left(-\frac{N}{2}+1\right)^2+S\right\} & \ddots & 0 \\ \ddots & \ddots & \ddots & \ddots & \ddots & \ddots & \ddots & \ddots \\ 0 & 0 & \ddots & S & 0 & 0 & \ddots & -\left\{k^2+\left(\frac{N}{2}-1\right)^2+S\right\} \end{bmatrix}.$$

This is the specific matrix construction for the case when $\alpha = 1$. However, as we showed for the one layer case, different values of α would only involve permuting coefficients in the matrix $\mathscr{M}$ and multiplying the value of $\mathscr{A}$ by α (the matrix $\mathscr{N}$ is the same for all values of α since the right-hand sides of (4.8) and (4.9) are independent of α).

If we now look at the system consisting of (4.8) and (4.10), we can construct a similar matrix form. The matrices $\mathscr{M}_1, \mathscr{N}_1$ and $\mathscr{N}_2$ will remain the same since $\mathscr{M}_1$ and $\mathscr{N}_1$ correspond to (4.8), and the right-hand side of (4.10) is identical to the right-hand side of (4.9). As for the remaining matrix, we find that for $\alpha = 1$, $\mathscr{M}_2$ is the $N \times 2N$ matrix:

$$\begin{bmatrix} 0 & 0 & \ddots & 0 & -\frac{N}{2}(\beta - SU) & -\mathscr{A}\ell & 0 & \ddots & 0 & 0 \\ 0 & 0 & \ddots & 0 & -\mathscr{A}\ell & \left(-\frac{N}{2}+1\right)(\beta - SU) & -\mathscr{A}\ell & \ddots & 0 & 0 \\ \ddots & \ddots & \ddots & \ddots & \ddots & \ddots & \ddots & \ddots & \ddots & \ddots \\ \ddots & \ddots & \ddots & \ddots & \ddots & \ddots & \ddots & \ddots & \ddots & \ddots \\ \ddots & \ddots & \ddots & \ddots & \ddots & \ddots & \ddots & \ddots & \ddots & \ddots \\ 0 & 0 & \ddots & 0 & 0 & 0 & 0 & \ddots & \mathscr{A}\ell & \left(\frac{N}{2}-1\right)(\beta - SU) \end{bmatrix}.$$

4.3 NUMERICAL RESULTS

We are now in a position where we can solve the linear stability problem numerically, though some care must be taken when doing this. Recall that the QG approximation holds provided the bottom topography under consideration is small-scale. In other words, our approximation is only valid given the amplitude of bottom irregularities is small in comparison to the bottom layer depth. If we assume the bottom layer depth to be 2000m, then physically, the greatest value of topographic amplitude sensible to consider is 1000m, since this is half the layer depth. Thus, we shall mainly restrict our attention to amplitudes of topography in the range 0—1000m. However, when looking for mathematical trends, we may consider amplitudes outside this range, despite the approximations not necessarily being valid.

Another point of note is numerical convergence. When solving problems numerically, we would like to know how good our approximation is relative to the exact solution. In most cases, we can improve our numerical solution by increasing the value of N (the number of grid points). In our case, to identify a sensible choice of N, we considered the numerical solutions for topography with 20 ridges. This is the greatest number of ridges we shall consider in this study, and so will produce the smallest scales, thus being the toughest case for numerical convergence. From this, we found that the difference between solutions with $N = 128$ and $N = 256$ has similarities, but with some distinct differences. However, when looking at $N = 256$ and $N = 512$, the solutions were very close to the same result. As a consequence of this, we shall use $N = 256$ in most cases, since the solutions obtained using $N = 512$ are much computationally time consuming in comparison to those obtained using $N = 256$. Hence, since there is not a massive disparity in the solutions obtained using either of these values of N, we shall favour the use of $N = 256$.

The Flat-Bottom Problem

Naturally, we would like to compare our findings when considering sinusoidal bottom irregularities with those found when considering a flat bottom. We have for the most part already formulated the problem in nondimensional form. The top layer goverance obviously remains the same as in (4.8), and the only difference for the bottom layer is we neglect terms due to topography in either (4.9) or (4.10) (this amounts to setting $\mathscr{A} = 0$). In other words, the system of equations governing the dynamics of fluid motion in a two-layer model, with a flat bottom, is given by:

$$\begin{aligned}
&\left\{\omega(k^2+\ell^2+S)+k\left[\beta-(k^2+\ell^2)U\right]\right\}\phi_1+S(kU-\omega)\phi_2=0,\\
&-\omega S\phi_1+\left\{\omega(k^2+\ell^2+S)+k(\beta-SU)\right\}\phi_2=0,
\end{aligned}$$

where we have expressed these differently to the layout of an eigenvalue problem since we are able to obtain the dispersion relation directly. Rewriting this system of equations in matrix form, we have that:

$$\begin{bmatrix}
\omega(k^2+\ell^2+S)+k\left\{\beta-(k^2+\ell^2)U\right\} & S(kU-\omega)\\
-\omega S & \omega(k^2+\ell^2+S)+k(\beta-SU)
\end{bmatrix}\begin{bmatrix}\phi_1\\ \phi_2\end{bmatrix}=\begin{bmatrix}0\\0\end{bmatrix}.$$

For this to have non-trivial solutions, we require that the determinant of the coefficient matrix is equal zero. This yields the dispersion relation:

$$\Big[\omega(K^2+S)+k(\beta-K^2U)\Big]\Big[\omega(K^2+S)+k(\beta-SU)\Big]+\omega(kU-\omega)S^2=0, \qquad (4.12)$$

where $K^2 = k^2 + \ell^2$. We can now solve the flat bottom case numerically.

Comparing Numerical Results

As we can see by comparing the distribution of unstable modes in the flat bottom case (illustrated in figure 4.1), with the distribution of unstable modes for zonal and meridional topography, with amplitude 400m (illustrated in 4.2 and 4.4 respectively), as we increase the number of ridges, α, the maximum growth rate in the presence of zonal topography appears to decrease, with the range of unstable modes shifting towards the short-wave end of the spectrum (shifting toward larger k). As for meridional topography, the maximum growth rate does not seem to change to that found in the flat bottom case, however, the spread of the distribution of unstable modes seemingly increases, but with a significant number of modes still collecting about the $\ell = 0$.

We can further compare with figures 4.3 and 4.5, those illustrating the distribution of unstable modes for zonal and meridional topography, respectively, with amplitude 800m. In the case of zonal topography, the maximum growth rate appears to have decreased slightly more with an increase in topographic amplitude, compared to that seen in figure 4.2 (to better visualise this observation, see figure 4.6). Regarding meridional topography, an increase in topographic amplitude still does not change the maximum growth rate, but the change in the distribution of unstable modes is more apparent for less ridges.

It is difficult to tell from our plots for the distribution of unstable modes, whether the number of modes increases, decreases, or simply remains the same, with changes in the number of topographic ridges. This information is presented in figure 4.7, and we find that in the case of meridional topography ($\eta_b = \mathscr{A}\sin(\alpha x)$), beyond a certain number of ridges, the number of modes appears to decrease with increasing α (for different topographic amplitudes). Concerning zonal topography ($\eta_b = \mathscr{A}\sin(\alpha y)$), this trend is not as clear, though the number of modes clearly fluctuates[1]. Figure 4.7 also presents the sum of all positive growth rates as a function of α. From this, we can see that in both cases of topography, there is a clear trend of the summation decreasing (or monotonically decreasing) as we increase the number of ridges.

[1]To get a better picture of how the number of unstable modes behaves as a function of α, we can consider a greater number of ridges.

Inspection of the dispersion relations illustrated in figures 4.8 and 4.9 for zonal topography again shows us that the growth rate of the unstable modes decreases with increasing α. Moreover, we see that when α transitions from $\alpha = 10$ to $\alpha = 15$, there appears to be separation of branches. This is supported in figures 4.10 and 4.11 ((α, k)-contour plots for the maximum growth rate in the presence of zonal topography, for $\mathscr{A} = 0.1$ and $\mathscr{A} = 0.1$ respectively), where we can see a separation of branches around $\alpha = 14$ in 4.10, and around $\alpha = 12$ in 4.11. This is representative of a bifurcation [26, pg. 45-80], where we have a single unstable region branching into two unstable regions separated by a stable region.

In figures 4.14, we illustrate how the maximum growth rate is affected by α and U in the presence of zonal bottom topography (for $\mathscr{A} = 0.1, 0.2$). The initial dark blue region corresponds to no unstable modes, and the regions following this have unstable modes of increasing growth rates. As we expect, increasing the background velocity in the upper layer increases the growth rate.

Contour plots of the perturbation streamfunctions corresponding to maximum growth rate in both the top and bottom layers, in the presence of zonal topography, can be found in figures 4.15, 4.16 and 4.17. The first two of these have $\mathscr{A} = 0.1$ with $\alpha = 1$ and $\alpha = 5$ respectively. The solutions are chains of eddies, oriented on the northern downward slopes (as opposed to the peaks or troughs of topography). As the number of topographic ridges increases, so does the number of eddy chains. Moreover, as we increase the number of ridges, the difference between the solutions in the top and bottom layers becomes more apparent, with the bottom layer streamfunctions having eddies 'smaller' than those seen in the top layer (the use of the term 'smaller' here corresponds to the eddies being weaker in the bottom layer due to the presence of topography). As we increase the topographic amplitude to $\hat{\mathscr{A}} = 800$m, we see in figure 4.17 that the chains consist of a greater number of eddies (in a smaller amount of space) than those in 4.16.

In figures 4.18, 4.19 and 4.20, we present the perturbation streamfunctions in each fluid layer, corresponding to maximum growth, but now for meridional topography. In this case, the solutions in both layers are meridional and equally spaced. Seemingly, increasing the number of ridges or the topographic amplitude does not appear to change the structure of the solutions in either of the layers. However, the solutions in the bottom layer are 'thinner' (weaker) than those in the top layer.

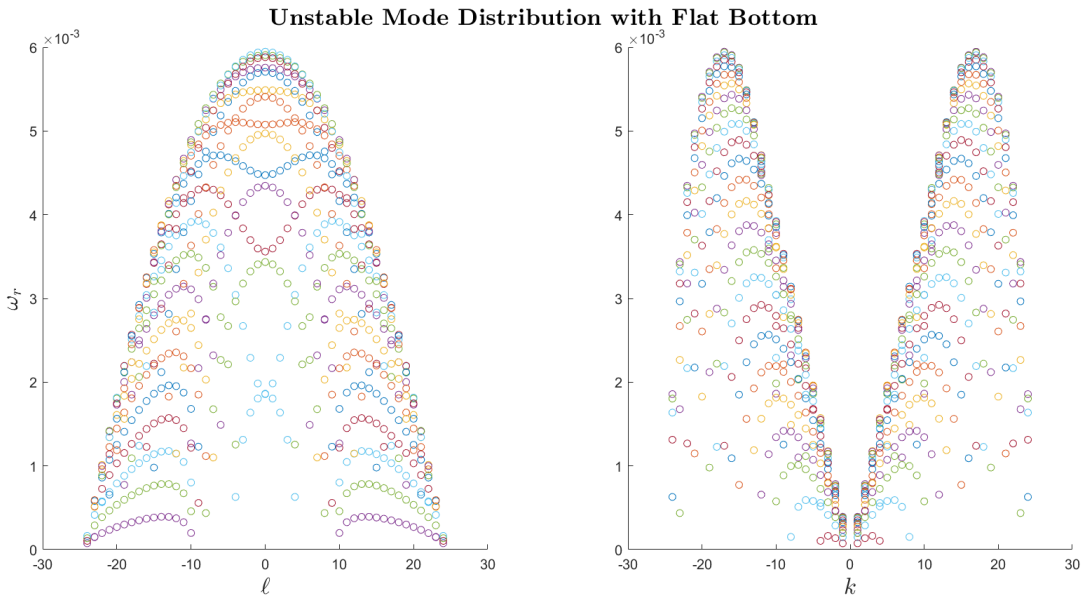

Figure 4.1: Nondimensional plots of growth rate, $\omega_i > 0$, against wavenumbers, ℓ and k, for $\hat{U} = 4\text{cm s}^{-1}$ (or $U = 0.013$), latitude $\theta_0 = 30°$ and $\hat{S} = 1.6 \times 10^{-9}\text{m}^{-2}$.

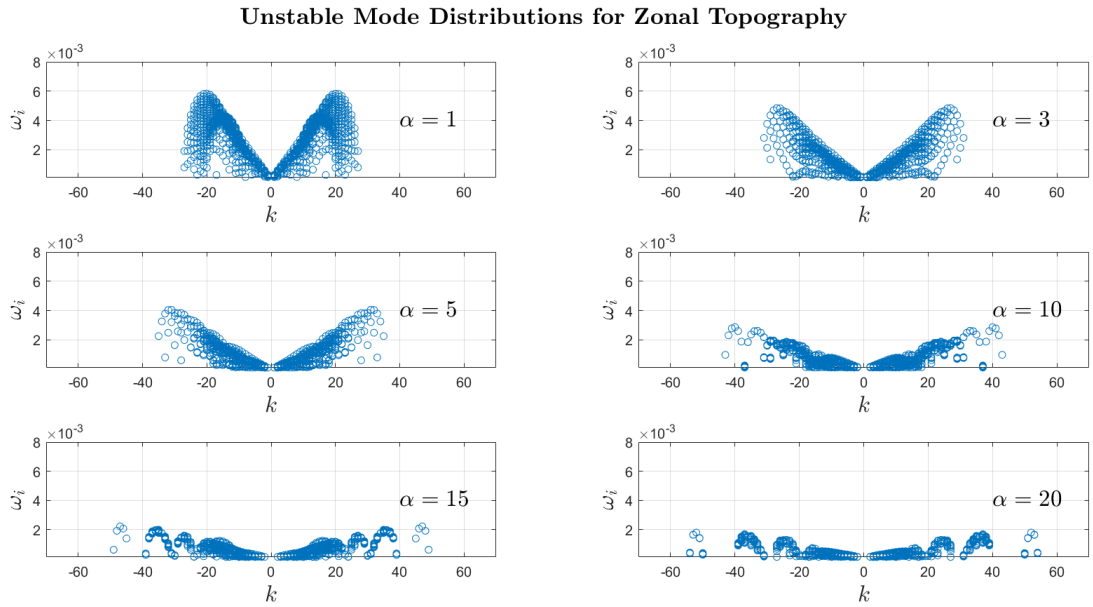

Figure 4.2: Nondimensional plots of growth rate, $\omega_i > 0$, against wavenumber, k, for zonal topography, with $N = 256$, $\hat{\mathscr{A}} = 400\text{m}$ (or $\mathscr{A} = 0.1$), $\alpha = (1, 3, 5, 10, 15, 20)$, $\hat{U} = 4\text{cm s}^{-1}$ (or $U = 0.013$), latitude $\theta_0 = 30°$ and $\hat{S} = 1.6 \times 10^{-9}\text{m}^{-2}$.

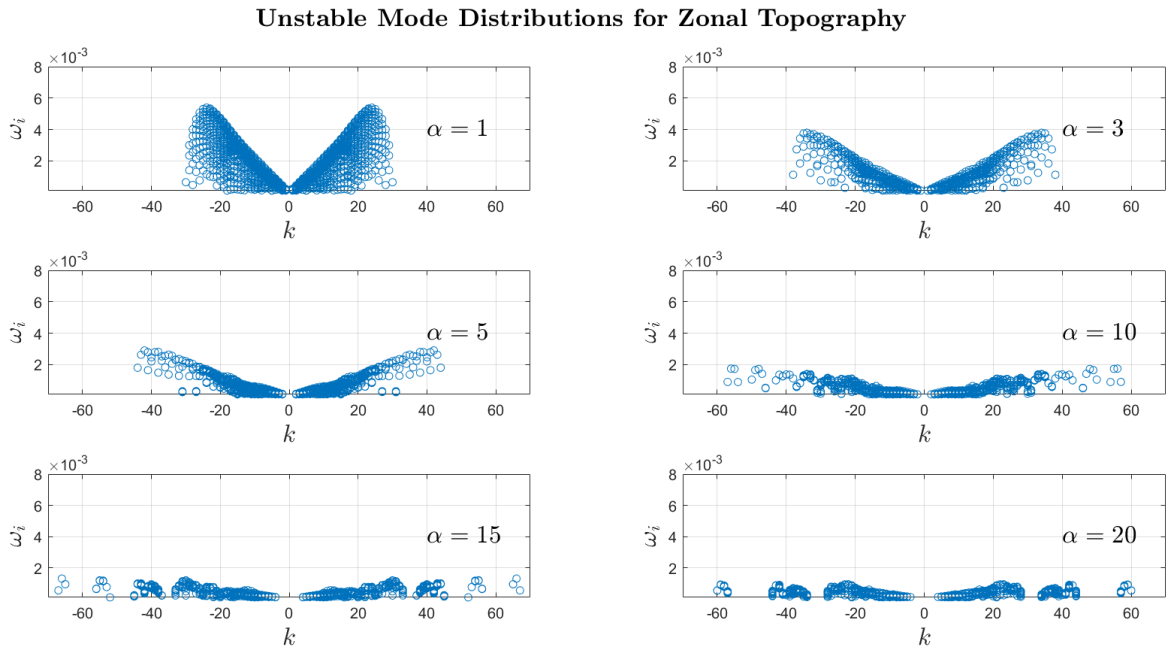

Figure 4.3: Nondimensional plots of growth rate, $\omega_i > 0$, against wavenumber, k, for zonal topography, with $N = 256$, $\hat{\mathscr{A}} = 800$m (or $\mathscr{A} = 0.2$), $\alpha = (1, 3, 5, 10, 15, 20)$, $\hat{U} = 4$cm s^{-1} (or $U = 0.013$), latitude $\theta_0 = 30°$ and $\hat{S} = 1.6 \times 10^{-9}$m^{-2}.

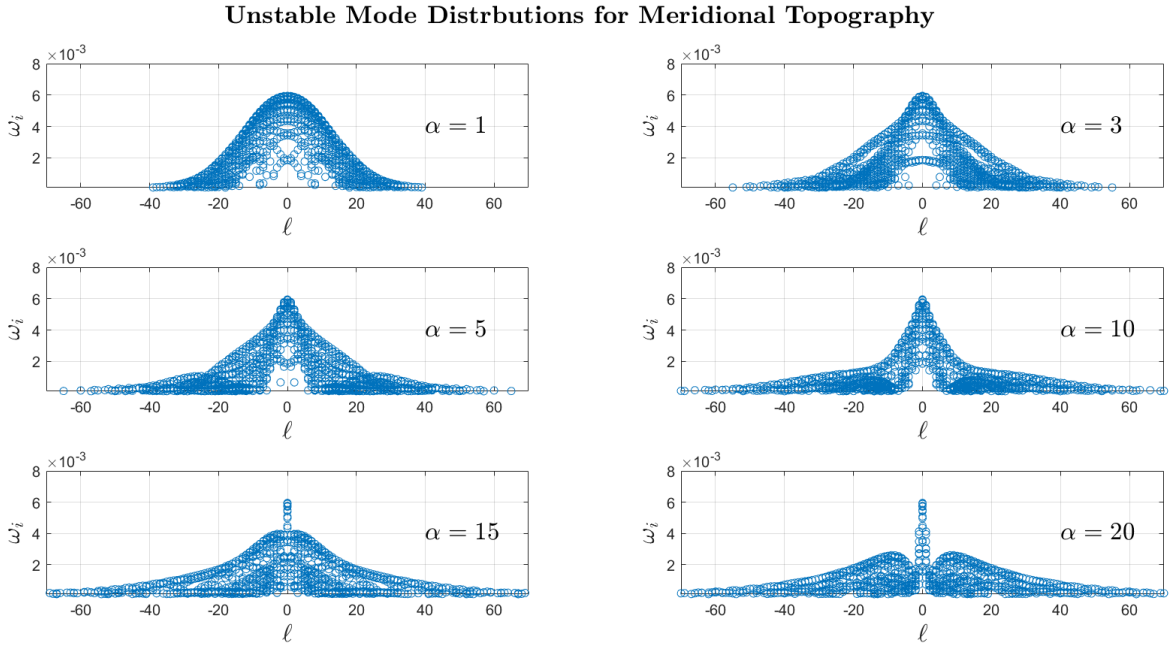

Figure 4.4: Nondimensional plots of growth rate, $\omega_i > 0$, against wavenumber, k, for meridional topography, with $N = 256$, $\hat{\mathscr{A}} = 400$m, $\alpha = (1, 3, 5, 10, 15, 20)$ $\hat{U} = 4$cm s^{-1} (or $U = 0.013$), latitude $\theta_0 = 30°$ and $\hat{S} = 1.6 \times 10^{-9}$m^{-2}.

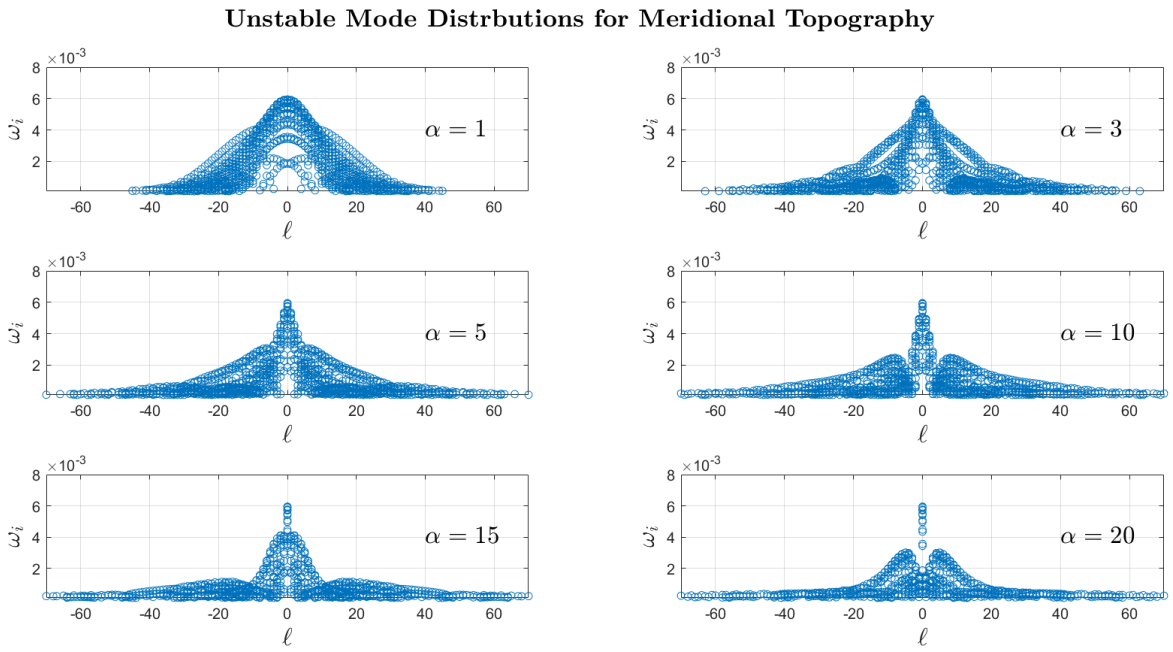

Figure 4.5: Nondimensional plots of growth rate, $\omega_i > 0$, against wavenumber, k, for meridional topography, with $N = 256$, $\hat{\mathscr{A}} = 800$m, $\alpha = (1, 3, 5, 10, 15, 20)$, $\hat{U} = 4\text{cm s}^{-1}$ (or $U = 0.013$), latitude $\theta_0 = 30°$ and $\hat{S} = 1.6 \times 10^{-9}\text{m}^{-2}$.

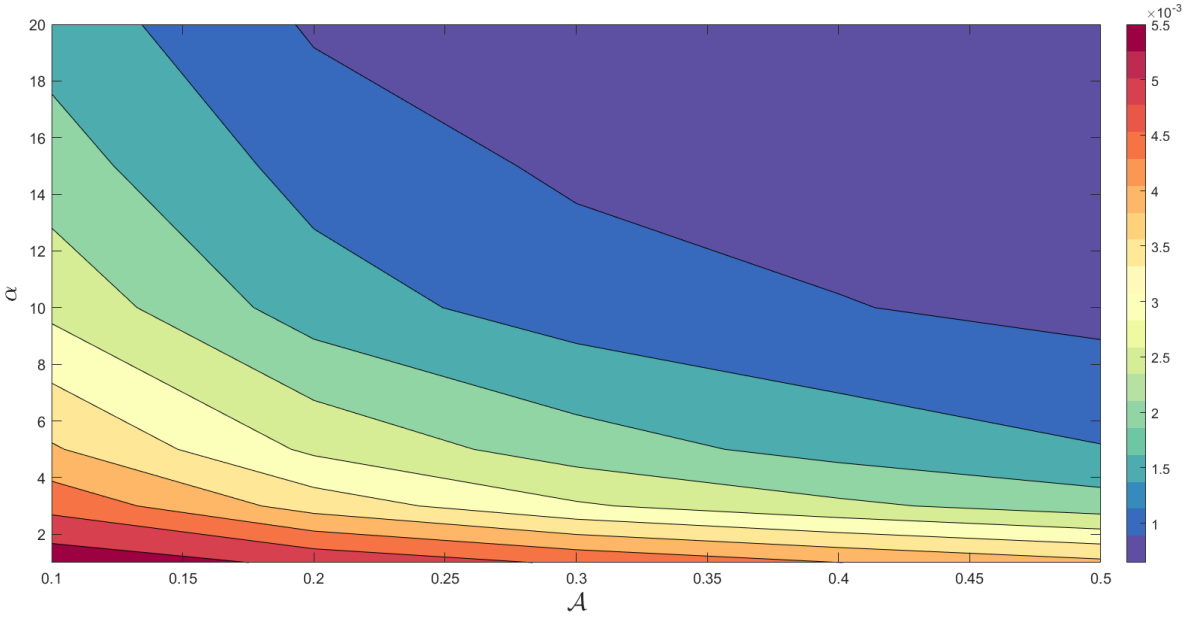

Figure 4.6: Nondimensional $(\alpha, \mathscr{A})$-contour plot for the maximum growth rate in the presence of zonal topography, with $N = 256$, $\hat{U} = 4\text{cm s}^{-1}$ (or $U = 0.013$), latitude $\theta_0 = 30°$ and $\hat{S} = 1.6 \times 10^{-9}\text{m}^{-2}$. Note that the QG approximation may not hold for $\mathscr{A} > 0.25$ (or $\hat{\mathscr{A}} > 1000$m), despite the trend of decreasing growth rate being consistent for increasing $\mathscr{A}$.

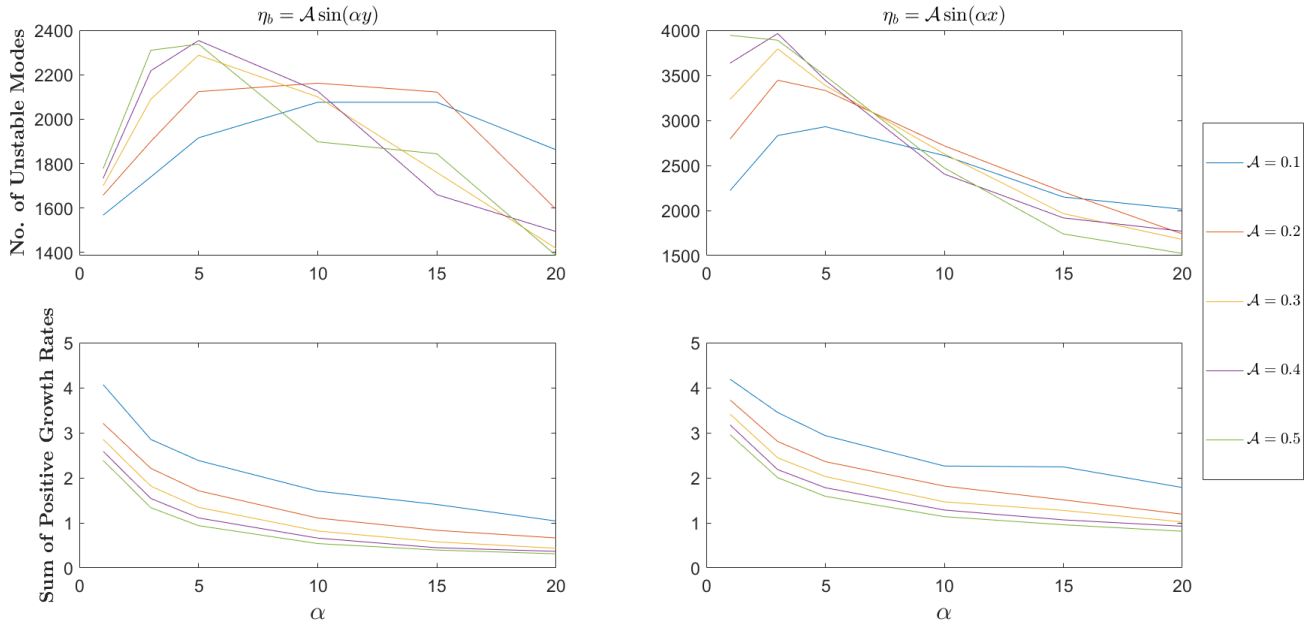

Figure 4.7: Plots for the number of unstable modes as a function of $alpha$, as well as plots for the sum of positive growth rates as a function of α. Note that the QG approximation may not hold for $\mathscr{A} > 0.25$ (or $\hat{\mathscr{A}} > 1000$m).

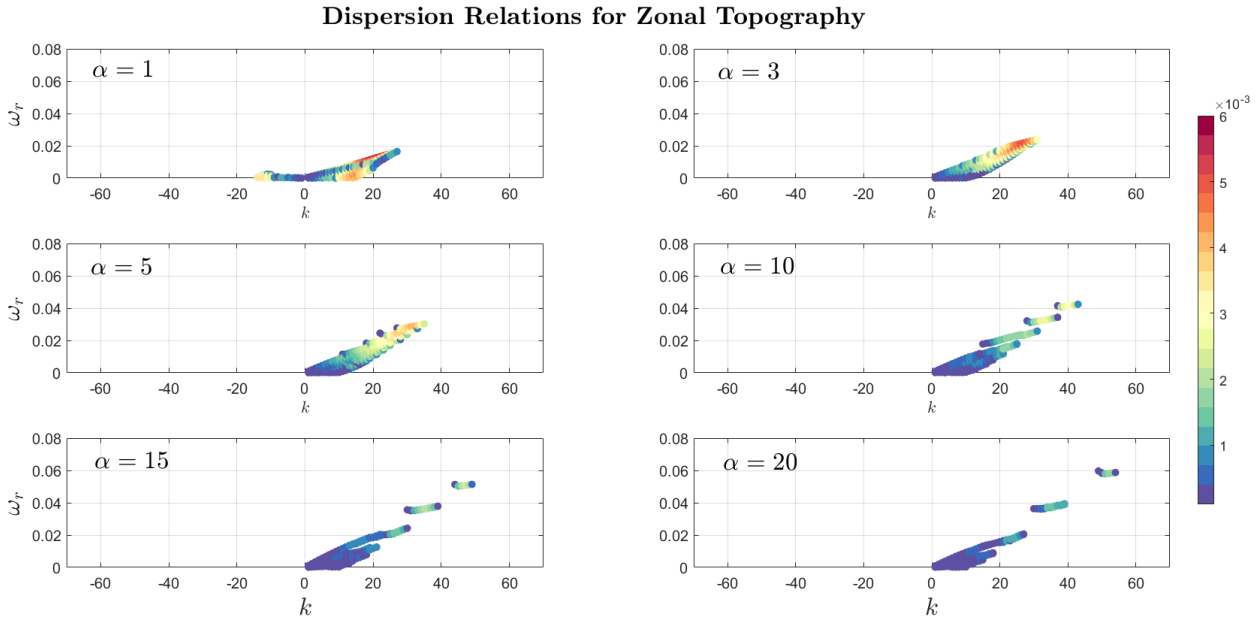

Figure 4.8: Nondimensional dispersion relations for zonal topography, with $N = 256$, $\hat{\mathscr{A}} = 400$m (or $\mathscr{A} = 0.1$), $\alpha = (1, 3, 5, 10, 15, 20)$, $\hat{U} = 4\text{cm s}^{-1}$ (or $U = 0.013$), latitude $\theta_0 = 30°$ and $\hat{S} = 1.6 \times 10^{-9}\text{m}^{-2}$.

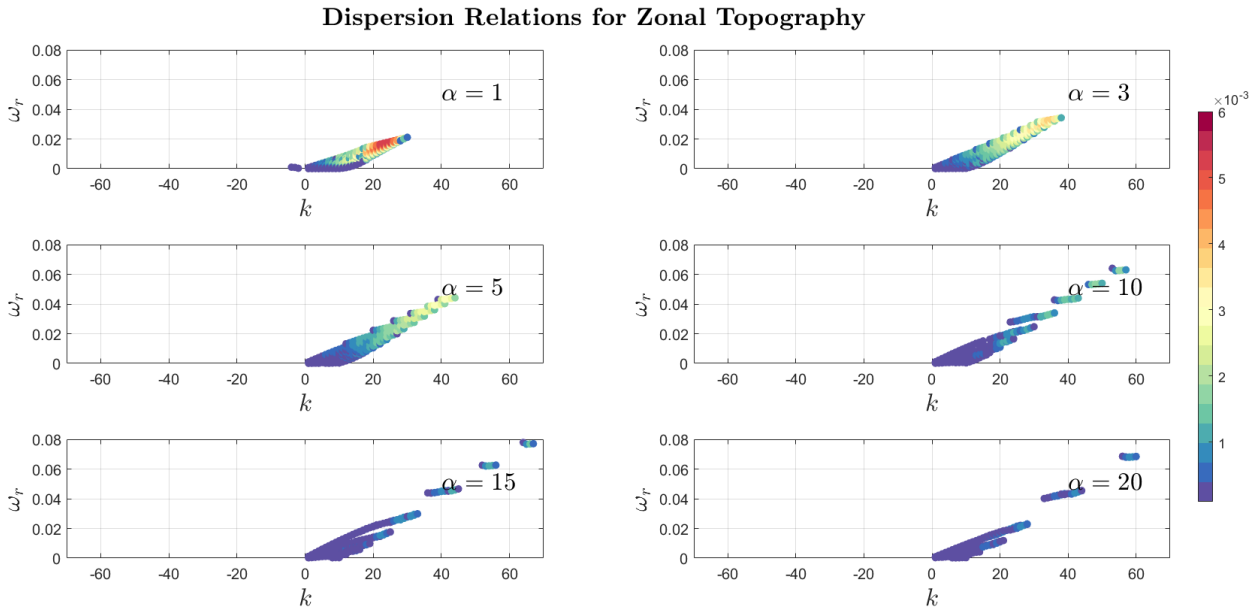

Figure 4.9: Nondimensional dispersion relations for zonal topography, with $N = 256$, $\hat{\mathscr{A}} = 800\text{m}$ (or $\mathscr{A} = 0.2$), $\alpha = (1, 3, 5, 10, 15, 20)$, $\hat{U} = 4\text{cm s}^{-1}$ (or $U = 0.013$), latitude $\theta_0 = 30°$ and $\hat{S} = 1.6 \times 10^{-9}\text{m}^{-2}$.

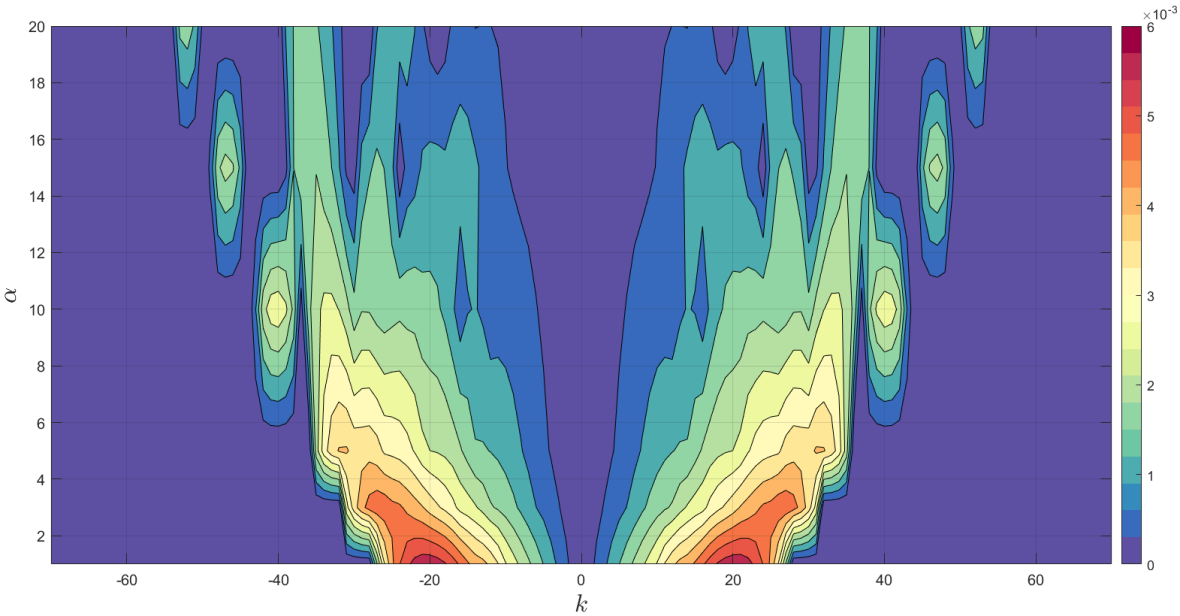

Figure 4.10: Nondimensional (α, k)-contour plot for the maximum growth rate in the presence of zonal topography, with $N = 256$, $\mathscr{A} = 0.1$ (or $\hat{\mathscr{A}} = 400\text{m}$), $\hat{U} = 4\text{cm s}^{-1}$ (or $U = 0.013$), latitude $\theta_0 = 30°$ and $\hat{S} = 1.6 \times 10^{-9}\text{m}^{-2}$.

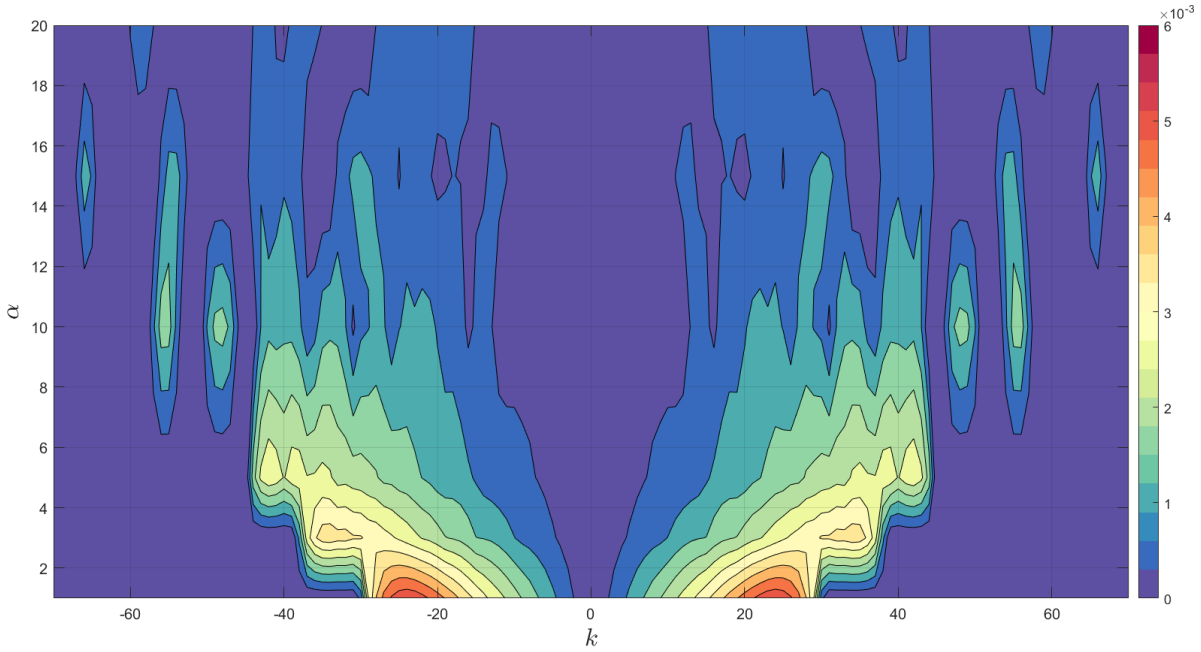

Figure 4.11: Nondimensional (α, k)-contour plot for the maximum growth rate in the presence of zonal topography, with $N = 256$, $\mathscr{A} = 0.2$ (or $\hat{\mathscr{A}} = 800\text{m}$), $\hat{U} = 4\text{cm s}^{-1}$ (or $U = 0.013$), latitude $\theta_0 = 30°$ and $\hat{S} = 1.6 \times 10^{-9}\text{m}^{-2}$.

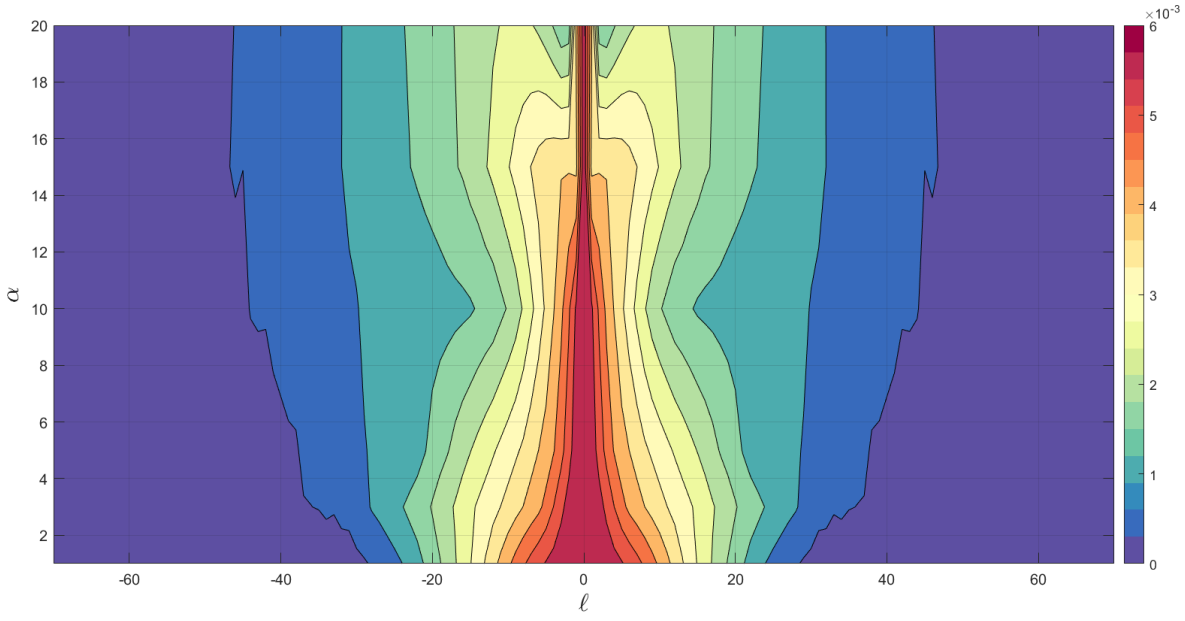

Figure 4.12: Nondimensional (α, ℓ)-contour plot for the maximum growth rate in the presence of meridional topography, with $N = 256$, $\mathscr{A} = 0.1$ (or $\hat{\mathscr{A}} = 400\text{m}$), $\hat{U} = 4\text{cm s}^{-1}$ (or $U = 0.013$), latitude $\theta_0 = 30°$ and $\hat{S} = 1.6 \times 10^{-9}\text{m}^{-2}$.

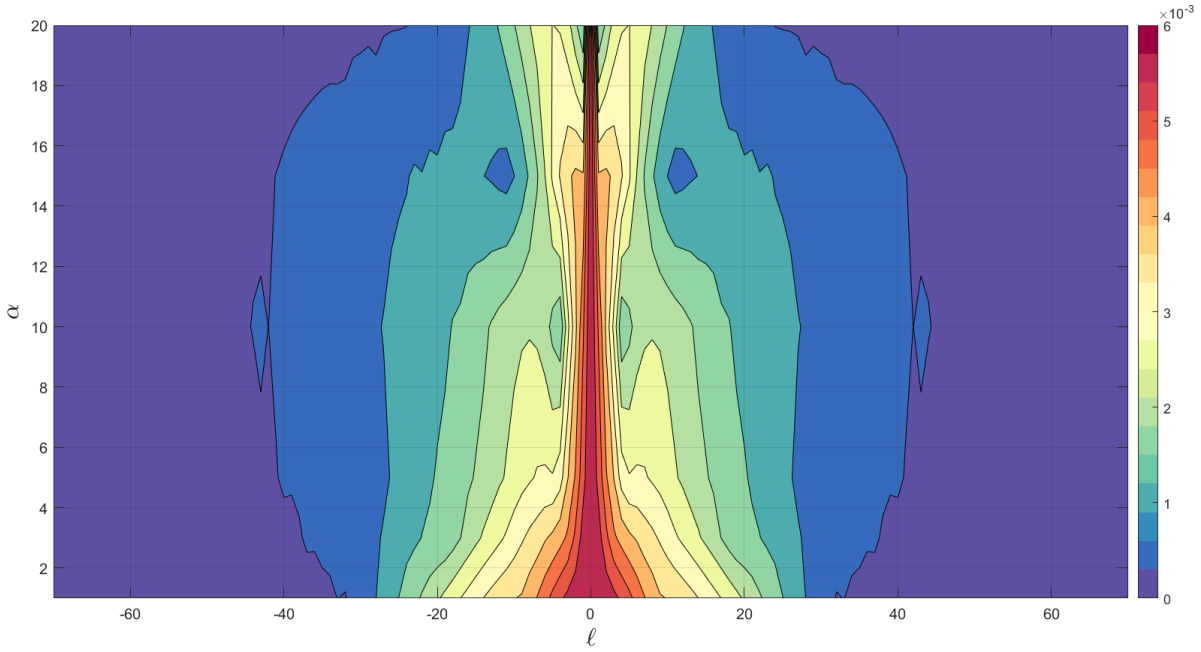

Figure 4.13: Nondimensional (α, ℓ)-contour plot for the maximum growth rate in the presence of meridional topography, with $N = 256$, $\mathscr{A} = 0.2$ (or $\hat{\mathscr{A}} = 800\text{m}$), $\hat{U} = 4\text{cm s}^{-1}$ (or $U = 0.013$), latitude $\theta_0 = 30°$ and $\hat{S} = 1.6 \times 10^{-9}\text{m}^{-2}$.

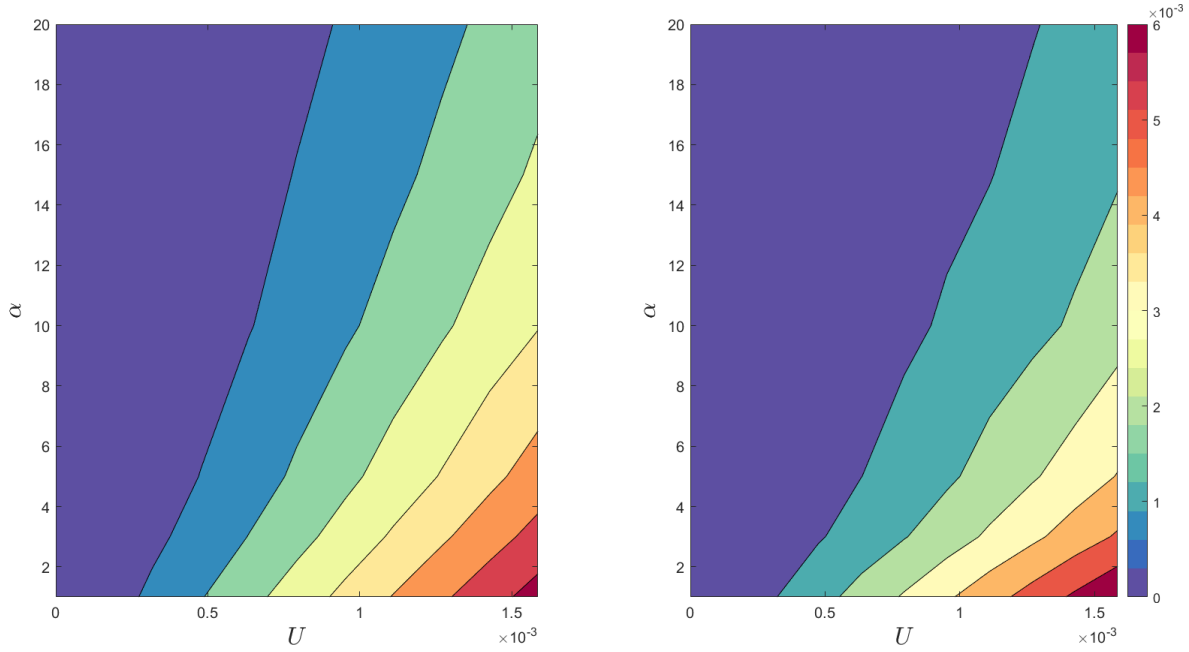

Figure 4.14: Nondimensional (α, U)-contour plot for the maximum growth rate in the presence of zonal topography, with $N = 256$, $\mathscr{A} = 0.1$ and $\mathscr{A} = 0.2$ respectively, latitude $\theta_0 = 30°$ and $\hat{S} = 1.6 \times 10^{-9}\text{m}^{-2}$.

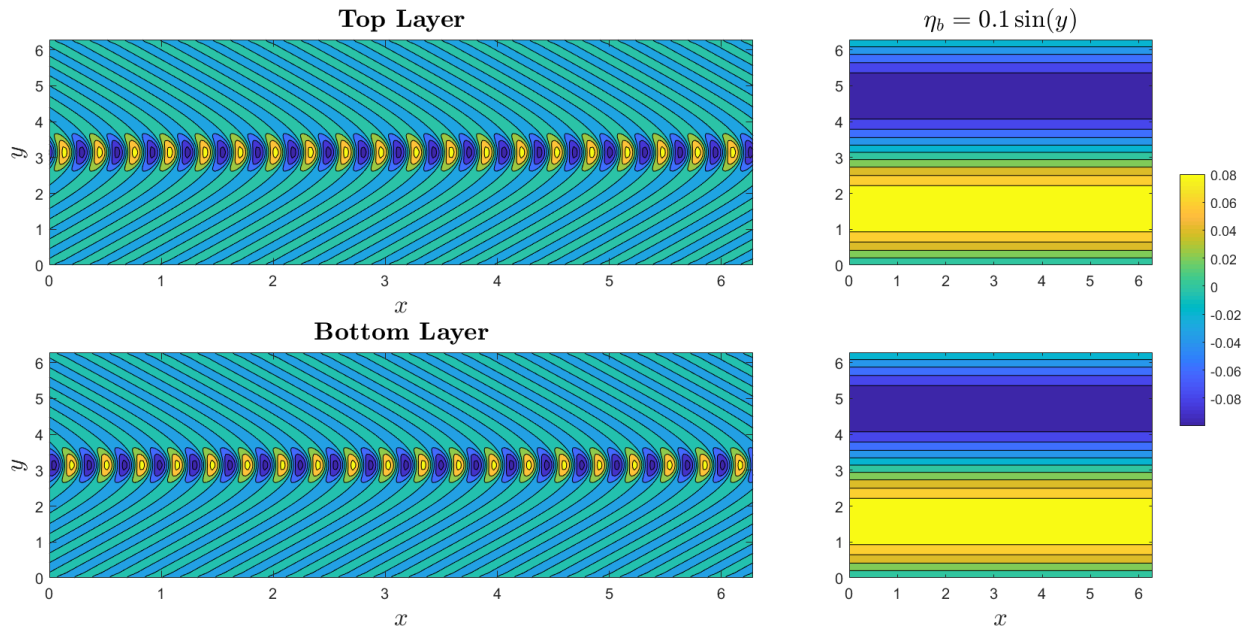

Figure 4.15: Left plots are contour plots for the perturbation streamfunctions corresponding to the maximum growth rates (in the top and bottom layers), in the presence of zonal topography, with $N = 256$, $\mathscr{A} = 0.1$, $\alpha = 1$, latitude $\theta_0 = 30°$ and $\hat{S} = 1.6 \times 10^{-9}\text{m}^{-2}$. The plots to the right are the orientation of topography. Note that the color bar only refers to the topography plots.

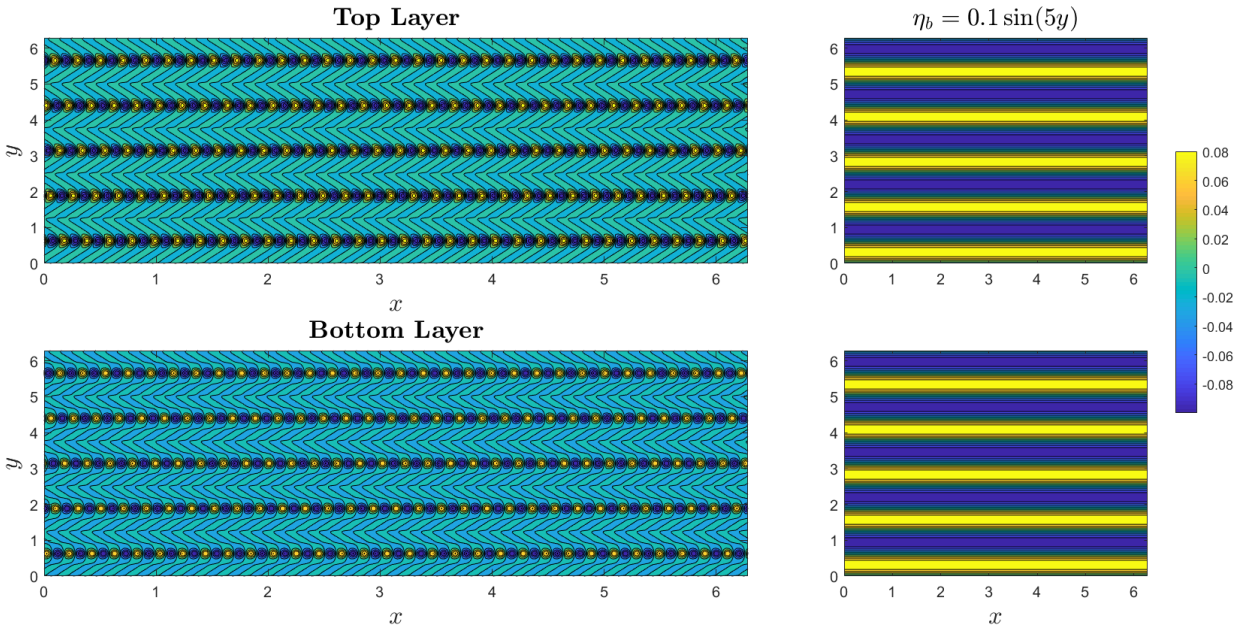

Figure 4.16: Left plots are nondimensional contour plots for the perturbation streamfunction corresponding to the maximum growth rates (in the top and bottom layers), in the presence of zonal topography, with $N = 256$, $\mathscr{A} = 0.1$, $\alpha = 5$, latitude $\theta_0 = 30°$ and $\hat{S} = 1.6 \times 10^{-9}\text{m}^{-2}$. The plots to the right are the orientation of topography. Note that the color bar only refers to the topography plots.

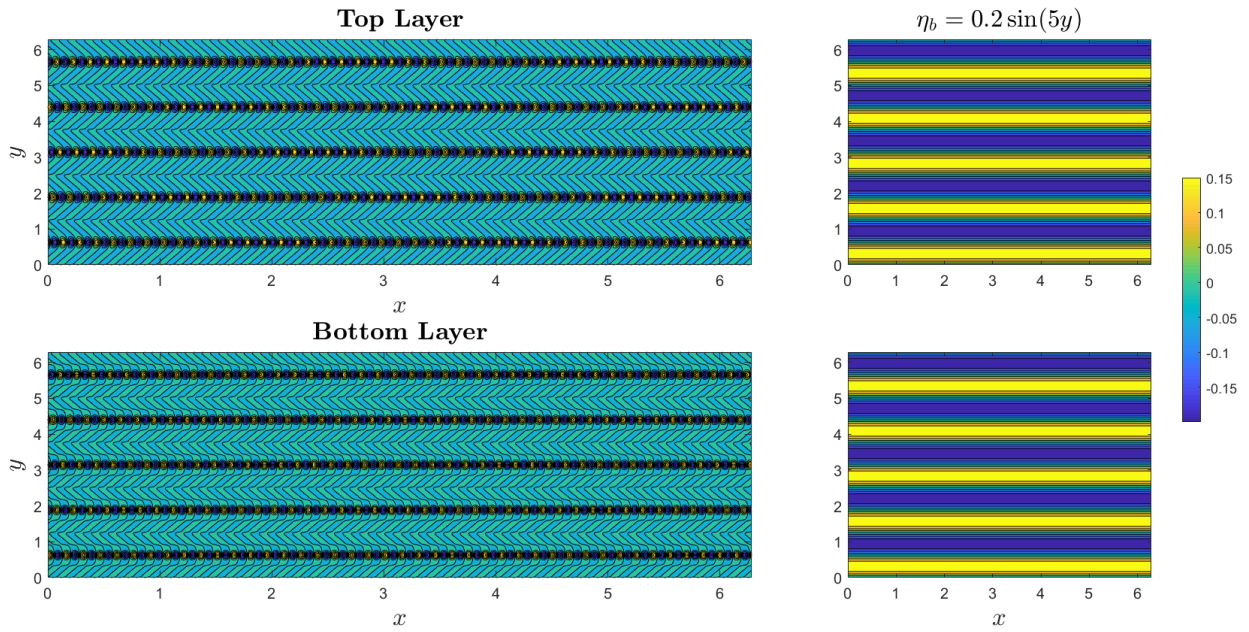

Figure 4.17: Left plots are nondimensional contour plots for the perturbation streamfunction corresponding to the maximum growth rates (in the top and bottom layers), in the presence of zonal topography, with $N = 256$, $\mathscr{A} = 0.2$, $\alpha = 5$, latitude $\theta_0 = 30°$ and $\hat{S} = 1.6 \times 10^{-9}\text{m}^{-2}$. The plots to the right are the orientation of topography. Note that the color bar only refers to the topography plots.

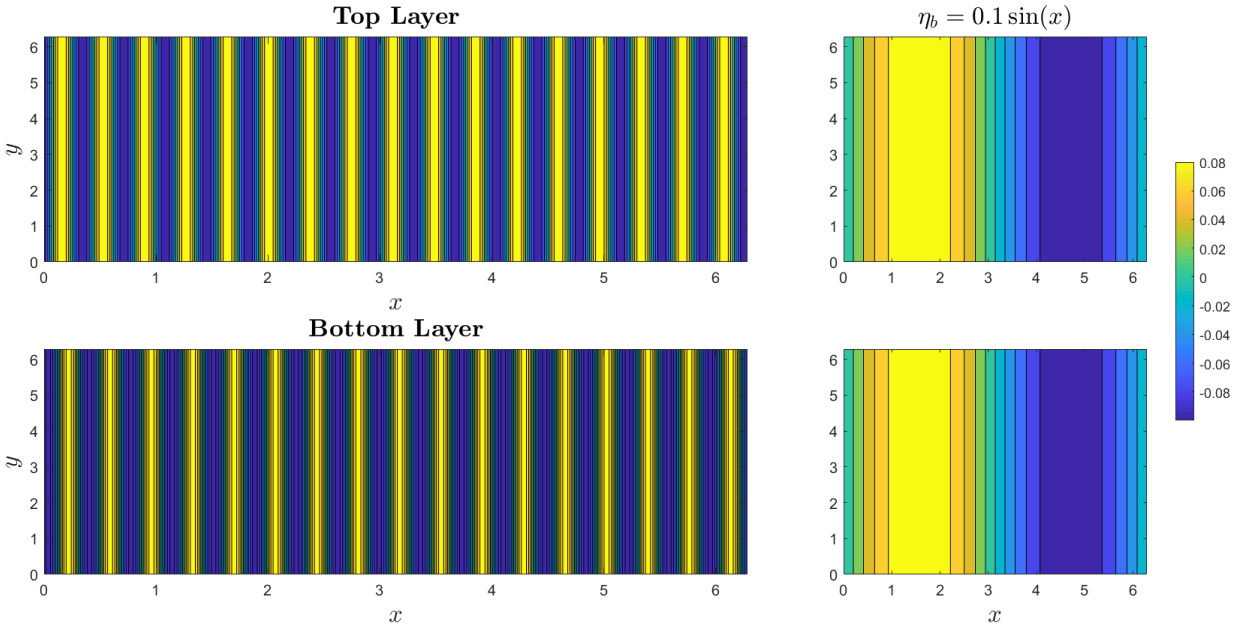

Figure 4.18: Left plots are nondimensional contour plots for the perturbation streamfunction corresponding to the maximum growth rates (in the top and bottom layers), in the presence of meridional topography, with $N = 256$, $\mathscr{A} = 0.1$, $\alpha = 1$, latitude $\theta_0 = 30°$ and $\hat{S} = 1.6 \times 10^{-9}\text{m}^{-2}$. The plots to the right are the orientation of topography. Note that the color bar only refers to the topography plots.

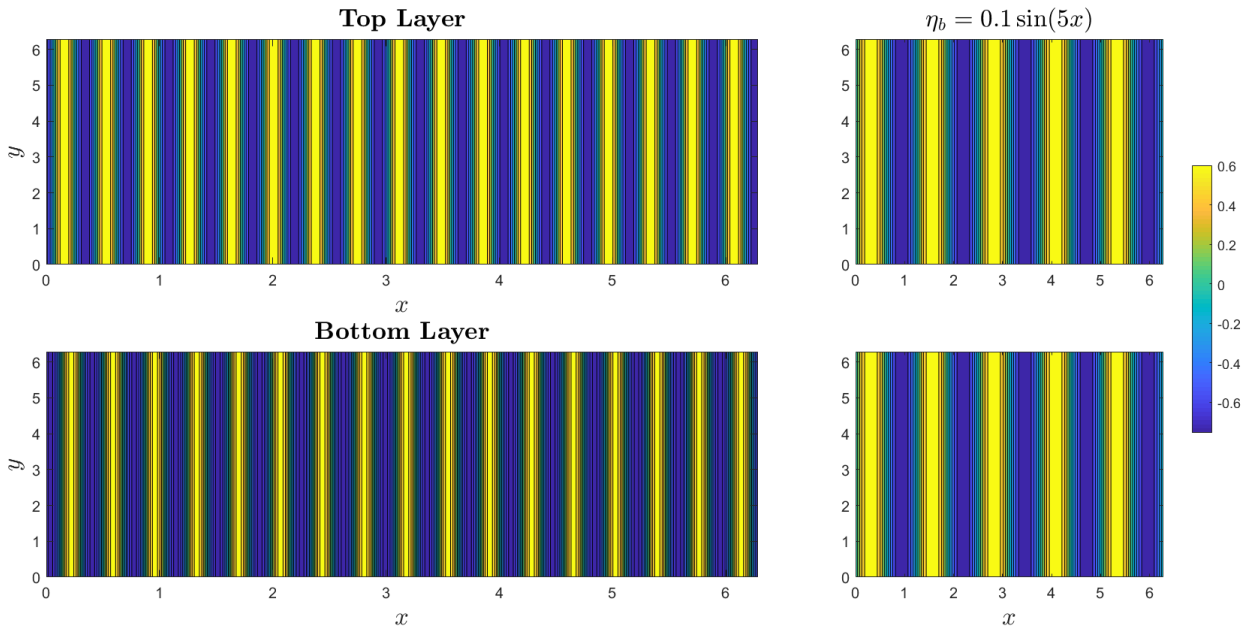

Figure 4.19: Left plots are nondimensional contour plots for the perturbation streamfunction corresponding to the maximum growth rates (in the top and bottom layers), in the presence of meridional topography, with $N = 256$, $\mathscr{A} = 0.1$, $\alpha = 5$, latitude $\theta_0 = 30°$ and $\hat{S} = 1.6 \times 10^{-9}\text{m}^{-2}$. The plots to the right are the orientation of topography. Note that the color bar only refers to the topography plots.

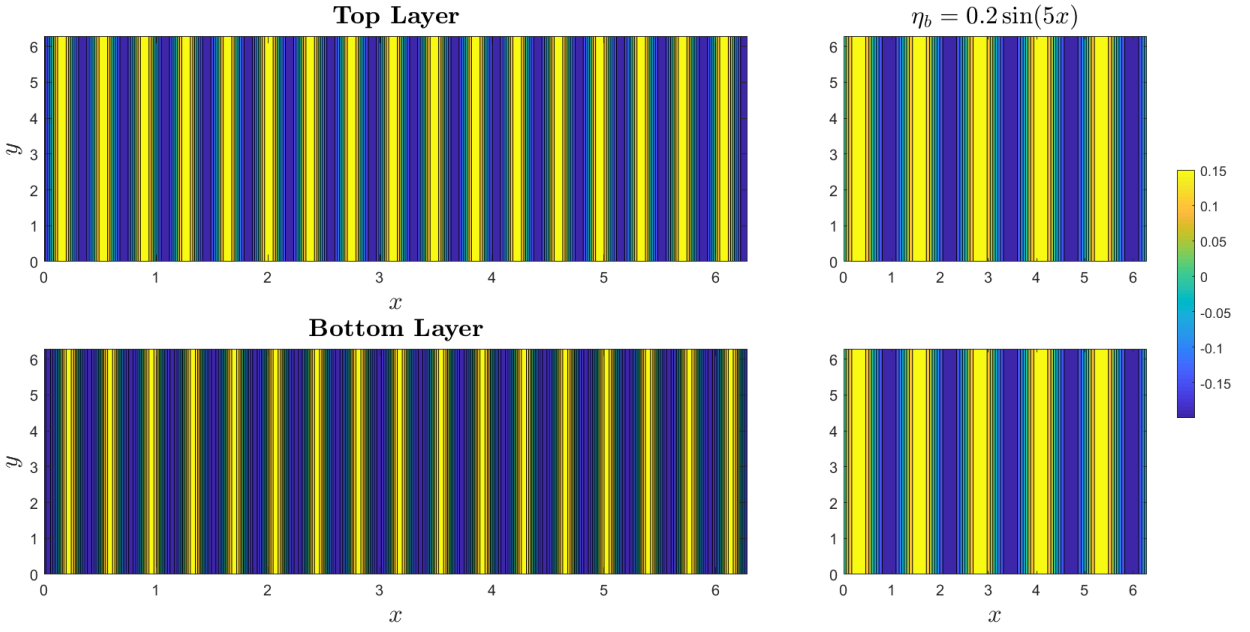

Figure 4.20: Left plots are nondimensional contour plots for the perturbation streamfunction corresponding to the maximum growth rates (in the top and bottom layers), in the presence of meridional topography, with $N = 256$, $\mathscr{A} = 0.2$, $\alpha = 5$, latitude $\theta_0 = 30°$ and $\hat{S} = 1.6 \times 10^{-9}\text{m}^{-2}$. The plots to the right are the orientation of topography. Note that the color bar only refers to the topography plots.

CHAPTER 5

TWO-LAYER ASYMPTOTIC ANALYSIS

In this chapter, rather than a numerical treatment of the two-layer problem, we attempt to solve the problem asymptotically. The aim of which is to compare the results obtained in this section with those found in chapter 4 when considering the numerical point of view. The reasoning behind why we wish to make this comparison is to assess the limitations of the asymptotic theory and determine scales of topography for which this approach breaks down. In particular, we would like to know how large the amplitude of topography must be before the asymptotic theory begins to disagree with our findings in the linear stability analysis.

Despite our focus being on the two-layer problem, the asymptotic theory can also be applied to a one-layer and other multi-layer models. In fact, Benilov has developed the asymptotic theory for waves over a one-layer beta plane with isolated, radially symmetric bottom irregularities [27], as well as zonal jets on a barotropic beta plane over sinusoidal topography [28]. The later of these papers was complemented by a follow-up paper, investigating the problem numerically [29]. In what follows, we shall take a look at an asymptotic analysis of the two-layer problem with sinusoidal topography presented by Benilov in [21]. We shall attempt to present the material in a clear and concise way, walking through all the technical details step by step. Again, credit for the results obtained in this section goes completely to Benilov, and we only include this material for the sake of completeness.

5.1 SMALL-SCALE ANALYSIS

NORMAL MODES

Recall that in chapter 4 we obtained the linearised system, (4.2), for the two-layer fluid model. If for the time being, we consider arbitrary bottom topography of the form $\hat{\eta}_b = \hat{\eta}_b(\hat{x}, \hat{y})$, then we have properties in the system which change w.r.t. space (an example in our case being the system PV), and so (4.2) is spatially inhomogeneous. As a consequence of this, we cannot guarantee the solutions $\hat{\psi}_j$ to depend on the horizontal coordinates, $(\hat{x}, \hat{y})$, harmonically. Despite this, we take inspiration from Benilov and consider normal mode solutions of the form:

$$\hat{\psi}_j(\hat{x}, \hat{y}, \hat{t}) = \hat{\phi}_j(\hat{\xi}) e^{i(\hat{k}\hat{x} + \hat{\ell}\hat{y} - \hat{\omega}\hat{t})}, \tag{5.1}$$

with wavevector $(\hat{k}, \hat{\ell})$, disturbance frequency $\hat{\omega}$ and $\hat{\xi} = \hat{\xi}(\hat{x}, \hat{y})$. This choice of solution is chosen for the sake of convenience and is intended to separate the harmonic spatial dependence from the spatial dependence due to bottom topography, which we have denoted by $\hat{\xi}$. In particular, if we were working with a flat bottomed ocean model, then our solutions would not have spatial dependence due to topography, and so our amplitude functions, $\hat{\phi}_j$, could be assumed constant. Since we considered sinusoidal topography with linear spatial dependence in chapter 5, we do the same here and set:

$$\hat{\eta}_b = \hat{\mathscr{A}} \sin(\hat{\xi}), \quad \hat{\xi} = \hat{\alpha}\hat{x} + \hat{\gamma}\hat{y}, \tag{5.2}$$

where $\hat{\mathscr{A}}$ is the topographic amplitude and $(\hat{\alpha}, \hat{\gamma})$ is the topographic wavevector. This choice of $\hat{\xi}$ is more general than the cases we considered in chapter 5. Nonetheless, we can simply set either $\hat{\alpha}$ or $\hat{\gamma}$ equal to zero depending on the case we wish to consider. Now with (5.1) and

(5.2) in mind, by means of the chain and product rules we obtain the system of derivatives:

$$\frac{\partial \hat{\eta}_b}{\partial \hat{x}} = \hat{\alpha}\frac{\mathrm{d}\hat{\eta}_b}{\mathrm{d}\hat{\xi}}, \tag{5.3a}$$

$$\frac{\partial \hat{\eta}_b}{\partial \hat{y}} = \hat{\gamma}\frac{\mathrm{d}\hat{\eta}_b}{\mathrm{d}\hat{\xi}}, \tag{5.3b}$$

$$\frac{\partial \hat{\psi}_j}{\partial \hat{t}} = -i\hat{\omega}\hat{\phi}_j e^{i(\hat{k}\hat{x}+\hat{\ell}\hat{y}-\hat{\omega}\hat{t})}, \tag{5.3c}$$

$$\frac{\partial \hat{\psi}_j}{\partial \hat{x}} = \left[\hat{\alpha}\frac{\mathrm{d}}{\mathrm{d}\hat{\xi}} + i\hat{k}\right]\hat{\phi}_j e^{i(\hat{k}\hat{x}+\hat{\ell}\hat{y}-\hat{\omega}\hat{t})}, \tag{5.3d}$$

$$\frac{\partial \hat{\psi}_j}{\partial \hat{y}} = \left[\hat{\gamma}\frac{\mathrm{d}}{\mathrm{d}\hat{\xi}} + i\hat{\ell}\right]\hat{\phi}_j e^{i(\hat{k}\hat{x}+\hat{\ell}\hat{y}-\hat{\omega}\hat{t})}, \tag{5.3e}$$

$$\frac{\partial^2 \hat{\psi}_j}{\partial \hat{x}^2} = \left[\hat{\alpha}^2\frac{\mathrm{d}^2}{\mathrm{d}\hat{\xi}^2} + 2i\hat{\alpha}\hat{k}\frac{\mathrm{d}}{\mathrm{d}\hat{\xi}} - \hat{k}^2\right]\hat{\phi}_j e^{i(\hat{k}\hat{x}+\hat{\ell}\hat{y}-\hat{\omega}\hat{t})}, \tag{5.3f}$$

$$\frac{\partial^2 \hat{\psi}_j}{\partial \hat{y}^2} = \left[\hat{\gamma}^2\frac{\mathrm{d}^2}{\mathrm{d}\hat{\xi}^2} + 2i\hat{\gamma}\hat{\ell}\frac{\mathrm{d}}{\mathrm{d}\hat{\xi}} - \hat{\ell}^2\right]\hat{\phi}_j e^{i(\hat{k}\hat{x}+\hat{\ell}\hat{y}-\hat{\omega}\hat{t})}. \tag{5.3g}$$

It follows when substituting this system of derivatives into (4.2a) that we have:

$$\begin{aligned}\left\{\left[-i\hat{\omega}+\hat{U}\left(\hat{\alpha}\frac{\mathrm{d}}{\mathrm{d}\hat{\xi}}+i\hat{k}\right)\right]\left[(\hat{\alpha}^2+\hat{\gamma}^2)\frac{\mathrm{d}^2\hat{\phi}_1}{\mathrm{d}\hat{\xi}^2}+2i(\hat{\alpha}\hat{k}+\hat{\gamma}\hat{\ell})\frac{\mathrm{d}\hat{\phi}_1}{\mathrm{d}\hat{\xi}}-(\hat{k}^2+\hat{\ell}^2)\hat{\phi}_1+\hat{S}_1(\hat{\phi}_2-\hat{\phi}_1)\right]\right.\\ \left.+(\hat{\beta}+\hat{S}_1\hat{U})\left(\hat{\alpha}\frac{\mathrm{d}\hat{\phi}_1}{\mathrm{d}\hat{\xi}}+i\hat{k}\hat{\phi}_1\right)\right\}e^{i(\hat{k}\hat{x}+\hat{\ell}\hat{y}-\hat{\omega}\hat{t})}=0.\end{aligned}$$

If we do the same for the bottom layer governance with topography, (4.2b), we find that:

$$\begin{aligned}\left\{-i\hat{\omega}\left[(\hat{\alpha}^2+\hat{\gamma}^2)\frac{\mathrm{d}^2\hat{\phi}_2}{\mathrm{d}\hat{\xi}^2}+2i(\hat{\alpha}\hat{k}+\hat{\gamma}\hat{\ell})\frac{\mathrm{d}\hat{\phi}_2}{\mathrm{d}\hat{\xi}}-(\hat{k}^2+\hat{\ell}^2)\hat{\phi}_2+\hat{S}_2(\hat{\phi}_1-\hat{\phi}_2)\right]\right.\\ \left.+(\hat{\beta}-\hat{S}_2\hat{U})\left[\hat{\alpha}\frac{\mathrm{d}\hat{\phi}_2}{\mathrm{d}\hat{\xi}}+i\hat{k}\hat{\phi}_2\right]+i\frac{\hat{f}_0(\hat{\gamma}\hat{k}-\hat{\alpha}\hat{\ell})}{\hat{H}_2}\frac{\mathrm{d}\hat{\eta}_b}{\mathrm{d}\hat{\xi}}\hat{\phi}_2\right\}e^{i(\hat{k}\hat{x}+\hat{\ell}\hat{y}-\hat{\omega}\hat{t})}=0.\end{aligned}$$

Therefore, if we divide through by the exponential terms, as well as by factors of $-i$, we are left with the top-layer equation:

$$\begin{aligned}\left[\hat{\omega}+\hat{U}\left(i\hat{\alpha}\frac{\mathrm{d}}{\mathrm{d}\hat{\xi}}-\hat{k}\right)\right]\left[(\hat{\alpha}^2+\hat{\gamma}^2)\frac{\mathrm{d}^2\hat{\phi}_1}{\mathrm{d}\hat{\xi}^2}+2i(\hat{\alpha}\hat{k}+\hat{\gamma}\hat{\ell})\frac{\mathrm{d}\hat{\phi}_1}{\mathrm{d}\hat{\xi}}-(\hat{k}^2+\hat{\ell}^2)\hat{\phi}_1+\hat{S}_1(\hat{\phi}_2-\hat{\phi}_1)\right]\\ +(\hat{\beta}+\hat{S}_1\hat{U})\left(i\hat{\alpha}\frac{\mathrm{d}\hat{\phi}_1}{\mathrm{d}\hat{\xi}}-\hat{k}\hat{\phi}_1\right)=0,\end{aligned} \tag{5.4}$$

and the bottom layer equation:

$$\hat{\omega}\Big[(\hat{\alpha}^2+\hat{\gamma}^2)\frac{\mathrm{d}^2\hat{\phi}_2}{\mathrm{d}\hat{\xi}^2}+2i(\hat{\alpha}\hat{k}+\hat{\gamma}\hat{\ell})\frac{\mathrm{d}\hat{\phi}_2}{\mathrm{d}\hat{\xi}}-(\hat{k}^2+\hat{\ell}^2)\hat{\phi}_2+\hat{S}_2(\hat{\phi}_1-\hat{\phi}_2)\Big] + (\hat{\beta}-\hat{S}_2\hat{U})\Big[i\hat{\alpha}\frac{\mathrm{d}\hat{\phi}_2}{\mathrm{d}\hat{\xi}}-\hat{k}\hat{\phi}_2\Big]-\frac{\hat{f}_0(\hat{\gamma}\hat{k}-\hat{\alpha}\hat{\ell})}{\hat{H}_2}\frac{\mathrm{d}\hat{\eta}_b}{\mathrm{d}\hat{\xi}}\hat{\phi}_2=0. \tag{5.5}$$

Nondimensional Scaling Analysis

So far, we have rewritten the model equations assuming a specific kind of perturbation solution, namely (5.1). Using these, we would now like to construct an asymptotic solution. To do such, we must first introduce small parameters to the problem. In chapter 4, we assumed that the length scales for bottom irregularities and the perturbation wavelength were relative in size to one another (we took this to be the barotropic Rossby radius). However, in the analysis that follows, we shall make the following assumptions:

- The zonal and meridional length scales of bottom irregularities, $\hat{L}_h$, are very small in comparison to the wavelength of the perturbation streamfunction, $\hat{\lambda}=(\hat{k}^2+\hat{\ell}^2)^{-1/2}$. In other words, we have that $\hat{L}_h \ll \hat{\lambda}$,
- The layer depths are equal, that is $\hat{H}_1=\hat{H}_2=\hat{H}$ (or $\hat{S}_1=\hat{S}_2=\hat{S}$),
- The vertical length scale of topography, $\hat{L}_h$ is very small relative to the bottom layer depth, i.e. $\hat{L}_v \ll \hat{H}$,
- The perturbation wavelength is relative in size to the barotropic Rossby radius, which we can write mathematically as $\hat{\lambda}=\mathcal{O}(\hat{R}_d)$, where $\hat{R}_d=\sqrt{\hat{g}'\hat{H}}/\hat{f}_0$ (as seen in chapter 4),
- By inspection of the exponential term, the perturbation frequency satisfies $\hat{\omega}\hat{t}=\mathcal{O}(\hat{k}\hat{x})$, or equivalently, $\hat{\omega}=\mathcal{O}(\hat{V}/\hat{\lambda})$, where $\hat{V}$ is the mean velocity in the top layer.

Of course, one question that is natural to ask when making these assumptions is what do we mean by the term 'small'. In particular, how do these small-scale ratios compare to one another in magnitude? To understand this, we must refer to real world data representative of our problem. The values for the layer depths, latitude, reduced gravity and background velocity used in Benilov's paper [21, pg. 2021] were taken from Nowlin and Klinck, which looked at the Antarctic Circumpolar Current [30]. These parameter values can be found in the table below, along with the topographic length scales used by Benilov.

Parameter	Value
$\hat{H}_1$	2000m
$\hat{H}_2$	2000m
θ_0	59°
$\hat{U}$	0.18ms^{-1}
$\hat{g}'$	$9.81 \times 5 \times 10^{-4}\text{ms}^{-2}$
$\hat{L}_h$	5000m
$\hat{L}_v$	200m

Table 5.1: Parameter values representative of the real world ocean, taken from [21, pg. 2021-2022], where $\hat{H}_j$ are the layer depths, θ_0 is the latitude, $\hat{U}$ is the background velocity in the top layer, $\hat{g}'$ is reduced gravity, and $\hat{L}_h$ and $\hat{L}_v$ are the horizontal length scales of bottom irregularities in the ocean model.

With these values, the barotropic Rossby radius can be calculated to be:

$$\hat{R}_d = \frac{\sqrt{9.81 \times 5 \times 10^{-4} \times 2000}}{1.2467 \times 10^{-4}} \approx 25123.1\text{m},$$

where the denominator is found using $\hat{f}_0 = 2\hat{\Omega}\sin(\theta_0)$, with $\hat{\Omega} = 2\pi/86400\text{s}^{-1}$. Thus, we find that $\hat{L}_h/\hat{R}_d \approx 0.2$. At the same time, we also have that $\hat{L}_v/\hat{H} = 0.1$, which appears similar in size to $\hat{L}_h/\hat{R}_d$, and so, for our convenience, we shall introduce the small parameter ϵ such that:

$$\frac{\hat{L}_h}{\hat{R}_d} = \frac{\hat{L}_v}{\hat{H}} = \epsilon \ll 1.$$

We now proceed by means of nondimensionalisation by writing:

$$\begin{aligned} (\hat{x}, \hat{y}) =& \hat{L}_h(x, y), \quad (\hat{k}, \hat{\ell}) = \frac{1}{\hat{R}_d\lambda}(k, \ell), \quad (\hat{\alpha}, \hat{\gamma}) = \frac{1}{\hat{L}_h}(\alpha, \gamma), \\ \hat{\omega} =& \frac{\hat{V}\omega}{\hat{R}_d\lambda}, \quad \hat{U} = \hat{V}U, \quad \hat{S} = \frac{S}{\hat{R}_d^2}, \end{aligned} \tag{5.6}$$

where we have set $\hat{\lambda} = \hat{R}_d\lambda$, for $\lambda = \mathcal{O}(1)$. Under the change of variables given in (5.6), it follows that:

$$\begin{aligned} \hat{\xi} &= \hat{\alpha}\hat{x} + \hat{\gamma}\hat{y} \\ &= \frac{\alpha}{\hat{L}_h}\hat{L}_h x + \frac{\gamma}{\hat{L}_h}\hat{L}_h y \\ &= \alpha x + \gamma y = \xi, \end{aligned}$$

where ξ is the dimensionless equivalent of $\hat{\xi}$. Since $\hat{\phi}_j$ are present in every term in (5.4) and (5.5), we can divide through by the corresponding dimensions, leaving us with the nondimensional equivalent, ϕ_j.

If we consider (5.4), then transforming according to (5.6) gives us:

$$\begin{aligned}
&\left[\frac{\hat{V}\omega}{\hat{R}_d\lambda}+\hat{V}U\left(i\frac{\alpha}{\hat{L}_h}\frac{\mathrm{d}}{\mathrm{d}\xi}-\frac{k}{\hat{R}_d\lambda}\right)\right]\left\{\frac{(\alpha^2+\gamma^2)}{\hat{L}_h^2}\frac{\mathrm{d}^2\phi_1}{\mathrm{d}\xi^2}+2i\frac{(\alpha k+\gamma\ell)}{\hat{L}_h\hat{R}_d\lambda}\frac{\mathrm{d}\phi_1}{\mathrm{d}\xi}-\frac{(k^2+\ell^2)\phi_1}{\hat{R}_d^2\lambda^2}\right.\\
&\left.+\frac{S(\phi_2-\phi_1)}{\hat{R}_d^2}\right\}+\left(\hat{\beta}+\frac{\hat{V}SU}{\hat{R}_d^2}\right)\left[i\frac{\alpha}{\hat{L}_h}\frac{\mathrm{d}\phi_1}{\mathrm{d}\xi}-\frac{k\phi_1}{\hat{R}_d\lambda}\right]=0\\
\implies&\frac{\hat{V}}{\hat{L}_h^3}\left[\frac{\hat{L}_h\omega}{\hat{R}_d\lambda}+U\left(i\alpha\frac{\mathrm{d}}{\mathrm{d}\xi}-\frac{\hat{L}_hk}{\hat{R}_d\lambda}\right)\right]\left\{(\alpha^2+\gamma^2)\frac{\mathrm{d}^2\phi_1}{\mathrm{d}\xi^2}+2i\frac{\hat{L}_h(\alpha k+\gamma\ell)}{\hat{R}_d\lambda}\frac{\mathrm{d}\phi_1}{\mathrm{d}\xi}-\frac{\hat{L}_h^2(k^2+\ell^2)\phi_1}{\hat{R}_d^2\lambda^2}\right.\\
&\left.+\frac{\hat{L}_h^2S(\phi_2-\phi_1)}{\hat{R}_d^2}\right\}+\frac{1}{\hat{L}_h}\left(\hat{\beta}+\frac{\hat{V}SU}{\hat{R}_d^2}\right)\left[i\alpha\frac{\mathrm{d}\phi_1}{\mathrm{d}\xi}-\frac{\hat{L}_hk\phi_1}{\hat{R}_d\lambda}\right]=0\\
\implies&\left[\frac{\hat{L}_h\omega}{\hat{R}_d\lambda}+U\left(i\alpha\frac{\mathrm{d}}{\mathrm{d}\xi}-\frac{\hat{L}_hk}{\hat{R}_d\lambda}\right)\right]\left\{(\alpha^2+\gamma^2)\frac{\mathrm{d}^2\phi_1}{\mathrm{d}\xi^2}+2i\frac{\hat{L}_h(\alpha k+\gamma\ell)}{\hat{R}_d\lambda}\frac{\mathrm{d}\phi_1}{\mathrm{d}\xi}-\frac{\hat{L}_h^2(k^2+\ell^2)\phi_1}{\hat{R}_d^2\lambda^2}\right.\\
&\left.+\frac{\hat{L}_h^2S(\phi_2-\phi_1)}{\hat{R}_d^2}\right\}+\left(\frac{\hat{\beta}\hat{L}_h^2}{\hat{V}}+\frac{\hat{L}_h^2SU}{\hat{R}_d^2}\right)\left[i\alpha\frac{\mathrm{d}\phi_1}{\mathrm{d}\xi}-\frac{\hat{L}_hk\phi_1}{\hat{R}_d\lambda}\right]=0.
\end{aligned}$$

This involves small-scale quantities by our construction, and so we can rewrite this in terms of ϵ. However, this equation contains the dimensionless quantity $\hat{\beta}\hat{L}_h^2/\hat{V}$, which we have yet to identify the size of (how it scales compared to the other small parameters in the problem). The value of which turns out to be:

$$\frac{\hat{\beta}\hat{L}_h}{\hat{V}}\approx\frac{1.1705\times10^{-11}\times5000^2}{0.18}\approx0.0016\mathrm{s}^{-1},$$

where we have made use of $\hat{\beta}=2\hat{\Omega}\cos(\theta_0)/\hat{r}_0$. Clearly, in relation to how we have defined ϵ, this quantity is smaller. Hence, we set $\hat{\beta}\hat{L}_h^2/\hat{V}=\epsilon^2\beta$, where $\beta=\mathcal{O}(1)$, as done in [27, pg. 264] (since $\hat{L}_v/\hat{H}=0.1^3=0.001$, it would perhaps make more sense to set $\hat{\beta}\hat{L}_h^2/\hat{V}=\epsilon^3\beta$, though this would be inconvenient when performing the asymptotic analysis, as will become apparent later on). Therefore, rewriting in terms of ϵ, we obtain the top-layer governance:

$$\begin{aligned}
&\left[\epsilon\omega^*+U\left(i\alpha\frac{\mathrm{d}}{\mathrm{d}\xi}-\epsilon k^*\right)\right]\left\{(\alpha^2+\gamma^2)\frac{\mathrm{d}^2\phi_1}{\mathrm{d}\xi^2}+2i\epsilon(\alpha k^*+\gamma\ell^*)\frac{\mathrm{d}\phi_1}{\mathrm{d}\xi}-\epsilon^2(k^{*2}+\ell^{*2})\phi_1\right.\\
&\left.+\epsilon^2S(\phi_2-\phi_1)\right\}+\epsilon^2(\beta+SU)\left[i\alpha\frac{\mathrm{d}\phi_1}{\mathrm{d}\xi}-\epsilon k^*\phi_1\right]=0,
\end{aligned}\tag{5.7}$$

where we have defined $(k^*,\ell^*,\omega^*)=(k,\ell,\omega)/\lambda$. Doing the same for the bottom-layer governance,

one finds that:

$$\begin{aligned}
&\frac{\hat{V}\omega}{\hat{R}_d\lambda}\left\{\frac{(\alpha^2+\gamma^2)}{\hat{L}_h^2}\frac{\mathrm{d}^2\phi_2}{\mathrm{d}\xi^2}+\frac{2i(\alpha k+\gamma\ell)}{\hat{L}_h\hat{R}_d\lambda}\frac{\mathrm{d}\phi_2}{\mathrm{d}\xi}-\frac{(k^2+\ell^2)\phi_2}{\hat{R}_d^2\lambda^2}+\frac{S(\phi_1-\phi_2)}{\hat{R}_d^2}\right\}\\
&+\left(\hat{\beta}-\frac{\hat{V}SU}{\hat{R}_d^2}\right)\left[i\frac{\alpha}{\hat{L}_h}\frac{\mathrm{d}\phi_2}{\mathrm{d}\xi}-\frac{k\phi_2}{\hat{R}_d\lambda}\right]-\frac{\hat{f}_0\hat{L}_v(\gamma k-\alpha\ell)}{\hat{H}\hat{L}_h\hat{R}_d\lambda}\frac{\mathrm{d}\eta_b}{\mathrm{d}\xi}\phi_2=0\\
\Longrightarrow\ &\frac{\hat{L}_h\omega^*}{\hat{R}_d}\left\{(\alpha^2+\gamma^2)\frac{\mathrm{d}^2\phi_2}{\mathrm{d}\xi^2}+\frac{2i\hat{L}_h(\alpha k^*+\gamma\ell^*)}{\hat{R}_d}\frac{\mathrm{d}\phi_2}{\mathrm{d}\xi}-\frac{\hat{L}_h^2(k^{*2}+\ell^{*2})\phi_2}{\hat{R}_d^2}+\frac{\hat{L}_h^2S(\phi_1-\phi_2)}{\hat{R}_d^2}\right\}\\
&+\left(\frac{\hat{\beta}\hat{L}_h^2}{\hat{V}}-\frac{\hat{L}_h^2SU}{\hat{R}_d^2}\right)\left[i\alpha\frac{\mathrm{d}\phi_2}{\mathrm{d}\xi}-\frac{\hat{L}_hk^*\phi_2}{\hat{R}_d}\right]-\frac{\hat{f}_0\hat{L}_v\hat{L}_h^2(\gamma k^*-\alpha\ell^*)}{\hat{H}\hat{R}_d\hat{V}}\frac{\mathrm{d}\eta_b}{\mathrm{d}\xi}\phi_2=0.
\end{aligned}$$

For us to be able to express this in ϵ-form, we must identify how the quantity $\hat{f}_0\hat{L}_b\hat{L}_h^2/\hat{H}\hat{R}_d\hat{V}$ scales relative to ϵ. A simple calculation reveals that:

$$\frac{\hat{f}_0\hat{L}_b\hat{L}_h^2}{\hat{H}\hat{R}_d\hat{V}}\approx 0.0693\approx\epsilon^2.$$

With this all in mind, we obtain the ϵ-equation for the bottom layer:

$$\begin{aligned}
&\omega^*\left\{(\alpha^2+\gamma^2)\frac{\mathrm{d}^2\phi_2}{\mathrm{d}\xi^2}+2i\epsilon(\alpha k^*+\gamma\ell^*)\frac{\mathrm{d}\phi_2}{\mathrm{d}\xi}-\epsilon^2(k^{*2}+\ell^{*2})\phi_2+\epsilon^2S(\phi_1-\phi_2)\right\}\\
&+\epsilon(\beta-SU)\left[i\alpha\frac{\mathrm{d}\phi_2}{\mathrm{d}\xi}-\epsilon k^*\phi_2\right]-\epsilon(\gamma k^*-\alpha\ell^*)\frac{\mathrm{d}\eta_b}{\mathrm{d}\xi}\phi_2=0,
\end{aligned}\tag{5.8}$$

where we have divided through by a common factor of ϵ. Now that we have derived the layer equations in terms of small parameters, we are now in a position where we can perform an asymptotic analysis.

5.2 AN ASYMPTOTIC SOLUTION

To begin our analysis, it is first convenient to rewrite (5.7) and (5.8) such that they are expressed in increasing powers of ϵ. If we omit the asterisk in (5.7) and (5.8), we have the top layer equation:

$$\begin{aligned}
&i\alpha U(\alpha^2+\gamma^2)\frac{\mathrm{d}^3\phi_1}{\mathrm{d}\xi^3}+\epsilon\left\{(\omega-kU)(\alpha^2+\gamma^2)-2\alpha U(\alpha k+\gamma\ell)\right\}\frac{\mathrm{d}^2\phi_1}{\mathrm{d}\xi^2}\\
&+i\epsilon^2\left\{\left\{\alpha\left[\beta-U(k^2+\ell^2)\right]+2(\omega-kU)(\alpha k+\gamma\ell)\right\}\frac{\mathrm{d}\phi_1}{\mathrm{d}\xi}+\alpha SU\frac{\mathrm{d}\phi_2}{\mathrm{d}\xi}\right\},\\
&+\epsilon^3\left\{\left[(kU-\omega)(k^2+\ell^2)-\omega S-\beta k\right]\phi_1+S(\omega-kU)\phi_2\right\}=0,
\end{aligned}\tag{5.9}$$

and the bottom layer equation:

$$\begin{aligned}&\omega(\alpha^2+\gamma^2)\frac{\mathrm{d}^2\phi_2}{\mathrm{d}\xi^2}+\epsilon\left\{i\Big[2\omega(\alpha k+\gamma\ell)+\alpha(\beta-SU)\Big]\frac{\mathrm{d}\phi_2}{\mathrm{d}\xi}+(\alpha\ell-\gamma k)\frac{\mathrm{d}\eta_b}{\mathrm{d}\xi}\phi_2\right\}\\&-\epsilon^2\left\{\Big[\omega(k^2+\ell^2+S)+k(\beta-SU)\Big]\phi_2-\omega S\phi_1\right\}=0.\end{aligned}\tag{5.10}$$

When working with equations of this type, we can attempt to seek solutions in the form of an ϵ-expansion, that is we look for solutions of the form:

$$\phi_j=\phi_j^{(0)}+\epsilon\phi_j^{(1)}+\epsilon^2\phi_j^{(2)}+\mathcal{O}(\epsilon^3),\quad \omega=\omega^{(0)}+\epsilon\omega^{(1)}+\epsilon^2\omega^{(2)}+\mathcal{O}(\epsilon^3).$$

Substitution of these solutions into (5.9) identifies that we have to solve the equations:

$$\begin{aligned}&\mathcal{O}(1):\quad i\alpha U(\alpha^2+\gamma^2)\frac{\mathrm{d}^3\phi_1^{(0)}}{\mathrm{d}\xi^3}=0,\\&\mathcal{O}(\epsilon):\quad i\alpha U(\alpha^2+\gamma^2)\frac{\mathrm{d}^3\phi_1^{(1)}}{\mathrm{d}\xi^3}+\Big[(\omega^{(0)}-kU)(\alpha^2+\gamma^2)-2\alpha U(\alpha k+\gamma\ell)\Big]\frac{\mathrm{d}^2\phi_1^{(0)}}{\mathrm{d}\xi^2}=0,\\&\mathcal{O}(\epsilon^2):\quad i\alpha U(\alpha^2+\gamma^2)\frac{\mathrm{d}^3\phi_1^{(2)}}{\mathrm{d}\xi^3}+\Big[(\omega^{(0)}-kU)(\alpha^2+\gamma^2)-2\alpha U(\alpha k+\gamma\ell)\Big]\frac{\mathrm{d}^2\phi_1^{(1)}}{\mathrm{d}\xi^2}\\&+\omega^{(1)}(\alpha^2+\gamma^2)\frac{\mathrm{d}^2\phi_1^{(0)}}{\mathrm{d}\xi^2}+i\left\{\alpha\Big[\beta-U(k^2+\ell^2)\Big]+2(\omega^{(0)}-kU)(\alpha k+\gamma\ell)\right\}\frac{\mathrm{d}\phi_1^{(0)}}{\mathrm{d}\xi}\\&+i\alpha SU\frac{\mathrm{d}\phi_2^{(0)}}{\mathrm{d}\xi}=0,\\&\mathcal{O}(\epsilon^3):\quad i\alpha U(\alpha^2+\gamma^2)\frac{\mathrm{d}^3\phi_1^{(3)}}{\mathrm{d}\xi^3}+\Big[(\omega^{(0)}-kU)(\alpha^2+\gamma^2)-2\alpha U(\alpha k+\gamma\ell)\Big]\frac{\mathrm{d}^2\phi_1^{(2)}}{\mathrm{d}\xi^2}\\&+\omega^{(1)}(\alpha^2+\gamma^2)\frac{\mathrm{d}^2\phi_1^{(1)}}{\mathrm{d}\xi^2}+\omega^{(2)}(\alpha^2+\gamma^2)\frac{\mathrm{d}^2\phi_1^{(0)}}{\mathrm{d}\xi^2}+i\alpha\Big[\beta-U(k^2+\ell^2)\Big]\frac{\mathrm{d}\phi_1^{(1)}}{\mathrm{d}\xi}\\&+2i(\omega^{(0)}-kU)(\alpha k+\gamma\ell)\frac{\mathrm{d}\phi_1^{(1)}}{\mathrm{d}\xi}+2i\omega^{(1)}(\alpha k+\gamma\ell)\frac{\mathrm{d}\phi_1^{(0)}}{\mathrm{d}\xi}+i\alpha SU\frac{\mathrm{d}\phi_2^{(1)}}{\mathrm{d}\xi}\\&+\Big[(kU-\omega^{(0)})(k^2+\ell^2)-\omega^{(0)}S-\beta k\Big]\phi_1^{(0)}+S(\omega^{(0)}-kU)\phi_2^{(0)}=0.\end{aligned}$$

In a similar fashion, we find that for (5.10), we have at each order of ϵ:

$$\mathcal{O}(1): \quad \omega^{(0)}(\alpha^2+\gamma^2)\frac{\mathrm{d}^2\phi_2^{(0)}}{\mathrm{d}\xi^2}=0,$$

$$\mathcal{O}(\epsilon): \quad \omega^{(0)}(\alpha^2+\gamma^2)\frac{\mathrm{d}^2\phi_2^{(1)}}{\mathrm{d}\xi^2}+\omega^{(1)}(\alpha^2+\gamma^2)\frac{\mathrm{d}^2\phi_2^{(0)}}{\mathrm{d}\xi^2}+i\Big[2\omega^{(0)}(\alpha k+\gamma\ell)+\alpha(\beta-SU)\Big]\frac{\mathrm{d}\phi_2^{(0)}}{\mathrm{d}\xi}$$
$$+(\alpha\ell-\gamma k)\frac{\mathrm{d}\eta_b}{\mathrm{d}\xi}\phi_2^{(0)}=0,$$

$$\mathcal{O}(\epsilon^2): \quad \omega^{(0)}(\alpha^2+\gamma^2)\frac{\mathrm{d}^2\phi_2^{(2)}}{\mathrm{d}\xi^2}+\omega^{(1)}(\alpha^2+\gamma^2)\frac{\mathrm{d}^2\phi_2^{(1)}}{\mathrm{d}\xi^2}+\omega^{(2)}(\alpha^2+\gamma^2)\frac{\mathrm{d}^2\phi_2^{(0)}}{\mathrm{d}\xi^2}$$
$$+i\Big[2\omega^{(0)}(\alpha k+\gamma\ell)+\alpha(\beta-SU)\Big]\frac{\mathrm{d}\phi_2^{(1)}}{\mathrm{d}\xi}+2i\omega^{(1)}(\alpha k+\gamma\ell)\frac{\mathrm{d}\phi_2^{(0)}}{\mathrm{d}\xi}+(\alpha\ell-\gamma k)\frac{\mathrm{d}\eta_b}{\mathrm{d}\xi}\phi_2^{(1)}$$
$$-\Big[\omega^{(0)}(k^2+\ell^2+S)+k(\beta-SU)\Big]\phi_2^{(0)}+\omega^{(0)}S\phi_1^{(0)}=0.$$

Notice that we have only considered up to order ϵ^2 in the bottom layer, whereas, in the top layer we also considered up to order ϵ^3. At first, this might seem like an arbitrary thing to do, however, we will see later on that the equation obtained at order ϵ^3 in the bottom layer will not be needed in our analysis.

Thanks to the presence of a small parameter, our problem has been reduced to solving several simpler problems. If we first restrict our attention to the leading order equations in both layers, after simplification, these result in:

$$\frac{\mathrm{d}^3\phi_1^{(0)}}{\mathrm{d}\xi^3}=0 \ \text{ and } \ \frac{\mathrm{d}^2\phi_2^{(0)}}{\mathrm{d}\xi^2}=0,$$

which clearly have solutions:

$$\phi_1^{(0)}=\frac{A_1^{(0)}\xi^2}{2}+B_1^{(0)}\xi+C_1^{(0)}, \ \ \phi_2^{(0)}=B_2^{(0)}\xi+C_2^{(0)},$$

where $A_j^{(0)}$, $B_j^{(0)}$ and $C_j^{(0)}$ are arbitrary constants. If we impose that these solutions are in fact bounded at infinity, that is they must satisfy the condition:

$$\lim_{\xi\to\infty}\phi_j^{(0)}(\xi)=0,$$

then our solutions conveniently reduce to:

$$\phi_j^{(0)}=C_j^{(0)}, \tag{5.11}$$

which are simply constants. Since the equations at leading order do not involve terms due to the presence of bottom topography, this tells us that we must analyse higher order terms

in the ϵ-expansion to understand the role bottom irregularities play. Turning our attention to the equations at order ϵ, as a consequence of (5.11), terms multiplied by derivatives of these solutions evaluate to zero. Thus, after some simplification, we find the equations at order ϵ to be:

$$\frac{\mathrm{d}^3\phi_1^{(1)}}{\mathrm{d}\xi^3}=0,\ \text{ and }\ \omega^{(0)}(\alpha^2+\gamma^2)\frac{\mathrm{d}^2\phi_2^{(1)}}{\mathrm{d}\xi^2}+(\alpha\ell-\gamma k)\frac{\mathrm{d}\eta_b}{\mathrm{d}\xi}C_2^{(0)}=0.$$

As we saw previously, the first of these equations has constant solutions, namely $\phi_1^{(1)}=C_1^{(1)}$. However, the later of which is not as trivial to solve, and in fact rearranges to:

$$\frac{\mathrm{d}^2\phi_2^{(1)}}{\mathrm{d}\xi^2}=\frac{C_2^{(0)}(\gamma k-\alpha\ell)}{\omega^{(0)}(\alpha^2+\gamma^2)}\frac{\mathrm{d}\eta_b}{\mathrm{d}\xi}.$$

Solving this for sinusoidal topography as in (5.2), and assuming the solution to be bounded, we have:

$$\phi_2^{(1)}=\frac{\mathscr{A}C_2^{(0)}(\alpha\ell-\gamma k)}{\omega^{(0)}(\alpha^2+\gamma^2)}\cos(\xi). \tag{5.12}$$

Notice that none of the solutions obtained thus far have involved β. This is because we have not yet considered higher order ϵ-equations. Now it should become apparent to the reader why we chose to set $\hat{\beta}\hat{L}_h^2/\hat{V}=\epsilon^2\beta$ rather than equal to $\epsilon^3\beta$, despite this perhaps being a more physically representative choice. If we chose the later of these, then we would have to consider even higher order equations before obtaining solutions involving β. This would of course be significantly more tedious.

Next, we consider equations obtained at order ϵ^2. If we make use of (5.11) and (5.12), we obtain $\mathrm{d}^3\phi_1^{(2)}/\mathrm{d}\xi^3=0$ and:

$$\begin{aligned}&\omega^{(0)}(\alpha^2+\gamma^2)\frac{\mathrm{d}^2\phi_2^{(2)}}{\mathrm{d}\xi^2}+\frac{\mathscr{A}C_2^{(0)}(\gamma k-\alpha\ell)}{\omega^{(0)}(\alpha^2+\gamma^2)}\Big\{\omega^{(1)}(\alpha^2+\gamma^2)\cos(\xi)+i\Big[2\omega^{(0)}(\alpha k+\gamma\ell)\\&+\alpha(\beta-SU)\Big]\sin(\xi)+\mathscr{A}(\gamma k-\alpha\ell)\cos^2(\xi)\Big\}-C_2^{(0)}\Big[\omega^{(0)}(k^2+\ell^2+S)+k(\beta-SU)\Big]\\&+C_1^{(0)}\omega^{(0)}S=0.\end{aligned} \tag{5.13}$$

Again, the first of these yield the constant solution:

$$\phi_1^{(2)}=C_1^{(2)}.$$

Clearly, (5.13) is more complicated, and requires some care when solving. By inspection of (5.13), we notice that since the trigonometric functions are bounded, we will have bounded

solutions if the remaining constant terms vanish. However, since $\cos^2(\xi) = 1/2\big[1+\cos(2\xi)\big]$, the constant term in (5.13) is in fact equal to:

$$C_1^{(0)}\omega^{(0)}S + C_2^{(0)}\left[\frac{\mathscr{A}^2(\gamma k-\alpha\ell)^2}{2\omega^{(0)}(\alpha^2+\gamma^2)} + (SU-\beta)k - \omega^{(0)}(k^2+\ell^2+S)\right].$$

With this equal to zero, we have an equation in two unknowns, meaning we require a second equation in order to solve for these constants. Since we have yet to find a second equation, we must consider equations obtained at order ϵ^3. It turns out such an equation can be found by considering the ϵ-expansion in the top layer. After some simplification (making use of the information obtained thus far), the ϵ^3-equation in the top layer reads as:

$$\begin{aligned} i\alpha U(\alpha^2+\gamma^2)\frac{\mathrm{d}^3\phi_1^{(3)}}{\mathrm{d}\xi^3} + \frac{i\mathscr{A}\alpha SUC_2^{(0)}(\gamma k-\alpha\ell)}{\omega^{(0)}(\alpha^2+\gamma^2)}\sin(\xi) + S(\omega^{(0)}-kU)C_2^{(0)} \\ + \left[(kU-\omega^{(0)})(k^2+\ell^2) - \omega^{(0)}S - k\beta\right]C_1^{(0)} = 0. \end{aligned} \tag{5.14}$$

Again, for this equation to have bounded solutions, we must have the constant terms equal to zero. Hence, we want to solve the pair of equations:

$$C_1^{(0)}\omega^{(0)}S + C_2^{(0)}\left[\frac{\mathscr{A}^2(\gamma k-\alpha\ell)^2}{2\omega^{(0)}(\alpha^2+\gamma^2)} + (SU-\beta)k - \omega^{(0)}(k^2+\ell^2+S)\right] = 0, \tag{5.15a}$$

$$\left[(kU-\omega^{(0)})(k^2+\ell^2) - \omega^{(0)}S - k\beta\right]C_1^{(0)} + S(\omega^{(0)}-kU)C_2^{(0)} = 0. \tag{5.15b}$$

Reformulating the system in matrix form, we have:

$$\begin{bmatrix} \omega^{(0)}S & \dfrac{\mathscr{A}^2(\gamma k-\alpha\ell)^2}{2\omega^{(0)}(\alpha^2+\gamma^2)} + (SU-\beta)k - \omega^{(0)}(k^2+\ell^2+S) \\ (kU-\omega^{(0)})(k^2+\ell^2) - \omega^{(0)}S - k\beta & S(\omega^{(0)}-kU) \end{bmatrix} \boldsymbol{C} = \boldsymbol{0},$$

with $\boldsymbol{C} = (C_1^{(0)}, C_2^{(0)})^T$ and $\boldsymbol{0} = (0,0)^T$. From linear algebra, we know that for this to have non-trivial solutions, the determinant of the matrix of coefficients must equal zero. Thus, we find the leading order dispersion relation for the two layer problem with sinusoidal topography to be (multiplying through by $\omega^{(0)}$):

$$\omega^2(\omega-kU)S^2 - \left[\frac{\sigma^2(\gamma k-\alpha\ell)^2}{(\alpha^2+\gamma^2)} + \omega(SU-\beta)k - \omega^2(K^2+S)\right]\left[K^2(kU-\omega) - \omega S - k\beta\right] = 0, \tag{5.16}$$

where we have introduced $\omega = \omega^{(0)}$, $\sigma^2 = \mathscr{A}^2/2$ and $K^2 = k^2+\ell^2$, as done in [21, pg. 2023]. Relating this back to our choices of bottom irregularities in chapter 4 (that being zonal and meridional topographies), the dispersion relation corresponding to zonal topography, (3.4), is given by:

$$\omega^2(\omega - kU)S^2 - \Big[(\sigma k)^2 + \omega(SU - \beta)k - \omega^2(K^2 + S)\Big]\Big[K^2(kU - \omega) - \omega S - k\beta\Big] = 0, \tag{5.17}$$

whereas, the dispersion relation corresponding to meridional topography, (3.5), is given by:

$$\omega^2(\omega - kU)S^2 - \Big[(\sigma \ell)^2 + \omega(SU - \beta)k - \omega^2(K^2 + S)\Big]\Big[K^2(kU - \omega) - \omega S - k\beta\Big] = 0. \tag{5.18}$$

These dispersion relations that we have obtained by making use of the asymptotic theory are the same as the dispersion relation for a flat-bottomed ocean, (4.12), with the addition of the topography term:

$$\frac{\sigma^2(\gamma k - \alpha \ell)^2}{\alpha^2 + \gamma^2} = \sigma^2 |\boldsymbol{k} \wedge \boldsymbol{\alpha}|, \tag{5.19}$$

where $\boldsymbol{k} = (k, \ell)$ and $\boldsymbol{\alpha} = (\alpha, \gamma)/\sqrt{\alpha^2 + \gamma^2}$. The cross product form is useful since it helps us identify when topography has the most influence on the stability of the flow, as well as the least influence. Since the cross product of two vectors vanishes when they are parallel to each other, the term due to topography disappears when the disturbance wavevector $\boldsymbol{k}$ is parallel to the topographic wavevector $\boldsymbol{\alpha}$. This corresponds to meridional topography, $\eta_b = \mathscr{A} \sin(\alpha x)$, not affecting the stability of the flow disturbance. In contrast with this, the topographic term attains a maximum when $\boldsymbol{k}$ and $\boldsymbol{\alpha}$ are perpendicular to one another, or rather, this tells us that zonal topography, $\eta_b = \mathscr{A} \sin(\gamma y)$, does affect the stability of the flow disturbance. Moreover, in [21, 2024-2025], Benilov solves the dispersion relation numerically and concludes that:

- Baroclinic instability is weakened by the presence of zonal topography,
- The range of unstable modes tends towards the short-wave end of the spectrum (towards greater values of k),
- Topography influence on baroclinic instability is relatively weak for flows in a thin top layer, but this influence increases as the width of the top layer increases.

From what we have see, it appears that there are both similarities and differences between the numerical solutions we have obtained and the conclusions due to Benilov's asymptotic approach. It is clear that both suggest that sinusoidal zonal topography acts to reduce the growth rate of unstable modes, as well as shifting the range of unstable modes towards the short-wave end of the spectrum. However, the asymptotic results due to Benilov tell us that meridional sinusoidal bottom irregularites have zero influence on the stability of the flow. From figures 4.1, 4.4 and 4.5, this appears to be true for the maximum growth rate of unstable modes, since this remains the same as the flat bottom case (regardless of increases in the number of ridges or topographic amplitude). On the other hand, figures 4.4 and 4.5 clearly show that meridional topography changes the distribution of unstable modes. Some of the modes do move towards the short-wave end of the spectrum (in agreement with Benilov's second conclusion), but other modes appear to collect about $\ell = 0$, which is not accounted for by Benilov's asymptotic theory.

Moreover, our observation of dispersion relations and (α, k)-contour plots for maximum growth for zonal topography reveal a bifurcation corresponding to some critical value of α (which seemingly decreases with increases in topographic amplitude, as seen in figures 4.10 and 4.11). The existence of such a bifurcation point is not made aware to us by the asymptotic theory. As can be seen from figure 4.7, the number of unstable modes seems to decrease when the number of ridges of meridional topography increases. Hence, the stability of unstable modes is influenced by meridional bottom irregularities, despite the asymptotic theory suggesting this has no influence on the stability of the flow.

CHAPTER 6

CONCLUSION

The numerical results obtained in this dissertation appear to agree with Benilov's asymptotic theory in some regards, but not in others. In terms of sinusoidal zonal topography, Benilov's conclusions are consistent with our findings. On the other hand, the existence of a bifurcation was identified by our numerical solution, but not the asymptotic solution. As for meridional topography, our numerical results show that the distribution of unstable modes in fact changes with increases in topographic amplitude and ridges (some of which move toward the short-wave end of the spectrum, and others collect about $\ell = 0$). Furthermore, despite the maximum growth rate remaining unchanged, the number of unstable modes decreases when increasing the number of ridges of topography. Thus, meridional topography has a clear influence on the stability of the flow, which is in disagreement with Benilov's findings. It would be interesting to see if this disagreement carries forward when considering higher order corrections in Benilov's asymptotic analysis.

An obvious extension to the material presented in this dissertation is the consideration of more than two fluid layers. A further possibility would have been the inclusion of numerical solutions to the two-layer problem in the presence of topography of the general Fourier form:

$$\hat{\eta}_b = \sum_{i=1}^{N} \left[\hat{\mathscr{A}}_i \sin(\hat{\alpha}_i \hat{x} + \hat{\gamma}_i \hat{y}) + \hat{\mathscr{B}}_i \cos(\hat{\kappa}_i \hat{x} + \hat{\tau}_i \hat{y}) \right].$$

The focus of this study was on a much simpler case, that being consideration of topography, taking the form of a sine function, varying in either the zonal or meridional directions (but never both). The reasoning behind these simple considerations was to produce a solid starting point. The number of routes we could have taken this problem down is endless, and so it makes little sense to overcomplicate the problem before we identify as much information as possible about the simpler case.

Despite having produced plots illustrating the critical shear over zonal topography numerically, it would be ideal for us to derive a necessary condition for the flow to become unstable., similar to the likes of Rayleigh's inflection point theorem [4, pg. 144-146] or the necessary condition derived over a constant slope in [20, pg. 792]. However, just because a necessary condition is satisfied, it does not always mean the flow is unstable. Nonetheless, this is still powerful information, and so it is important to derive such a condition. It would also be interesting to compare the critical shear in the topographic case with that obtained in the flat bottom case.

Another point worth addressing is one concerning the solutions obtained for the perturbation streamfunctions in each fluid layer. In this thesis, we only presented contour plots for solutions corresponding to the maximum growth rate. Despite this being interesting information, the structure of solutions corresponding to other growth rates could differ to that seen in figures 4.15-4.20. The extent of these differences is unknown, and is worth investigating in the future to see if any interesting patterns arise.

There is room for improvement in some of the numerical results obtained. For example, figure 4.7 showed that beyond a certain value of α, the number of unstable modes decreases with increases in α. Unfortunately, no obvious trend applied for zonal topgraphy. This might be due to considering topographic amplitudes greater than 1000m. Such amplitudes are outside the assumptions of the QG approximation, and so these solutions do not necessarily hold physically. If instead we considered more topographic amplitudes between $0-1000$m, we might be able to identify some form of trend. Regardless, even when considering such amplitudes, we identified a clear trend for the sum of positive growth rates for both types of topography, that being the sum decreases when α increases. To verify this, it is worth considering more topographic amplitudes between $0-1000$m. Finally, we favoured the use of $N = 256$ in our investigation since it appeared to give us similar results to those obtained using $N = 512$, as well as not being anywhere near as time consuming. Despite this, it might prove useful to solve the problem numerically for $N = 512$ and compare with the results obtained for $N = 256$.

Appendices

Throughout the construction of this thesis, I have written MATLAB code to obtain numerical solutions and produce various plots. For reference, I present these codes in this appendix.

.1 FLAT BOTTOM CODES

MATRIX FUNCTION

```
%{
    Two-layer QG matrix formulation with flat bottom
    Num is the number of grid points used
    k and l are the zonal and meridional wavenumbers respectively
    beta is the meridional gradient of the Coriolis parameter
    S is the stratification parameter
    U is the background velocity shear
%}

function [M, N] = QG_Two_Layer_Matrix_Flat(Num, k, l, S, beta, U)

    % Preallocation:
    M = zeros(2, 2);
    N = zeros(2, 2);

    K = k^2 + l^2;

    %Matrix elements, where w*M = N:
    M(1, 1) = K + S;
    M(1, 2) = -S;
    M(2, 1) = -S;
    M(2, 2) = K + S;

    N(1, 1) = -k*(beta - K*U);
    N(1, 2) = -k*S*U;
    N(2, 1) = 0;
    N(2, 2) = -k*(beta - S*U);
```

STABILITY CODE

```
%% ------------ Two-Layer Flat Linear Stability Analysis ------------ %%
clear variables

% ---------- Model Parameters ----------- %

Num = 256;
theta = 30; % latitude in degrees
Omega = 2*pi/86400; % Earth's rotation
% leading order Coriolis parameter:
f0 = 2*Omega*sin(theta*pi/180);
H = 2000; % Top/bottom layer depth
g = 9.81;
Rd = sqrt(g*2*H)/f0; % Barotropic deformation radius
rE = 6.4*10^6; % Radius of Earth

% meridional gradient of Coriolis parameter:
beta_dim = 2*Omega*cos(theta*pi/180)/rE;
S_dim = 1/25000^2; % Stratification parameter
U_dim = 0.04; % Background velocity in top layer

% Length and velocity scales:
Lh = Rd/(2*pi);
Lv = 2*H;
V = f0*Rd/(2*pi);

% Nondimensional variables:
beta = beta_dim*Lh^2/V;
S = Lh^2*S_dim;
U = U_dim/V;

% Wavenumbers:
k = -Num/2: 1: Num/2 - 1;
l = k;

% Preallocation:
eig_val = zeros(length(k), length(l), 2);
eig_vec = zeros(length(k), length(l), 2, 2);
tic
for i = 1: length(k)
    for j = 1: length(l)
```

```
        [M, N] = QG_Two_Layer_Matrix_Flat(Num, k(i), l(j), S, beta, U);
        [vec, lambda] = eig(N, M); % Solves M*vec = N*vec*lambda,
                                   % for matrices vec and lambda (diagonal)
        eig_val(i, j, :) = diag(lambda);
        eig_vec(i, j, :, :) = vec;
    end
end
toc

%% ------------ Distribution of Unstable Modes ------------ %%
for i = 1: Num
wi1 = squeeze(imag(eig_val(i, :, 1)));
k1 = k(wi1 > 0);
wi1 = squeeze(wi1(wi1 > 0));
wi2 = squeeze (imag(eig_val(i, :, 2)));
k2 = k(wi2 > 0);
wi2 = squeeze(wi2(wi2 > 0));
wi3 = squeeze (imag(eig_val(:, i, 1)));
k3 = k(wi3 > 0);
wi3 = squeeze(wi3(wi3 > 0));
wi4 = squeeze (imag(eig_val(:, i, 2)));
k4 = k(wi4 > 0);
wi4 = squeeze(wi4(wi4 > 0));
figure(1)
subplot(1, 2, 1)
plot(k1, wi1, 'o')
hold on
plot(k2, wi2, 'o')
subplot(1, 2, 2)
plot(k3, wi3, 'o')
hold on
plot(k4, wi4, 'o')
end
```

.2 TOPOGRAPHY CODE

MATRIX FUNCTION

```
%{
```

```
    Two-layer QG matrix formulation with sinusoidal bottom topography
    Num is the number of grid points used
    k and l are the zonal and meridional wavenumbers respectively
    S is the stratification parameter
    beta is the meridional gradient of the Coriolis parameter
    Amp and alpha denote the amplitude and wavelength of topography
    Top defines the topography under consideration
    U is the background velocity shear
%}

function [M, N] = QG_Two_Layer_Matrix(Num, k, l, S, beta, ...
                                      Amp, alpha, Top, U)

    % Preallocation:
    M = zeros(2*Num);
    N = zeros(2*Num);

    K1 = k.^2 + l.^2;
    K2 = k.^2 + l.^2 + S;

    if Top == 1 % Bottom irregularities with meridional variation
        for j = 1: Num
            % Elements of the matrix N
            N(j, j) = -K2(j);
            N(j, j + Num) = S;
            N(j + Num, j) = S;
            N(j + Num, j + Num) = -K2(j);
            % Elements of the matrix M
            M(j, j) = k*(beta - K1(j)*U);
            M(j, j + Num) = k*S*U;
            M(j + Num, j + Num) = k*(beta - S*U);
            if l(j) - alpha ≥ l(1)
                M(j + Num, j + Num - alpha) = Amp*alpha*k;
            end
            if l(j) + alpha ≤ l(end)
                M(j + Num, j + Num + alpha) = Amp*alpha*k;
            end
        end

    elseif Top == 2 % Bottom irregularities with zonal variation
```

```
        for j = 1: Num
            % Elements of the matrix N
            N(j, j) = -K2(j);
            N(j, j + Num) = S;
            N(j + Num, j) = S;
            N(j + Num, j + Num) = -K2(j);
            % Elements of the matrix M
            M(j, j) = k(j)*(beta - K1(j)*U);
            M(j, j + Num) = k(j)*S*U;
            M(j + Num, j + Num) = k(j)*(beta - S*U);
            if k(j) - alpha ≥ k(1)
                 M(j + Num, j + Num - alpha) =  -Amp*alpha*l;
            end
            if k(j) + alpha ≤ k(end)
                M(j + Num, j + Num + alpha) = -Amp*alpha*l;
            end
        end
    else
        disp('Error: Make sure the value for Top is either 1 or 2!')
    end

end
```

Stability Code for Variable Topographic Amplitude

```
%% ------------ Two-Layer Linear Stability Analysis ------------ %%
clear variables

Top = 1; % Top = 1 corresponds to topography Amp*sin(alphy*y)
         % Top = 2 corresponds to topography Amp*sin(alphy*y)

% ---------- Model Parameters ----------- %

Num = 256;
theta = 30; % latitude in degrees
Omega = 2*pi/86400; % Earth's rotation

% leading order Coriolis parameter:
f0 = 2*Omega*sin(theta*pi/180);
```

```
15
16 H = 2000; % Top/bottom layer depth
17 g = 9.81;
18 Rd = sqrt(g*2*H)/f0; % Barotropic deformation radius
19 rE = 6.4*10^6; % Radius of Earth
20
21 % meridional graident of Coriolis parameter:
22 beta_dim = 2*Omega*cos(theta*pi/180)/rE;
23
24 S_dim = 1/25000^2; % Stratification parameter
25 U_dim = 0.04; % Background velocity in top layer
26
27 % Loop for amplitude column vector:
28 Amp_dim = [400, 800, 1200, 1600, 2000];
29
30 % Length and velocity scales:
31 Lh = Rd/(2*pi);
32 Lv = 2*H;
33 V = f0*Rd/(2*pi);
34
35 % Nondimensional variables:
36 Amp = Amp_dim/Lv;
37 beta = beta_dim*Lh^2/V;
38 S = Lh^2*S_dim;
39 U = U_dim/V;
40
41 % topographic ridges:
42 alpha = [1, 3, 5, 10, 15, 20];
43
44 % wavenumbers:
45 k = -Num/2: 1: Num/2 - 1;
46 l = k;
47
48 % ---------- Eigenfrequencies and Eigenmodes ----------- %
49
50 % Preallocation:
51 eig_vec = zeros(length(alpha), length(k), 2*Num, 2*Num);
52 eig_val = zeros(length(alpha), 2*Num^2);
53 max_growth = zeros(length(Amp), length(alpha), length(k));
54
```

```
tic
for i = 1: length(Amp)
    for j = 1: length(alpha)
        for m = 1: length(k)

            if Top == 1
                [M, N] = QG_Two_Layer_Matrix(Num, k(m), l, S, ...
                    beta, Amp(i), alpha(j), Top, U);
                % Array to store k values for alpha:
                k_arr(j, (m - 1)*2*Num + 1 :m*2*Num) = k(m);
            elseif Top == 2
                [M, N] = QG_Two_Layer_Matrix(Num, k, l(m), S, ...
                    beta, Amp(i), alpha(j), Top, U);
                % Array to store l values for alpha:
                k_arr(j, (m - 1)*2*Num + 1 : m*2*Num) = l(m);
            end

            [vec, lambda] = eig(M, N);
            % Solves M*vec = N*vec*lambda,
            % for matrices vec and lambda (diagonal)

            eig_vec(j, m, :, :) = vec(:, :);
            % Column vectors of matrix output
            % are eigenvectors of eigenfunctions for each eigenvalue

            eig_val(j, (m - 1)*2*Num + 1 : m*2*Num) = diag(lambda);
            % Stores array of eigenfrequencies for each (k, Amp, alpha)

            % store maximum growth rates:
            max_growth(i, j, m) = max(imag(diag(lambda)));

        end
    end

    % save files for use later:
    filename = sprintf('Data_Top_%d_Amp_%d_Num_256.mat', Top, Amp_dim(i));
    save(filename, 'k_arr', 'eig_vec', 'eig_val', 'k', '-v7.3')
    clear eig_val eig_vec
    % command to clear eig variables and renew for every Amp value
end
```

```
toc
file_name = sprintf('Max_Growth_Top_%d_U_4_Num_256.mat', Top);
save(file_name, 'max_growth', 'k', 'Amp', 'alpha', '-v7.3')
```

Stability Code for Variable Background Velocity

```
%% ------------ Two-Layer Linear Stability Analysis ------------ %%
clear variables

Top = 1;

% ---------- Model Parameters ----------- %

Num = 128;
theta = 30;
Omega = 2*pi/86400;
f0 = 2*Omega*sin(theta*pi/180);
H = 2000;
g = 9.81;
Rd = sqrt(g*2*H)/f0;
rE = 6.4*10^6;
beta_dim = 2*Omega*cos(theta*pi/180)/rE;
S_dim = 1/25000^2;

% Vector of background velocities:
U_dim = [0, 0.005, 0.01, 0.015, 0.02, 0.025, ...
    0.03, 0.035, 0.04, 0.045, 0.05];

% Loop for amplitude column vector:
Amp_dim = 400;

% Length and velocity scales:
Lh = Rd/(2*pi);
Lv = 2*H;
V = f0*Rd/(2*pi);

% Nondimensional variables:
Amp = Amp_dim/Lv;
beta = beta_dim*Lh^2/V;
```

```
S = Lh^2*S_dim;
U = U_dim/V;

alpha = [1, 3, 5, 10, 15, 20];

k = -Num/2: 1: Num/2 - 1;
l = k;

% ---------- Eigenfrequencies and Eigenmodes ----------- %

% Preallocation:
eig_vec = zeros(length(alpha), length(k), 2*Num, 2*Num);
eig_val = zeros(length(alpha), 2*Num^2);
max_growth = zeros(length(U), length(alpha), length(k));

% Same code as QG_Two_Layer_Stability,
% but for varying U and fixed Amp:
tic
for i = 1: length(U)
    for j = 1: length(alpha)
        for m = 1: length(k)

            if Top == 1
                [M, N] = QG_Two_Layer_Matrix(Num, k(m), l, S, ...
                    beta, Amp, alpha(j), Top, U(i));
                k_arr(j, (m - 1)*2*Num + 1 :m*2*Num) = k(m);
            elseif Top == 2
                [M, N] = QG_Two_Layer_Matrix(Num, k, l(m), S, ...
                    beta, Amp, alpha(j), Top, U(i));
                k_arr(j, (m - 1)*2*Num + 1 : m*2*Num) = l(m);
            end

            [vec, lambda] = eig(M, N);
            eig_vec(j, m, :, :) = vec(:, :);
            eig_val(j, (m - 1)*2*Num + 1 : m*2*Num) = diag(lambda);
            max_growth(i, j, m) = max(imag(diag(lambda)));

        end
    end
    filename = sprintf('Data_Top_%d_U_%d_Amp_1_Num_128.mat', Top, U_dim(i));
```

```
    save(filename, 'k_arr', 'eig_vec', 'eig_val', 'k', '-v7.3')
    clear eig_val eig_vec
end
toc
file_name = sprintf('Max_Growth_Top_%d_Amp_1_Num_128.mat', Top);
save(file_name, 'max_growth', 'k', 'Amp', 'alpha', '-v7.3')
```

PLOTS

```
clear variables
LB = flipud(brewermap(20,'Spectral')); % Colour scheme for instability plots

% Loading saved files storing eigenvalues
% and eigenvectors for different Amp
% values and different topography:

% Zonal topography data:

load('Data_Top_1_Amp_0400_Num_256.mat');
% load('Data_Top_1_Amp_0800_Num_256.mat');
% load('Data_Top_1_Amp_1200_Num_256.mat');
% load('Data_Top_1_Amp_1600_Num_256.mat');
% load('Data_Top_1_Amp_2000_Num_256.mat');
load('Max_Growth_Top_1_U_4_Num_256.mat');

% Meridional topography data:

% load('Data_Top_2_Amp_0400_Num_256.mat');
% load('Data_Top_2_Amp_0800_Num_256.mat');
% load('Data_Top_2_Amp_1200_Num_256.mat');
% load('Data_Top_2_Amp_1600_Num_256.mat');
% load('Data_Top_2_Amp_2000_Num_256.mat');
% load('Max_Growth_Top_2_U_4_Num_256.mat');

Num = 256;
alpha = [1, 3, 5, 10, 15, 20];
% Top = 2; % use when loading Top_2 files
Top = 1; % use when loading Top_1 files
l = k;
```

```
31
32 % Define array of k-values for each alpha
33 % to use for scatter plots:
34 for j = 1: length(alpha)
35     for m = 1: length(k)
36         k_arr(j, (m - 1)*2*Num + 1 :m*2*Num) = k(m);
37     end
38 end
39
40
41 %% ------------ Growth Rates of Unstable Modes ------------ %%
42 figure(1)
43 for j = 1: 6
44     wi = imag(eig_val(j, :));
45     subplot(3, 2, j)
46     plot(k_arr(j, :), wi, 'o')
47     ax = gca;
48     ax.FontSize = 12;
49     xlim([-70, 70])
50     ylim([0.0001, 0.008])
51     ylabel('$\omega_i$', 'Interpreter', 'latex', 'fontsize', 20)
52     grid on
53     txt1 = ['$$\alpha = ' num2str(alpha(j)) '$$'];
54     t1 = text(40, 0.004, txt1, 'Interpreter', 'latex');
55     t1.FontSize = 20;
56     if Top == 1
57        xlabel('$k$', 'Interpreter', 'latex', 'fontsize', 20)
58     elseif Top == 2
59            xlabel('$\ell$', 'Interpreter', 'latex', 'fontsize', 20)
60     end
61 end
62
63
64 %% ------------ Contour Plots ------------ %%
65
66 % Maximum growth rates for alpha vs k (or l):
67 figure(2)
68 contourf(k, alpha, squeeze(max_growth(1, :, :)))
69 % 1 corresponds to Amp_dim = 400m, 2 corresponds to Amp_dim = 800m, ect.
70 ax = gca;
```

```
ax.FontSize = 12;
ylabel('$\alpha$', 'Interpreter', 'latex', 'fontsize', 20)
xlim([-70, 70])
ylim([1, 20])
grid on
colorbar()
colormap(LB)
caxis([0, 0.006])
if Top == 1
    xlabel('$k$', 'Interpreter', 'latex', 'fontsize', 20)
elseif Top == 2
       xlabel('$\ell$', 'Interpreter', 'latex', 'fontsize', 20)
end

%% ------------ Dispersion Relation Scatter Plots (Unstable Modes only!) -----

figure(3)
for j = 1: 6
    subplot(3, 2, j)
    wi = imag(eig_val(j, :));
    wi (wi ≤ 0) = nan;
    wr = real(eig_val(j, :));
    scatter(k_arr(j, :), wr, [], wi, 'o', 'filled')
    ax = gca;
    ax.FontSize = 12;
    ylabel('$\omega_r$', 'Interpreter', 'latex', 'fontsize', 20)
    colormap(LB)
    caxis([0.0001, 0.006])
    box on
    grid on
    txt1 = ['$$\alpha = ' num2str(alpha(j)) '$$'];
    t1 = text(40, 0.05, txt1, 'Interpreter', 'latex');
    t1.FontSize = 20;
    if Top == 1
        xlabel('$k$', 'Interpreter', 'latex', 'fontsize', 20)
        xlim([-70, 70])
        ylim([0, 0.08])
    elseif Top == 2
        xlabel('$\ell$', 'Interpreter', 'latex', 'fontsize', 20)
        xlim([-70, 70])
```

```
111         ylim([0, 0.08])
112     end
113 end
114
115
116 %% ------------ No. of Unstable Modes as Function of alpha ------------ %%
117
118 %% ------------ Eigenmode Plots (corresponding to maximum growth rates) ------
119
120 x = linspace(0, 2*pi, Num);
121 y = linspace(0, 2*pi, Num);
122 [X, Y] = meshgrid(x, y);
123
124     for j = 1: length(alpha)
125         [A(j), I(j)] = max(squeeze(imag(eig_val(j, :))));
126         % I is the index of the maximum mode
127         i = floor(I(j)/(2*Num)) + 1;
128         % i is the wavenumber corresponding
129         % to the maximum mode
130         m = rem(I(j), 2*Num);
131         B(:, j) = squeeze(eig_vec(j, i, :, m));
132         max_k(j) = i;
133     end
134
135 psi1 = 0*X;
136 psi2 = 0*X;
137 for i = 1: Num
138      % use for zonal topography:
139        psi1 = psi1 + B(i, 1)*exp(1j*(k(max_k(1))*X + l(i)*Y));
140        psi2 = psi2 + B(i + Num, 1)*exp(1j*(k(max_k(1))*X + l(i)*Y));
141        % use for meridional topography:
142 %        psi1 = psi1 + B(i, 1)*exp(1j*(k(max_k(1))*Y + l(i)*X));
143 %        psi2 = psi2 + B(i + Num, 1)*exp(1j*(k(max_k(1))*Y + l(i)*X));
144
145 end
146
147 figure(5)
148 subplot(2, 3, [1 2])
149 contourf(x, y, real(psi1))
150 ax = gca;
```

```
ax.FontSize = 12;
xlabel('$x$', 'Interpreter', 'latex', 'fontsize', 20)
ylabel('$y$', 'Interpreter', 'latex', 'fontsize', 20)
title('\textbf{Top Layer}', 'Interpreter', 'latex', ...
    'fontsize', 20)
subplot(2, 3, 3)
contourf(x, y, (0.1)*sin(alpha(1)*Y)); % use for Top = 1
% contourf(x, y, (0.1)*sin(alpha(1)*X)); % use for Top = 2
ax = gca;
ax.FontSize = 12;
title('$\eta_b = 0.1\sin(y)$', 'Interpreter', 'latex', ...
    'fontsize', 20)
subplot(2, 3, [4 5])
contourf(x, y, real(psi2))
ax = gca;
ax.FontSize = 12;
xlabel('$x$', 'Interpreter', 'latex', 'fontsize', 20)
ylabel('$y$', 'Interpreter', 'latex', 'fontsize', 20)
title('\textbf{Bottom Layer}', 'Interpreter', 'latex', ...
    'fontsize', 20)
subplot(2, 3, 6)
contourf(x, y, (0.1)*sin(alpha(1)*Y)); %use for Top = 1
% contourf(x, y, (0.1)*sin(alpha(1)*X)); % use for Top = 2
ax = gca;
ax.FontSize = 12;
xlabel('$x$', 'Interpreter', 'latex', 'fontsize', 20)
```

```
clear variables
alpha = [1, 3, 5, 10, 15, 20];

% Loading saved files:
file_list1 = dir('Data_Top_1_Amp*.mat');
file_list2 = dir('Data_Top_2_Amp*.mat');
for k = 1: length(file_list1)
    s1 = load(file_list1(k).name);
    for i = 1: length(alpha)
        tmp1 = squeeze(s1.eig_val(i, :));
        tmp1 = tmp1 (imag(tmp1) > 0);
        % Number of unstable modes:
```

```
        N1(k, i) = length(tmp1);
        % Sum of complex modes:
        sum_eig1(k, i) = sum(tmp1);
    end
end
for k = 1: length(file_list2)
    s2 = load(file_list2(k).name);
    for i = 1: length(alpha)
        tmp2 = squeeze(s2.eig_val(i, :));
        tmp2 = tmp2 (imag(tmp2) > 0);
        N2(k, i) = length(tmp2);
        sum_eig2(k, i) = sum(tmp2);
    end
end

s = load('Data_Amp_0_Num_256');
for i = 1: length(k)
    tmp3 = squeeze(s.eig_val(i, :));
    tmp3 = tmp3 (imag(tmp3) > 0);
    N3(i) = length(tmp3);
    sum_eig3(i) = sum(tmp3);
end
l = k;
for i = 1: length(l)
    tmp4 = squeeze(s.eig_val(:, i));
    tmp4 = tmp4 (imag(tmp3) > 0);
    N4(i) = length(tmp4);
    sum_eig4(i) = sum(tmp4);
end

figure(1)
% Plots of unstable modes as a function
% of alpha:
subplot(2, 2, 1)
% zonal topography:
plot(alpha, N1, '-')
xlabel('$\alpha$', 'Interpreter', 'latex', ...
    'fontsize', 20)
ylabel('\textbf{Number of Unstable Modes}', ...
    'Interpreter', 'latex', 'fontsize', 12)
```

```
53 title('$\eta_b = \mathcal{A}\sin(\alpha y)$', ...
54     'Interpreter', 'latex', 'fontsize', 20)
55 legend('$\mathcal{A} = 0.1$', '$\mathcal{A} = 0.2$', ...
56     '$\mathcal{A} = 0.3$', '$\mathcal{A} = 0.4$', ...
57     '$\mathcal{A} = 0.5$', 'Interpreter', 'latex')
58
59 subplot(2, 2, 2)
60 % meridional topography:
61 plot(alpha, N2, '-')
62 xlabel('$\alpha$', 'Interpreter', 'latex', ...
63     'fontsize', 20)
64 ylabel('\textbf{Number of Unstable Modes}', ...
65     'Interpreter', 'latex', 'fontsize', 12)
66 title('$\eta_b = \mathcal{A}\sin(\alpha x)$', ...
67     'Interpreter', 'latex', 'fontsize', 20)
68 legend('$\mathcal{A} = 0.1$', '$\mathcal{A} = 0.2$', ...
69     '$\mathcal{A} = 0.3$', '$\mathcal{A} = 0.4$', ...
70     '$\mathcal{A} = 0.5$', 'Interpreter', 'latex')
71
72 % plots of sum of all positive growth rates
73 % as a function of alpha:
74 subplot(2, 2, 3)
75 % zonal topography:
76 plot(alpha, imag(sum_eig1), '-')
77 xlabel('$\alpha$', 'Interpreter', 'latex',...
78     'fontsize', 20)
79 ylabel('\textbf{Sum of Growth Rates of all Unstable Modes}', ...
80     'Interpreter', 'latex', 'fontsize', 12)
81 title('$\eta_b = \mathcal{A}\sin(\alpha y)$', ...
82     'Interpreter', 'latex', 'fontsize', 20)
83 legend('$\mathcal{A} = 0.1$', '$\mathcal{A} = 0.2$', ...
84     '$\mathcal{A} = 0.3$', '$\mathcal{A} = 0.4$', ...
85     '$\mathcal{A} = 0.5$', 'Interpreter', 'latex')
86
87 subplot(2, 2, 4)
88 % meridional topography:
89 plot(alpha, imag(sum_eig2), '-')
90 xlabel('$\alpha$', 'Interpreter', 'latex', ...
91     'fontsize', 20)
92 ylabel('\textbf{Sum of Growth Rates of all Unstable Modes}',...
```

```
93      'Interpreter', 'latex', 'fontsize', 12)
94  title('$\eta_b = \mathcal{A}\sin(\alpha y)$', ...
95      'Interpreter', 'latex', 'fontsize', 20)
96  legend('$\mathcal{A} = 0.1$', '$\mathcal{A} = 0.2$', ...
97      '$\mathcal{A} = 0.3$', '$\mathcal{A} = 0.4$', ...
98      '$\mathcal{A} = 0.5$', 'Interpreter', 'latex')
```

BIBLIOGRAPHY

[1] John Billingham and Andrew C King. *Wave motion*. Number 24. Cambridge university press, 2000.

[2] Philip G Saffman. *Vortex dynamics*. Cambridge university press, 1992.

[3] Anatoly I Ruban. *Fluid Dynamics: Part 3 Boundary Layers*. Oxford University Press, 2017.

[4] Philip Drazin, William Reid, and FH Busse. Hydrodynamic stability, 1982.

[5] Andy C King, John Billingham, and Stephen Robert Otto. *Differential equations: linear, nonlinear, ordinary, partial*. Cambridge University Press, 2003.

[6] Paul C Matthews. *Vector calculus*. Springer Science & Business Media, 2012.

[7] Martin Anthony and Michele Harvey. *Linear algebra: concepts and methods*. Cambridge University Press, 2012.

[8] Arieh Iserles. *A first course in the numerical analysis of differential equations*. Number 44. Cambridge university press, 2009.

[9] Larry Wasserman. *All of statistics: a concise course in statistical inference*. Springer Science & Business Media, 2013.

[10] P Berloff and Igor Kamenkovich. On spectral analysis of mesoscale eddies. part i: Linear analysis. *Journal of Physical Oceanography*, 43(12):2505–2527, 2013.

[11] P Berloff and Igor Kamenkovich. On spectral analysis of mesoscale eddies. part ii: Nonlinear analysis. *Journal of Physical Oceanography*, 43(12):2528–2544, 2013.

[12] Stephen I Thomson and Michael E McIntyre. Jupiter's unearthly jets: A new turbulent model exhibiting statistical steadiness without large-scale dissipation. *Journal of the Atmospheric Sciences*, 73(3):1119–1141, 2016.

[13] Hemant Khatri and Pavel Berloff. Role of eddies in the maintenance of multiple jets embedded in eastward and westward baroclinic shears. *Fluids*, 3(4):91, 2018.

[14] IV Shevchenko, PS Berloff, David Guerrero-López, and JE Roman. On low-frequency variability of the midlatitude ocean gyres. *Journal of Fluid Mechanics*, 795:423–442, 2016.

[15] Peter B Rhines and William R Young. A theory of the wind-driven circulation. i. mid-ocean gyres. *J. Mar. Res*, 40(3):559–596, 1982.

[16] Dmitri Kondrashov and Pavel Berloff. Stochastic modeling of decadal variability in ocean gyres. *Geophysical Research Letters*, 42(5):1543–1553, 2015.

[17] Hemant Khatri and Pavel Berloff. Tilted drifting jets over a zonally sloped topography: effects of vanishing eddy viscosity. *Journal of Fluid Mechanics*, 876:939–961, 2019.

[18] Hemant Khatri and Pavel Berloff. A mechanism for jet drift over topography. *Journal of Fluid Mechanics*, 845:392–416, 2018.

[19] RM Samelson and J Pedlosky. Local baroclinic instability of flow over variable topography. *Journal of fluid mechanics*, 221:411–436, 1990.

[20] Changheng Chen and Igor Kamenkovich. Effects of topography on baroclinic instability. *Journal of Physical Oceanography*, 43(4):790–804, 2013.

[21] ES Benilov. Baroclinic instability of two-layer flows over one-dimensional bottom topography. *Journal of physical oceanography*, 31(8):2019–2025, 2001.

[22] Geoffrey K Vallis. *Atmospheric and oceanic fluid dynamics*. Cambridge University Press, 2017.

[23] James C McWilliams, C James, James C McWilliams, and Jim McWilliams. *Fundamentals of geophysical fluid dynamics*. Cambridge University Press, 2006.

[24] Joseph Pedlosky. *Geophysical fluid dynamics*. Springer Science & Business Media, 2013.

[25] David J Acheson. Elementary fluid dynamics, 1991.

[26] Steven H Strogatz. *Nonlinear dynamics and chaos: with applications to physics, biology, chemistry, and engineering*. CRC Press, 2018.

[27] ES Benilov. Waves on the beta-plane over sparse topography. *Journal of Fluid Mechanics*, 423:263–273, 2000.

[28] ES Benilov. The stability of zonal jets in a rough-bottomed ocean on the barotropic beta plane. *Journal of physical oceanography*, 30(4):733–740, 2000.

[29] ES Benilov, J Nycander, and DG Dritschel. Destabilization of barotropic flows small-scale topography. *Journal of Fluid Mechanics*, 517:359–374, 2004.

[30] Worth D Nowlin Jr and John M Klinck. The physics of the antarctic circumpolar current. *Reviews of Geophysics*, 24(3):469–491, 1986.